ABSTRACT

Title of dissertation: Multi-scale Modeling and Computations

Linbao Zhang, Doctor of Philosophy, 2009

Dissertation directed by: Professor Jian-Guo Liu
Department of Mathematics

In the rarefied gas dynamics, the classic kinetic models are more accurate and complicated, while the fluid models are much simpler but fail in some cases. In this thesis, we propose a new local up-scaling model to couple Euler equations with the kinetic model when the previous up-scaling model in [19] does not apply, e.g. when the Boltzmann equation is solved by the particle method, like DSMC. By means of the first order Chapman-Enskog expansion we propose a new NSLU model to couple the Navier-Stokes equations with the kinetic models. We also propose the zero-moment projection based on the macro-micro decomposition ([34]) to correct the non-fluid part in the up-scaling models.

Numerical tests of these local up-scaling models have been done in various

multi-scale problems, including the Jin-Xin relaxation model for the traveling shock, 1D1D BGK model for the dynamics of a small perturbation of an equilibrium, 1D3D BGK model for the stationary shock and the simulation of a planar Couette flow by direct simulation of Monte Carlo (DSMC) for the Boltzmann equation.

The implicit-explicit scheme for the relaxation models is applied, which is shown to preserve the positiveness of the distribution function, the conservation laws and entropy inequality. Numerical results show that the zero-projection is necessary to ensure the stability and accuracy for the up-scaling models, especially when non-kinetic schemes are applied in the moment equations. NSLU model must be applied to replace the up-scaling model in [19] if the macroscopic approximation is the viscous fluid.

The similar scaling exists in the relaxation-time model for the semiconductor device when electric field is low. The DrDiLU model based on drift-diffusion model for the diode is proposed which is similar to NSLU model for the rarefied gas. Numerical experiments show it is stable and accurate compared with the results from the relaxation-time model.

MULTI-SCALE MODELING AND COMPUTATIONS

by

Linbao Zhang

Dissertation submitted to the Faculty of the Graduate School of the
University of Maryland, College Park in partial fulfillment
of the requirements for the degree of
Doctor of Philosophy
2009

Advisory Committee:
  Professor Jian-Guo Liu
  Professor Manussos Grillakis
  Professor C. David Levermore
  Professor Matei Machedon
  Professor Konstantina Trivisa

DEDICATION

To my father, Wangli Zhang and my mother, Guihua Bai;

To my wife, Bo Li;

To my daughter, Yun-Mo Zhang.

ACKNOWLEDGEMENTS

The thesis dissertation marks the end of a long and eventful journey for which there are many people that I would like to acknowledge for their support along the way.

First of all I would like to express my sincere appreciation to my advisor, Jian-Guo Liu. I especially want to thank for his guidance and constant support both on my research and on my life. His perpetual energy, enthusiasm in research and optimistic attitude toward life have motivated me a lot. In addition, he is always patient, understanding and willing to help. I can get his prompt assistance when needed all the time.

I thanks the committee members: Manussos Grillakis, David Levermore, Matei Machedon and Konstantina Trivisa. In particular, I would like to thank David Levermore for his precious suggestions and comments, which help to improve my writing and understanding of this subject.

Definitely I will miss my doctoral years at Maryland. I am grateful to all my friends here, for being the surrogate family during these years. I will treasure their

friendship for the rest of my life.

My deepest gratitude goes to my wife for her love, encouragement and patience throughout all these years. I had to be away from her for months when she was pregnant. For these and much more, I am forever in her debt. I also owe a lot to my parents-in-law. They took care of our baby so I could be fully devoted to the dissertation. This dissertation is simply impossible without them.

At last I want to thank my parents. Both of them had worked industriously to support the family and spare no effort to provide their six children the best education as they can. Like all other simply perfect mother, my mother spent her whole life to raise her children without any complaint in spite of all the hardships in the life. However, after I, her youngest kid, graduated from the college, she left us forever. In many nights these years, I met her in the dreams. Although she is no longer with us, I am sure she shares all the happy moments with us in the heaven. I cannot ask for more from my father. His everlasting love and constant support are what I rely on whenever I encounter difficulties.

<div align="center">Table of Contents</div>

vi

List of Figures

Chapter 1

Introduction

In nature, things are made up of atoms or molecules and the processes occur at the atomic scale (micro scale). For example, the mean free path of nitrogen at 298 K and a pressure of 0.01 atm is $6.68 \times 10^{-6} m$ and mean free time is $2.68 \times 10^{-8} s$. However events in our daily lives are happening at a much larger geometric dimensions and much slower pace (macro scales). In our numerical simulation for the 1D stationary shock, the ratio of macro length scale to micro length scale is around 10^6. Due to the multi-scale feature, there are two ways to model the rarefied gas dynamics: kinetic models and fluid models.

In the thesis we will focus on the spacial multi-scale problems. The Knudsen number κ is usually used as a rough indicator of the scales which is the ratio of the mean free path to a typical macroscopic length. As noted in [7], a more precise κ, or the local κ is obtained if the macroscopic length $L = |U/\frac{\partial U}{\partial x}|$, where U is the

macroscopic quantities such as $\rho, \mathbf{u}$ or T. If $\kappa \approx O(1)$, the kinetic models must be applied. However, the kinetic models are often not only too complex to be dealt with, but also because it contains too much information of little interest. When $\kappa \ll 1$, the system is close to equilibrium state so the simpler fluid models may be applied. These fluid models will fail when $\kappa \approx O(1)$.

A typical example is the simulation of reentry problems in aerodynamics, where the system is close to equilibrium far from the reentry body, while non-equilibrium effects are very large close to the body. Another example is the simulation of combustion wave. Ignition will occur in a local region over a certain temperature and affect the whole system afterwards. It may not happen if we won't resolve the small scales in the local region. In these cases, the multi-scale modeling is needed to solve the problems efficiently and accurately.

One straightforward way to deal with these cases is that we may apply different models in different regions, i.e. the domain decomposition model. The domain decomposition model (DD) has also been widely used in molecular dynamics problems. A lot of work has been done in this area [22, 48]. It has also been applied to couple the kinetic model with the continuum model, [9].

Heterogeneous multi-scale Model was proposed by E and Engquist in [20]. The basic principle of HM model is that one should start with a macro solver, taking into account as much as possible what is known about the macro process, and use the

micro model to provide the missing macro data that are necessary for implementing the macro solver. In [20], they propose the conservation laws as the macro solver and the missing macro data is the fluxes.

It is well-known the Euler equations can be derived from the zeroth order of Chapman-Enskog expansion, which describes the dynamics of the equilibrium state. Therefore we may choose the Euler equations as the macro solver which will be solved in the entire region and solve an additional equation for the non-equilibrium part to provide the corrections (up-scaling) of the macro model which are needed in the kinetic region. This is the local up-scaling (ELU1) model proposed by Degond, Liu and Mieussens in [19].

In a lot of cases, the dynamics of fluid should be better modeled as viscous fluid instead of inviscid fluid. Therefore we may replace the Euler equations by the Navier-Stokes equations as the macro solver. By means of the first order Chapman-Enskog expansion we propose a new NSLU model to couple the Navier-Stokes equations with the kinetic models. In this model, the Navier-Stokes system will be solved in the whole region. The additional equation for the non-fluid part obtained from the kinetic model is solved in kinetic sub-region to supply the up-scaling for the Navier-Stokes equations.

From the Chapman-Enskog expansion, the non-fluid part in the ELU1 and NSLU models should make no contribution to the macroscopic quantities. There-

fore we propose the zero-moment projection based on the macro-micro decomposition [34] to correct the non-fluid part in the computation of the up-scaling models. Numerical simulations show the zero-moment projection improves not only the accuracy, but also the stability of the numerical schemes, especially when the non-kinetic schemes are used for the macro solver.

The equation for the non-equilibrium part is needed for the ELU1 model, which can't be obtained if the particle method for the kinetic models is used, such as Direction Simulation of Monte Carlo (DSMC) for the Boltzmann equation. By rewriting the up-scaling terms in terms of the original distribution function f instead of non-equilibrium part, we propose a new local up-scaling model (ELU2) which enables us to couple Euler equations with the Boltzmann equation.

To compare the results of the up-scaling models with the kinetic models, we also did the simulation of the kinetic models in the whole region. In order to remove the stiffness of the relaxation models due to the small knudsen number in the fluid region, we apply the implicit-explicit scheme for the relaxation model, which is shown to preserve the positiveness, the conservation laws and the entropy inequality.

For the simulation of the semiconductor device: 1D GaAs n^+-n-n^+ diode, we take the relaxation-time model (RT) as the kinetic model. It is known the similar scaling structure exists when electric field is low. The DrDiLU model based on

4

drift-diffusion model (DrDi) for the diode is proposed from the first order Chapman-Enskog expansion. Numerical experiments show it is stable and accurate, esp. on the regions where the doping profile has big gradient. When the electric field is high, the macroscopic model is the high field (HF) model, [14]. Due to the complicated distribution function of the high field model, the up-scaling model can't be obtained. In this case, we did a comparison of the DD model and RT model, which shows no improvement compared with the HF model.

In the following we present a brief overview of each chapter:

1. Chapter 2 is the introduction of the kinetic models and the fluid models for the rarefied gas dynamics, their connections and the corresponding numerical methods which will be used in the multi-scale modeling. The kinetic models include the Boltzmann equation, the BGK model and some other models. The fluid models include Euler equations and Navier-Stokes equations. The numerical methods include DSMC for the Boltzmann equation and the discrete velocity method for the BGK model, the flux splitting methods for Euler equations and Navier-Stokes equations.

2. In chapter 3, we review some existing multi-scale models, such as DD model and HM model. The derivations of the local up-scaling models are shown for ELU1, ELU2 and NSLU models. Also we discuss the corresponding numerical schemes for these models.

3. In chapter 4, similar to the NSLU model, when the electric field is low, the DrDiLU model is derived based on the DrDi model from the RT model to simulate the 1D GaAs $n^+ - n - n^+$ diode. If the electric field is high, the DD model to couple the high-field model with the relaxation model is used.

4. In chapter 5, we will concentrate on the numerical tests of the multi-scale models. We begin with an artificial multi-scale problem constructed from the Jin-Xin relaxation model for the inviscid Burger's equation. The ELU1 and NSLU models will be used to compute a traveling shock problem. Then it is followed by the BGK model for the rarefied gas. We will consider an initial-value problem for 1D1D case and a stationary shock problem for 1D3D case. The ELU1 model, ELU2 and NSLU models will be used in the computation. We also simulate a 2D planar Couette flow to show how to use the ELU2 model to get a smoother profile from the DSMC result of the Boltzmann equation. In last example, we will do a diode simulation for the semiconductor using the DrDiLU model when the electric field is low. When electric field is high, we apply DD model to couple the HF model with the RT model.

5. In appendix A, the derivation of the Boltzmann equation for the hard-sphere molecules [10] is shown which is helpful to understand the algorithm of DSMC. It is followed by a list of different types of molecular models including the hard-

6

sphere model. Then two examples are given to shown that the local Knudsen number κ is not a sufficient condition to demarcate the region. The zero-moment projection formulas for 1D1D BGK and 1D3D BGK models are given in section D. They are needed in the numerical experiments in chapter 5.

From the numerical results, we see the implicit-explicit scheme for the relaxation models is stable for the relaxation models for all κ. Also zero-moment projection is very important for stability and accuracy. It is necessary to apply the projection for the stability if other schemes are used than kinetic scheme. When the viscous fluid model is needed to describe the leading behavior of the fluid dynamics, ELU1 model should be replaced by NSLU model coupling fluid model (Navier-Stokes equations) with kinetic models to avoid modeling error. ELU2 model is an alternate up-scaling model to couple the Euler equations with the kinetic models. It resolves the difficulty of ELU1 model which can't be obtained in some cases to implement the local up-scaling.

In [28], the authors got an asymptotic preserving scheme for the relaxation model by balancing the transport term and the relaxation term. Because of the successful separation of different scales in the different equations, the up-scaling models should be a new way to get an asymptotic preserving scheme. We will leave the theoretic analysis for the ELU1 and NSLU models as the future work.

So far we only did one-way coupling for the ELU2 model in the simulation of

7

2D Couette flow and enforced the conservation of mass and momentum. A better result should be obtained if the energy conservation is also enforced. Two-way coupling for ELU2 model may also accelerate the convergence of DSMC.

Chapter 2

Kinetic Models and Fluid Models

In this chapter, we present the background material needed for multi-scaling modeling, i.e. the classic kinetic models and the fluid models for the rarefied gas dynamics. The kinetic models include the Boltzmann equation, the BGK model and some other models and the fluid models include Euler equations and Navier-Stokes equations.

The appropriate boundary conditions for the models are reviewed to describe the interaction of the gas and the solid boundary. Then we will show how to extract the macroscopic variable functions $\rho, \mathbf{u}, \theta$ of the gas from the microscopic variable function f and the asymptotic derivation of the fluid models from the kinetic models (Chapman-Enskog expansion).

In the last two sections, we will review some popular numerical methods to

kinetic and fluid models. The numerical methods include Direct Simulation of Monte Carlo (DSMC) for the Boltzmann equation and the discrete velocity method for the BGK models, the flux splitting methods for Euler equations and Navier-Stokes equations. These numerical methods will be applied in the numerical schemes of the multi-scaling models.

2.1   Kinetic Models

To deal with the gas dynamics, the kinetic models recognize the particulate structure of the gas as a a myriad of discrete molecules and ideally provide information on the position, velocity, and state of every molecule at all times. For the rarefied gas, the kinetic models describe the evolution of the distribution function f with time, where $f(t, \mathbf{x}, \boldsymbol{\xi})$ denotes number density of the molecules, which appear at the position $\mathbf{x}$ at time t with the velocity $\boldsymbol{\xi}$.

The most famous example of the kinetic models is the Boltzmann equation. The Boltzmann equation for the hard-sphere molecule is reviewed, whose derivation from the Boltzmann-Grad limit is given in appendix A. Then the collision invariants and equilibrium are defined for the Boltzmann equation and followed by the Boltzmann's H-theorem. Some other kinetic model such as discrete velocity model, BGK model are reviewed in the end of section. These simplified models have been used for years to provide useful insight into non-equilibrium problems. In the numerical

experiments, we will mainly concentrate on the BGK model as the kinetic model.

2.1.1   Boltzmann Equation for Hard-Sphere Molecules

Let $f(t, \mathbf{x}, \boldsymbol{\xi})$ be the expected number density distribution of the particles at time t at the point $(\mathbf{x}, \boldsymbol{\xi})$ in the phase space. Then the evolution of f for the hard-sphere monatomic particles is governed by the Boltzmann equation:

$$\frac{\partial f}{\partial t} + \boldsymbol{\xi} \cdot \nabla_{\mathbf{x}} f = Q(f, f), \tag{2.1}$$

The quadratic integral collision operator $Q(f, f)$ is

$$Q(f, f) = \int_{R^3} \int_{B^-} (f' f_1' - f f_1) \mathrm{d}^2 V \cos \theta d\Omega d\boldsymbol{\xi}_1, \tag{2.2}$$

Here $f = f(t, \mathbf{x}, \boldsymbol{\xi})$, $f_1 = f(t, \mathbf{x}, \boldsymbol{\xi}_1)$, $f' = f(t, \mathbf{x}, \boldsymbol{\xi}')$, $f_1' = (t, \mathbf{x}, \boldsymbol{\xi}_1')$. d is the diameter of the particle, $\pi - 2\theta$ is the deflection angle and $V = |\boldsymbol{\xi} - \boldsymbol{\xi}'|$ is the relative speed. Ω is the unit solid angle. The post-collision velocities $(\boldsymbol{\xi}', \boldsymbol{\xi}_1')$ are related to the pre-collision velocities $(\boldsymbol{\xi}, \boldsymbol{\xi}_1)$ by

$$\boldsymbol{\xi}' = \boldsymbol{\xi} - \mathbf{n}[\mathbf{n} \cdot (\boldsymbol{\xi} - \boldsymbol{\xi}_1)], \qquad \boldsymbol{\xi}_1' = \boldsymbol{\xi}_1 + \mathbf{n}[\mathbf{n} \cdot (\boldsymbol{\xi} - \boldsymbol{\xi}_1)], \tag{2.3}$$

where $\mathbf{n}$ is the unit vector along $\boldsymbol{\xi} - \boldsymbol{\xi}'$.

The Boltzmann equation is obtained from the binary collisions of molecules, while DSMC simulate the collision integral in a similar way. To help understand DSMC, the derivation of the Boltzmann equation for the hard-sphere molecules [11]

10

is shown in the appendix A. There are some other molecular models, [7]. These models are more physical models that can be handled by DSMC too. We put a list of these molecule models in appendix B and leave the multi-scaling modeling based on these molecular models for future study.

2.1.2 Collision Invariants, Equilibria and the H-Theorem

Let $(\boldsymbol{\xi}_1, \boldsymbol{\xi}_2)$ and $(\boldsymbol{\xi}'_1, \boldsymbol{\xi}'_2)$ be the velocities of two particles before and after collision. Let ϕ be a function of $\boldsymbol{\xi}$. If

$$\phi(\boldsymbol{\xi}_1) + \phi(\boldsymbol{\xi}_2) = \phi(\boldsymbol{\xi}'_1) + \phi(\boldsymbol{\xi}'_2), \tag{2.4}$$

we call ϕ a collision invariant. From the conservation of mass, moment and energy in the collisions, we can get the five elementary collision invariants: $1, \boldsymbol{\xi}, \frac{1}{2}|\boldsymbol{\xi}|^2$. Any linear combination of them is also a general collision invariant. It has been shown that any collision invariant can be written as the linear combination of the elementary collision invariants, [10].

From the symmetry of the collision process, for any function $\phi(\boldsymbol{\xi})$, we may derive

$$\int \phi Q(f,f) d\boldsymbol{\xi} = \frac{1}{2} \int_{R^3} \int_{R^3} \int_B f f_1 (\phi' + \phi'_1 - \phi - \phi_1) V \sigma d\Omega d\boldsymbol{\xi}_1 d\boldsymbol{\xi}, \tag{2.5}$$

Therefore $\int \phi Q(f,f) d\boldsymbol{\xi} = 0$ for any f if ϕ is a collision invariant.

In particular the solution of $Q(f,f) = 0$ is called a local equilibrium of the

Boltzmann equation denoted by $\mathcal{M}$. In this case, it can be shown that $\log \mathcal{M}$ is a collision invariant, [11]. Then $\log \mathcal{M}$ must be a linear combination of the elementary collision invariants and can only take a form of the Maxwellian :

$$\mathcal{M}[n, \mathbf{u}, T] = \frac{n}{(2\pi RT)^{\frac{3}{2}}} \exp\left(-\frac{|\boldsymbol{\xi} - \mathbf{u}|^2}{2RT}\right), \tag{2.6}$$

where $n = \int \mathcal{M}d\boldsymbol{\xi}$, $\mathbf{u} = \frac{1}{n}\int \boldsymbol{\xi}\mathcal{M}d\boldsymbol{\xi}$ and $RT = \frac{1}{3n}\int |\boldsymbol{\xi}|^2 \mathcal{M}d\boldsymbol{\xi} - \frac{1}{3}|\mathbf{u}|^2$. Here R is the specific gas constant equal to the Boltzmann constant k_B divided by the molecular mass m. In the next section we will see $n, \mathbf{u}, T$ will be the macroscopic number density, velocity, and temperature.

Next if we define

$$\mathcal{H} = \int_{R^3} f \log f d\boldsymbol{\xi}, \quad \mathcal{S} = \int_{R^3} \log f \; Q(f, f)d\boldsymbol{\xi}, \tag{2.7}$$

From the symmetry of the collision, we obtain

$$\mathcal{S} = \int_{R^3} \log f \; Q(f, f)d\boldsymbol{\xi} = \frac{1}{4}\int_{R^3}\int_{R^3}\int_{B}(f'f_1' - ff_1)\log\left(\frac{ff_1}{f'f_1'}\right)V\sigma d\Omega d\boldsymbol{\xi}_1 d\boldsymbol{\xi}, \tag{2.8}$$

Because of the inequality $(x - y)\log(y/x) \leq 0$ for all $x > 0, y > 0$, we get $S \leq 0$. Here the equality holds if and only if f is a Maxwellian.

For the space-homogeneous case, multiply both sides of the Boltzmann equation by $\log f$ and integrate it over the velocity space, we get

$$\frac{\partial \mathcal{H}}{\partial t} = \mathcal{S} \leq 0 \tag{2.9}$$

This implies the famous Boltzmann's H-theorem (for the space-homogeneous case): **$\mathcal{H}$ is a decreasing quantity unless f is a Maxwellian.** In the non-homogeneous case, we introduce $H = \int_\Omega \mathcal{H} d\mathbf{x}$ and obtain

$$\frac{dH}{dt} \leq \int_{\partial\Omega} \left(\int_{R^3} \boldsymbol{\xi} f \log f d\boldsymbol{\xi} \right) \cdot dS, \tag{2.10}$$

where dS is the oriented surface element on $\partial\sigma$. In the case where the gas does not exchange mass and energy with a solid boundary, we also have $\frac{dH}{dt} \leq 0$.

The H-theorem shows that Boltzmann equation has a basic feature of irreversibility: The quantities $\mathcal{H}$ and H always decrease in time. This H has the properties of entropy (except for the sign). In the equilibrium state, we may have $H = -(1/R)\eta$ where η is the entropy of the gas (see p.65, [11]).

2.1.3   Other Kinetic Models

Because of the complicated nature of the collision integral, it is very difficult to deal with the Boltzmann equation. Therefore, some alternative simpler expressions have been proposed for the collision term. This simplification brings about various kinetic models.

1. **Discrete Velocity Models:** This kind of models uses the prearranged discrete set of velocities which changes the collision integral to be a finite summation. For example in one space dimension, the Broadwell model describes a

gas as composed of molecules of only three speeds $0, \pm 1$ with a binary collision law and spatial variation in one dimension.

2. **BGK Model:** A simple and most widely known collision model was brought by P.L.Bhatnagar, E.P.Gross, and M.Krook at 1954 in [5]. In this BGK model, the collision term $Q(f, f) = \frac{1}{\tau}(\mathcal{M} - f)$, where $\tau = Cn^{-1}T^{\omega-1}$ is the relaxation time which is inversely proportional to the density and may also depend on the temperature. $\mathcal{M}$ is the local Maxwellian.

There no precise relation between the Boltzmann equation and the BGK collision model. The BGK model does however have the most important feature of the Boltzmann equation, i.e.

1. Five collision invariants are $1, \boldsymbol{\xi}, \frac{1}{2}|\boldsymbol{\xi}|^2$,

2. Null space of Q consists of Maxwellians,

3. Tendency to a Maxwellian distribution (H-theorem), i.e. $\int_{R^3} \log f Q(f, f) d\boldsymbol{\xi} \leq 0$, and

$$\int_{R^3} \log f Q(f, f) d\boldsymbol{\xi} = 0 \Leftrightarrow f \text{ is a Maxwellian.}, \qquad (2.11)$$

The mathematical theory of the BGK model is slightly simpler than that of the Boltzmann equation. Numerical simulations are also easier, especially by deterministic methods. However the Prandtl number $Pr = \mu/c_p \kappa$ turns out to be

14

unity for the BGK model, where it is smaller than 1 in the case of Boltzmann equation. This model is generalized (Ellipsoidal Statistical model) by substituting a locally anisotropic 3D Gaussian in place of the local Maxwellian (which is an isotropic Gaussian), [27]. Andries and Perthame proved an entropy inequality for the ES model in 2001, [1].

2.2 Fluid Models

Considering the examples of classical fluid dynamics, we usually are only interested in the macroscopic properties of the fluid, for example, mass density(ρ), velocity field $(\mathbf{u}) = (u_1, u_2, u_3)^T \in R^3$, pressure$(p)$, temperature$(T)$ and so on, all of which are functions of $(t, \mathbf{x})$ only. In the following, we will only consider the compressible fluids, whose equations can be easier derived from the Boltzmann equation or kinetic models than the incompressible fluids. There are two well-known models for the fluid: Euler fluid (or perfect) and the Navier-Stokes (or viscous) fluid.

2.2.1 Euler Equations

From the laws of conservation of mass, momentum, and total energy for the compressible inviscid fluid, the Euler equations can be written in the following conser-

vative form:

$$\begin{cases} \partial_t \rho + \nabla_x \cdot (\rho \mathbf{u}) = 0, \\[2mm] \partial_t(\rho \mathbf{u}) + \nabla_x \cdot (\rho \mathbf{u} \otimes \mathbf{u} + pI) = 0, \\[2mm] \partial_t(\rho e) + \nabla_x \cdot ((\rho e + p)\mathbf{u}) = 0, \end{cases} \qquad (2.12)$$

where the specific total energy $e = \epsilon + \frac{1}{2}|\mathbf{u}|^2$ and ϵ is the specific internal energy

which is related to the temperature T. I is the identity tensor.

To close the above system, a pressure law for p from thermodynamics is needed.

For example, for a polytropic ideal gas, from the equations of the state, we have

$$p = R\rho T, \qquad p = (\gamma - 1)\rho \epsilon, \quad \gamma > 1, \qquad (2.13)$$

For example, for the monatomic gas $\gamma = \frac{5}{3}$, we have $\epsilon = \frac{3}{2}\theta = \frac{3}{2}RT$.

2.2.2 Navier-Stokes Equations

Another model of the compressible fluid flow is the Navier-Stokes equations, which

describes the motion of the viscous fluids. The system of equations reads as follows:

$$\begin{cases} \partial_t \rho + \nabla_x \cdot (\rho \mathbf{u}) = 0, \\[2mm] \partial_t(\rho \mathbf{u}) + \nabla_x \cdot (\rho \mathbf{u} \otimes \mathbf{u}) + \nabla_x p = \nabla_x \cdot \Sigma, \\[2mm] \partial_t(\rho e) + \nabla_x \cdot (\rho e + p)\mathbf{u})) = \nabla_x \cdot (\Sigma \cdot \mathbf{u} + \mathbf{q}) \end{cases} \qquad (2.14)$$

For Newtonian fluids, the constitutive relation for the viscous stress tensor Σ

16

is

$$\Sigma = \mu \left(\nabla_x \mathbf{u} + \nabla_x \mathbf{u}^T - \frac{2}{3} \nabla_x \cdot \mathbf{u} I \right), \tag{2.15}$$

if we neglect the bulk viscosity. Here μ is the dynamic viscosity coefficient.

Also we assume that heat diffusion is governed by Fourier's law, i.e. $\mathbf{q} = k \nabla_x T$ with k the thermal conductivity and T the temperature.

Given the viscosity μ and the thermal conductivity k, to complete the system of the Navier-Stokes equations we still need the equations of states to express the pressure p and the energy density e in terms of $\rho, \mathbf{u}$ and T. For example, we may use the equations of the state for a polytropic ideal gas again.

2.3   Boundary Conditions

Because both kinetic and fluid models contain space derivatives, they should be equipped with suitable boundary conditions to be well-posed problems. There are two types of boundary conditions: actual boundary conditions and artificial boundary conditions. The actual boundary conditions describe the interactions of gas molecules with the boundary interface in the bounded domain while the artificial boundary conditions are necessary if the spatial domain is unbounded. In this section, we will discuss the actual boundary conditions for the solid boundary. The artificial boundary conditions will be discussed in the specific numerical examples.

17

2.3.1   Boundary Conditions for Kinetic Models

As for kinetic models, we need to impose boundary conditions for the distribution function $f(t, \mathbf{x}, \boldsymbol{\xi})$. There are two simple models proposed by Maxwell in [35] for the interaction of a stationary equilibrium gas with a solid surface that maintains equilibrium: **specular reflection** and **diffusion reflection**.

Specular reflection is perfectly elastic with molecular velocity component normal to the surface being reversed, while those parallel to the surface remain unchanged, i.e.

$$Rf(t, \mathbf{x}, \boldsymbol{\xi}) = f(t, \mathbf{x}, \boldsymbol{\xi} - 2(\mathbf{c} \cdot \mathbf{n})\mathbf{n}), \tag{2.16}$$

in which $\mathbf{x} \in \partial\Omega$, $\mathbf{c} \cdot \mathbf{n} \geq 0$, where $\mathbf{n}$ is the unit normal vector of $\partial\Omega$ pointed outward and $\mathbf{c} = \boldsymbol{\xi} - \mathbf{u}_w$ is the relative velocity of the molecule to the wall. $\mathbf{u}_w(\mathbf{x})$ is the velocity of the surface.

In diffusion reflection, the velocity of each molecule after reflection is independent of its initial velocity. However, the velocities of the reflected molecules as a whole are distributed in accordance with the half-range equilibrium or Maxwellian distribution for the molecules that are directed away from the surface, i.e.

$$Mf(t, \mathbf{x}, \boldsymbol{\xi}) = \frac{\mu}{(2\pi RT_w)^{3/2}} \exp\left\{ -\frac{|\mathbf{c}|^2}{2RT_w} \right\}, \tag{2.17}$$

in which $\mathbf{x} \in \partial\Omega$, $\mathbf{c} \cdot \mathbf{n} \geq 0$, where $\mathbf{c} = \boldsymbol{\xi} - \mathbf{u}_w$ and T_w are respectively, the relative velocity of the molecule to the wall and the temperature of the wall, while μ is to

18

be determined to keep the conservation of mass at the surface of the wall, i.e.

$$\int_{\mathbf{c}\cdot\mathbf{n}\geq 0} Mf(t,\mathbf{x},\boldsymbol{\xi})|\mathbf{c}\cdot\mathbf{n}|d\boldsymbol{\xi} = \int_{\mathbf{c}\cdot\mathbf{n}<0} f(t,\mathbf{x},\boldsymbol{\xi})|\mathbf{c}\cdot\mathbf{n}|d\boldsymbol{\xi}, \tag{2.18}$$

Accordingly we get $\mu = \sqrt{\frac{2\pi}{RT_w}} \int_{\mathbf{c}\cdot\mathbf{n}<0} f(t,\mathbf{x},\boldsymbol{\xi})|\mathbf{c}\cdot\mathbf{n}|d\boldsymbol{\xi}$.

From a physical point of view, we assume that at the solid boundary condition a fraction α of the molecules is absorbed by the wall and then re-emitted with the velocities corresponding to those in a still gas at the temperature with the same velocity as the wall's, while the remaining portion $(1-\alpha)$ is perfectly reflected. This is equivalent to impose for the ingoing velocities:

$$f(t,\mathbf{x},\boldsymbol{\xi}) = (1-\alpha)Rf(t,\mathbf{x},\boldsymbol{\xi}) + \alpha Mf(t,\mathbf{x},\boldsymbol{\xi}), \tag{2.19}$$

in which $\mathbf{x} \in \partial\Omega, \quad (\boldsymbol{\xi}-\mathbf{u}_w)\cdot\mathbf{n} \geq 0$. Here α is called the accommodation coefficient.

2.3.2   Boundary Conditions for Fluid Models

The fluid models also need appropriate boundary conditions for $\rho, \mathbf{u}, T$ to be well-posed.

We know Euler equations describes the dynamics of compressible inviscid fluid. If the boundary is assumed to be an impermeable rigid wall, i.e. the fluid does not cross the boundary but may move tangentially, we may require:

$$\mathbf{u}\cdot\mathbf{n} = 0, \tag{2.20}$$

19

where **n** stands for the outer normal vector of the boundary.

Since Euler equations is a system of conservation laws, for artificial boundary we may also need to impose inflow and/or out-flow conditions by linearization (page 443, [24]).

Because Navier-Stokes system describes the dynamics of compressible viscous fluid, it is second order in space. Therefore we may apply the usual Dirichlet boundary conditions for the boundary like

$$\mathbf{u} = \mathbf{u}_w, \quad T = T_w, \tag{2.21}$$

where the subscript w means the corresponding values of the boundary. This boundary condition is inconsistent with the kinetic boundary condition at the first order in κ. The slip boundary conditions are often used in the numerical computation which allow jumps of the velocity and temperature in a mean free path (see p.428, [46]).

2.4 From the Kinetic Model to the Fluid Model: C-E Expansion

Now we have two different levels of models: kinetic models and fluid models. We use different variable functions to describe the dynamics of the gas. There are several questions we may ask:

1. Since we are familiar with the macroscopic quantities, for example the density,

the velocity or the temperature, etc. How do we obtain these information from the kinetic model or from the distribution function $f(t, \mathbf{x}, \boldsymbol{\xi})$?

2. The fluid models are simpler and efficient to compute and the kinetic models are more accurate. For a specific problem, how do we tell which model we should choose? How do these two levels of models relate to each other?

The answers to these questions are important for the multi-scale modeling and will be given in the following sections.

2.4.1 Three Moments of the Distribution Function f

Given the number density distribution function $f(t, \mathbf{x}, \boldsymbol{\xi})$, we may obtain the macroscopic quantities by taking different moments of f with respect to $\boldsymbol{\xi}$ as follows.

In the following we will use the notation $\langle h(\boldsymbol{\xi}) \rangle = \int_{R^3} h(\boldsymbol{\xi}) d\boldsymbol{\xi}$.

The number density and the velocity field in the physical space is:

$$n(\mathbf{x}, t) = \langle f \rangle, \qquad \mathbf{u}(\mathbf{x}, t) = \frac{\langle \boldsymbol{\xi} f \rangle}{\langle f \rangle} = \frac{1}{n} \langle \boldsymbol{\xi} f \rangle, \qquad (2.22)$$

Let m be the mass of the molecule. Then the density $\rho = m \cdot n$.

The total energy E is:

$$E = \rho e = \frac{1}{2} \langle |\boldsymbol{\xi}|^2 f \rangle = \rho \epsilon + \frac{1}{2} \rho |\mathbf{u}|^2, \qquad (2.23)$$

here e is the specific total energy and $\epsilon =$ is the specific internal energy, then $\rho \epsilon = \frac{1}{2} \langle |\mathbf{c}|^2 f \rangle$, where $\mathbf{c} = \boldsymbol{\xi} - \mathbf{u}$ is the thermal velocity.

21

The pressure tensor $\mathbf{P}$ is defined as

$$\mathbf{P} = \langle \mathbf{c} \otimes \mathbf{c} f \rangle, \tag{2.24}$$

The scalar pressure may be identified as the isotropic part of the pressure tensor (Pascal's principle) at least in the case of equilibrium or for non-equilibrium situations in the case of monatomic ideal gas, i.e.

$$p = \frac{1}{3} trace \mathbf{P} = \frac{1}{3} \langle |\mathbf{c}|^2 f \rangle, \tag{2.25}$$

Notice we have $2\rho\epsilon = 3p$. Therefore $p = \frac{3}{2}\rho\epsilon$. Combined with the Boyle's law for ideal gas $p = R\rho T$ we have $\epsilon = \frac{3}{2}RT$.

2.4.2 Scaling of Kinetic Equation

In order to get the scaling of the kinetic model, we need a dimensionless kinetic equation. Denote by T a typical time, by L a typical length, by w a typical molecular velocity, by n the number density, by σ_T the total collision cross-section, then the scalings of the quantities in the Boltzmann equation are as follows:

$$\partial_t f = O(T^{-1}f); \quad \boldsymbol{\xi} \cdot \nabla_{\mathbf{x}} f = O(wL^{-1}f); \quad Q(f,f) = O(nw\sigma_T f^2) \tag{2.26}$$

If we take the hard-sphere model as an example, then $\sigma_T = \pi \mathrm{d}^2$ where d is the molecular diameter. From an elementary argument, the mean free path l, i.e. the average length of the free flight of a molecule between two successive collisions

has $l \approx (n\mathrm{d}^2)^{-1}$. Accordingly the mean free time θ will be: $\theta = l/w$. The non-dimensional Knudsen number is defined as $\kappa = l/L$. Suppose the length and time scales can be taken to be comparable, and $l/L \approx \theta/T$ (it is called hydrodynamic scaling), then we get the dimensionless kinetic equation:

$$\partial_t f + \boldsymbol{\xi} \cdot \nabla_{\mathbf{x}} f = \frac{1}{\kappa} Q(f, f), \tag{2.27}$$

If $\kappa = O(1)$ or bigger, then the system is not at equilibrium state, we have to use the kinetic models to get the details, i.e. the distribution function $f(t, \mathbf{x}, \boldsymbol{\xi})$. When the Knudsen number is very small ($\kappa \ll 1$), we need $Q(f, f)$ to be close to zero. Therefore the system is very close to an equilibrium state. This means the dynamics of the system could be described using the macroscopic quantities, whose evolutions are governed by the fluid models. From the Chapman-Enskog expansion based on the Knudsen number, we will see these fluid models are exactly the Euler equations or the Navier-Stokes equations.

2.4.3 Chapman-Enskog Expansion

Since we only need the Chapman-Enskog (C-E) expansion for the BGK model in the multi-scale modeling, we will use the BGK model instead of the Boltzmann equation to get the fluid models by the C-E expansion. For the C-E expansion of the general Boltzmann equation, see chapter V in [11] or [31].

The dimensionless BGK model is

$$\partial_t f + \boldsymbol{\xi} \cdot \nabla_x f = \frac{1}{\kappa} \nu (\mathcal{M} - f), \qquad (2.28)$$

Here the collision frequency $\nu = \frac{1}{\tau}$ and $\mathcal{M}$ is the Maxwellian.

2.4.3.1 Zero-Order Expansion

The only $O(\kappa^{-1})$ term in the BGK model is the right-hand-side. The zero-order expansion means we set the right-hand-side to be zero and notice the only solution of $Q(f) = 0$ is the local Maxwellian. Plug

$$f(t, \mathbf{x}, \boldsymbol{\xi}) = \mathcal{M}[\rho, \mathbf{u}, T] = \frac{\rho}{(2\pi RT)^{\frac{3}{2}}} \exp\left(-\frac{|\boldsymbol{\xi} - \mathbf{u}|^2}{2RT}\right), \qquad (2.29)$$

into the expressions of the stress tensor and heat flux, we obtain

$$\Sigma = \rho \langle (\boldsymbol{\xi} - \mathbf{u}) \otimes (\boldsymbol{\xi} - \mathbf{u}) f \rangle = \rho RT I = p I, \mathbf{q} = 0, \qquad (2.30)$$

This is exactly the constitutive relation for the Euler equations. Therefore when the system's κ is very small (e.g. ≤ 0.002, [7]), we may treat the system as the compressible inviscid fluid and choose the Euler equations to model the system.

2.4.3.2 First-Order Expansion

Next we consider $O(1)$ terms in the BGK model, i.e. $f = \mathcal{M} + \kappa g_1$, where $g_1 = \partial_t \mathcal{M} + \boldsymbol{\xi} \cdot \nabla_x \mathcal{M}$. In the term $\partial_t \mathcal{M}$, we may eliminate the time derivatives of the

24

macroscopic variables by means of the Euler equation without changing the order of truncation error. Let $\mathbf{c} = \boldsymbol{\xi} - \mathbf{u}$ be the peculiar velocity of the molecules, after some formal manipulation, we get $f = f_1 + O(\kappa^2)$, where

$$f_1 = \left\{ 1 - \kappa \frac{1}{\nu} \left[\mathbf{c} \cdot \left(\left(\frac{m|\mathbf{c}|^2}{2\theta} - \frac{5}{2} \right) \nabla_x (\ln T) \right) + \frac{m}{\theta} (\mathbf{c} \otimes \mathbf{c} - |\mathbf{c}|^2 I) : \nabla_x \mathbf{u} \right] \right\} \mathcal{M},$$

$$(2.31)$$

where m is the molecule's mass. It can easily be checked the $O(\kappa)$ term in f has no contribution to the equilibrium of f.

Plug f_1 into the expressions of the stress tensor and heat flux again and ignore the $O(\kappa^2)$ terms, we get

$$\Sigma = \frac{\rho RT}{\nu} \left[\nabla \mathbf{u} + \nabla \mathbf{u}^T - \frac{2}{3} \nabla \cdot \mathbf{u} I \right],$$

$$\mathbf{q} = -\frac{5}{2} R \frac{\rho RT}{\nu} \nabla T,$$

Compared with the Navier-Stokes equation, the coefficient of viscosity μ and the thermal conductivity k are

$$\mu = \frac{\rho RT}{\nu}, \quad k = \frac{5}{2} R \frac{\rho RT}{\nu}, \tag{2.32}$$

In this way we get the Navier-Stokes equation for the compressible fluid. When the system's $\kappa \leq 0.1$, we may neglect the $O(\kappa^2)$ term in f and use the Navier-Stokes equations to model it, [7]. The system is treated as the compressible viscous fluid.

The specific heat at constant pressure is $c_p = \frac{5}{2} R$ for the monatomic gas. Therefore the Prandtl number $Pr = \frac{5}{2} c_p \mu / k = 1$ which is different from the observed

quantity which is close to $\frac{2}{3}$. A correction to the BGK model (Ellipsoidal Statistical model, [27]) is obtained by substituting a locally anisotropic 3D Gaussian in place of the local Maxwellian which gives the same Navier-Stokes equations as the full Boltzmann equation. An H-theorem of this model is proved in [1].

2.5   Numerical Methods to the Kinetic Models

Numerical solutions of the Boltzmann equation based on finite different methods meet with severe computational requirement due to the large number of independent variables $(t, \mathbf{x}, \boldsymbol{\xi})$ and the very large number of operations required to evaluate the collision term. This paved the way to the development of simulation schemes, such as Direct Simulation of Monte Carlo (DSMC) method [7] which have become a powerful tool for practical calculations. DSMC has been rigorously proven to yield approximations to solutions of the Boltzmann equation, provided the number of test molecules is sufficiently large, [47].

For other kinetic models, such as BGK model or discrete velocity model, owing to the simplified collision term, it is possible to apply the conventional methods of hyperbolic equations for some simple flow geometries.

2.5.1 Direct Simulation of Monte Carlo for Boltzmann Equation

In Direct Simulation of Monte Carlo (DSMC), the state of the system is given by the positions and velocities of simulated particles. It models a gas flow as 10^{3-8} of simulated "molecules", with each of them representing a large number of real gas molecules (10^{12-17}). As the simulated molecules move through the computational domain, they may collide with one another as well as with physical boundaries. The position coordinates $\mathbf{x}$ and velocity components $\boldsymbol{\xi}$ of the simulated molecule are modified with time. The molecular properties are then sampled to determine the macroscopic flow quantities.

Consider the Boltzmann equation for the monatomic rarefied gas

$$\partial_t f + \boldsymbol{\xi} \cdot \nabla_{\mathbf{x}} f = Q(f, f) \tag{2.33}$$

where the collision kernel is

$$Q(f, f) = \int_{R^3} \int_0^{2\pi} \int_0^{\frac{\pi}{2}} (f'f_1' - f f_1) V \sigma d\boldsymbol{\xi}_1 d\epsilon d\theta, \tag{2.34}$$

here V is the relative speed and σ is the differential collision cross-section.

The essential DSMC approximation of the Boltzmann equation is the uncoupling, over a small time step($\approx$ the mean free time), of the translational motion($\partial_t f + \boldsymbol{\xi} \cdot \nabla_{\mathbf{x}} f = 0$) and the binary collisions $\partial_t f = Q(f, f)$, which can be described as follows respectively.

27

1. Translation: The solution to $\partial_t f + \boldsymbol{\xi} \cdot \nabla_{\mathbf{x}} f = 0$ is

$$f(t, \mathbf{x}, \boldsymbol{\xi}) = f(0, \mathbf{x}, \boldsymbol{\xi}), \tag{2.35}$$

which corresponds to the translational motion of the gas particles. Therefore for the ith particle, we only need to set its new position to be

$$\mathbf{X}_i(t^{n+1}) = \mathbf{X}_i(t^n) + \Delta t \boldsymbol{\xi}(t^n), \tag{2.36}$$

Also we need to deal with the interaction of the gas with the solid surface in this step. We may have the specular reflection for the particle colliding with the wall:

$$\boldsymbol{\xi}^* = \boldsymbol{\xi}(t^n) - 2(\mathbf{c} \cdot \mathbf{n})\mathbf{n}, \tag{2.37}$$

here $\mathbf{n}$ is the unit normal vector of $\partial \Omega$ pointed outward and $\mathbf{c} = \boldsymbol{\xi} - \mathbf{u}_w$ is the relative velocity of the molecule to the wall.

We may also apply the diffusion boundary condition. In this case, the particle colliding with the wall is absorbed and a new particle is emitted from the wall with the velocity $\boldsymbol{\xi}^*$ randomly generated from the biased Maxwellian distribution

$$P(t, \mathbf{x}, \boldsymbol{\xi}) = C|\mathbf{c} \cdot \mathbf{n}| \exp\left\{-\frac{|\mathbf{c}|^2}{2RT_w}\right\}, \tag{2.38}$$

here C is determined by $\int_{\mathbf{c} \cdot \mathbf{n} < 0} P d\boldsymbol{\xi} = 1$. The velocities of the molecules away from the boundary will not change in the translation step.

2. Collision:

28

In this step we solve $\partial_t f = Q(f, f)$. This corresponds to the binary collisions between the molecules. The whole computation domain is divided into small cells whose magnitude is around a fraction of mean free path. For any two molecules in the same cell, we consider there are some possibility that they will collide and the binary collisions will be done cell by cell. In order to do the binary collision, first we need to determine the number of collisions in each cell and the probability of the chosen pair to collide. Secondly we need to compute the post-collision of the particles.

Suppose each simulated molecule represents N_p physical molecules. The average number of simulated molecules in the fixed cell is N_c and the volume of the cell is V_c. Let $V = |\boldsymbol{\xi}_2 - \boldsymbol{\xi}_1|$ be the relative speed between two simulated molecules. Then the probability of these two selected molecules in Δt time interval to collide is $\sigma_T V \Delta t / V_c$. Considering repetition because of the large number of N_p physical molecules that each simulated molecule represents, there are $N_c^2/2$ pairs in the cell. Since the number of molecules in each cell varies in time according to Poisson statistics, $N_c(N_c - 1)$ has an average equal to $\overline{N_c}^2$ [12]. Hence the total number of the selected pairs of the simulated molecules in Δt will be $N_p \frac{N_c(N_c-1)}{2}$ and the probability of the collision between the selected pair is $\frac{\sigma_T V \Delta t}{V_c}$. Therefore the average number of collisions will be $N_p \frac{N_c(N_c-1)}{2} \cdot \frac{\overline{\sigma_T V} \Delta t}{V_c}$ where $\overline{\sigma_T V}$ is the mean value of $\sigma_T V$ for all pairs of molecules, since generally σ_T is a function of relative speed V.

Because $N_p N_c(N_c - 1)/2$ is very big and the collision probability $\frac{\overline{\sigma_T V} \Delta t}{V_c}$ is very small, the above method is inefficient. We may apply Bird's No Time Counter method (NTC) to maximize the efficiency in the following way:

Let the number of trials be $N_t = N_p \frac{N_c(N_c-1)}{2} \cdot \frac{(\sigma_T V)_{max} \Delta t}{V_c}$, which can be determined before the collision. It can be set initially to a reasonably large value and will be automatically updated if a larger value is encountered during the sampling. Then the probability of collision for each pair of molecules is $P = \frac{\sigma_T V}{(\sigma_T V)_{max}}$ which can be obtained after the selection of the pair of molecules. Then the total expected number of collisions will be $N_t * P$, same as before.

Next we need to compute the post-collision velocity for the molecules. When the collision occurs between the molecules i and j, the relative speed $V = |\boldsymbol{\xi}_i - \boldsymbol{\xi}_j|$ is unchanged, which can be proved using the conservation laws for the binary collision. Therefore the relative velocity

$$\mathbf{V}^* = V[\cos\chi \mathbf{e_1} + \sin\chi \cos\epsilon \mathbf{e_2} + \sin\chi \sin\epsilon \mathbf{e_3}] \tag{2.39}$$

Here $\chi = \pi - 2\theta$ is the deflection angle and ϵ is the azimuthal angle. These two angles are derived in the following way:

Let b be the distance of closest approach of the undisturbed trajectories in the center of mass frame so we have $\cos(\frac{\chi}{2}) = \frac{b}{d}$ for HS model, where d is the radius of the molecule.

Since b is very small compared with the distance of the molecules and each sim-

ulated molecule represents lots of physical molecules, we may assume the incoming molecules are uniformly distributed in the collision cross-section disk whose radius is d, i.e. b^2/d^2 is a uniformly distributed random variables distributed in $[0, 1)$ and ϵ is uniformly distributed in $[0, 2\pi)$, which will be denoted by R_1 and $2\pi R_2$. R_1 and R_2 are uniformly distributed random variables in $[0, 1)$. Therefore $\cos\chi = 2R_1^{1/\alpha} - 1$.

Once we have the reflection angle χ and the azimuthal angle ϵ, we may get the post-collision velocity from the above expression. The post-collision velocities of the two molecules are obtained in the following way:

$$\boldsymbol{\xi}_i^* = \frac{\boldsymbol{\xi}_i + \boldsymbol{\xi}_j}{2} + \frac{1}{2}\mathbf{V}^*, \qquad \boldsymbol{\xi}_j^* = \frac{\boldsymbol{\xi}_i + \boldsymbol{\xi}_j}{2} - \frac{1}{2}\mathbf{V}^*, \tag{2.40}$$

In this collision step, the positions of the molecules will not change. When all the collisions are done, we obtain the new velocities of each molecule.

When the simulation is done in each time step, we can obtain the macroscopic quantities by means of sampling. Let N_s be the total number of simulated molecules, then the molecule's number density distribution function in the phase space is

$$f(\mathbf{x}, \boldsymbol{\xi}, t^{n+1}) = \sum_{i=1}^{N_s} \delta(\mathbf{x} - \mathbf{X}_i(t^{n+1}))\delta(\boldsymbol{\xi} - \boldsymbol{\xi}_i(t^{n+1})), \tag{2.41}$$

Then the number of molecules N_j^{n+1} who lie in the cell $I_j = [x_j, x_j + \Delta x]$ at $t = t^{n+1}$ is

$$N_j^{n+1} = \int_{I_j} \langle f(\mathbf{x}, \boldsymbol{\xi}, t^{n+1}) \rangle dx = \sum_{i=1,\ X_i \in I_j}^{N_s} 1, \tag{2.42}$$

31

We may obtain the number density n_i^{n+1} at cell I_i at t^{n+1} as

$$n_j^{n+1} = N_j^{n+1}/V_c, \tag{2.43}$$

where V_c is the volume of the cell.

The macroscopic velocity $\mathbf{u}_j^{n+1}$ at cell I_j at t^{n+1} is obtained by

$$\mathbf{u}_j^{n+1} = \frac{\int_{I_j} \langle \boldsymbol{\xi} f(\mathbf{x}, \boldsymbol{\xi}, t^{n+1}) \rangle dx}{\int_{I_j} \langle f(\mathbf{x}, \boldsymbol{\xi}, t^{n+1}) \rangle dx} = \frac{1}{N_j^{n+1}} \left(\sum_{i=1,\ X_i \in I_j}^{N_s} \boldsymbol{\xi}_i \right), \tag{2.44}$$

We also get the macroscopic temperature T_j^{n+1} at cell I_j at t^{n+1} from the unbiased estimate

$$T_j^{n+1} = \frac{\int_{I_j} \langle |\boldsymbol{\xi} - \mathbf{u}|^2 f(\mathbf{x}, \boldsymbol{\xi}, t^{n+1}) \rangle dx}{3 \int_{I_j} \langle f(\mathbf{x}, \boldsymbol{\xi}, t^{n+1}) \rangle dx} = \frac{1}{3(N_i^{n+1} - 1)} \sum_{i=1,\ X_i \in I_j}^{N_s} |\boldsymbol{\xi}_i - \mathbf{u}_j^{n+1}|^2, \tag{2.45}$$

For steady state computation, the long time average will be used as the output result, i.e.

$$n_j = \frac{1}{N_t} \sum_{n=1}^{N_t} n_j^n, \quad u_j = \frac{1}{N_t} \sum_{n=1}^{N_t} u_j^n, \quad T_j = \frac{1}{N_t} \sum_{n=1}^{N_t} T_j^n, \tag{2.46}$$

where N_t is the number of iterations.

Here is a flow chart for the standard DSMC algorithm.

DIRECT SIMULATION MONTE CARLO (DSMC)
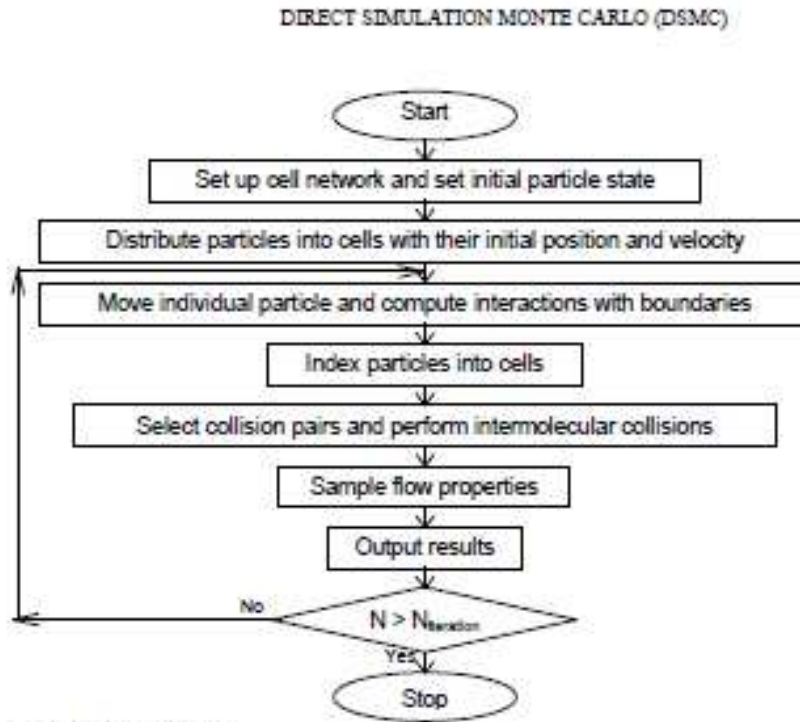
Fig. 1. DSMC flowchart.

Figure 2.1: Flow Chart for DSMC, pasted from [42]

2.5.2 Numerical Methods to Other Kinetic Models

Because of the simplified collision term of the BGK model or discrete velocity models, we may apply the direct numerical approach to solve these models. Here we take the finite difference method for the BGK model as an example. The distribution function $f(t, \mathbf{x}, \boldsymbol{\xi})$ will be represented by its numerical value over a network of points in phase space.

For simplicity, we take $1D1D$ dimensional case as an example, i.e. 1D physical space and 1D velocity space. In the following, we will write ξ_1 as ξ in the 1D velocity case. The BGK model is written as

$$\partial_t f + \xi \partial_x f = \frac{1}{\tau}(\mathcal{M} - f), \tag{2.47}$$

where $\mathcal{M} = \frac{n}{\sqrt{2\pi RT}} \exp\{-\frac{(\xi-u)^2}{2RT}\}$ and $\tau = Cn^{-1}T^{\omega-1}$. Here C and ω are constants.

When solving BGK model, the main difficulty is the velocity discretization. It is difficult to preserve the important properties, such as the positiveness of f, the conservation laws of mass, momentum and energy, as well as the entropy inequality.

In order to get a conservative and entropy decreasing discrete scheme for BGK model, as stated in [37], we may apply a nontrivial discrete approximation of $\mathcal{M}$ defined by a minimum entropy principle.

We assume $-M \leq \xi \leq N$ where M, N are the given bounds for ξ. Let $\Pi = \{\xi_k | \xi_k = k\Delta\xi\}$ be the uniform discrete grid points set with size $\Delta\xi$ and $\mathcal{K}$ be the corresponding set for the index k. $f_k(t, x)$ is assumed to be an approximation of $f(t, x, \xi_k)$.

Then we obtain the macroscopic quantities by

$$\langle g \rangle_\mathcal{K} = \sum_{k \in \mathcal{K}} g_k \Delta\xi, \tag{2.48}$$

therefore the first three moments are $\boldsymbol{\rho} = \langle \boldsymbol{\phi} f \rangle_\mathcal{K}$ where $\boldsymbol{\phi} = (1, \xi, \frac{1}{2}\xi^2)$ are the collision invariants. In the following we will use $\boldsymbol{\phi}_k = (1, \xi_k, \frac{1}{2}\xi_k^2)$.

Also the discrete entropy is $H_\mathcal{K}[f] = \langle f \log f \rangle_\mathcal{K}$.

The discrete approximation to $\mathcal{M}$ is denoted by $\mathcal{E}$ which minimize the discrete entropy

$$H_\mathcal{K}[\mathcal{E}] = \min \left\{ H_\mathcal{K}[g], \ g \geq 0, \quad \text{s.t.} \langle \boldsymbol{\phi} g \rangle_\mathcal{K} = \boldsymbol{\rho} \right\}, \tag{2.49}$$

In the continuous case the minimizer will be the local Maxwellian. It is not the case here because of the numerical integration error. It is shown in [37] that $\mathcal{E}_k = \exp(\boldsymbol{\alpha} \cdot \boldsymbol{\phi}_k)$ where $\boldsymbol{\alpha}$ is determined by the other minimization problem

$$J(\boldsymbol{\alpha}) = \min\{\langle \exp(\boldsymbol{\beta} \cdot \boldsymbol{\phi}_k) \rangle_\mathcal{K} - \boldsymbol{\beta} \cdot \boldsymbol{\rho}; \quad \boldsymbol{\beta} \in R^3 \}, \tag{2.50}$$

For simplicity, we use Euler forward method to discretize the tempal derivative. Space discretization for $\xi \partial_x f$ is done by the upwind conservative scheme from the hyperbolic equation, i.e.

$$\xi \partial_x f \approx D^-(\xi^+ f) + D^+(\xi^- f), \tag{2.51}$$

where $\xi^+ = \max\{\xi, 0\}$, $\xi^- = \min\{\xi, 0\}$ and $D^+(D^-)$ is the forward(backward) difference operator defined as

$$D^+ f = \frac{1}{\Delta x}(f_{i+1} - f_i), \quad D^- f = \frac{1}{\Delta x}(f_i - f_{i-1}), \tag{2.52}$$

The subscript i is the index along the x-direction.

Here is the first order numerical explicit scheme for the BGK model:

$$f_{i,k}^{n+1} = f_{i,k}^n - \Delta t (D^-(\xi_k^+ f_{i,k}^n) + D^+(\xi_k^- f_{i,k}^n)) + \frac{\Delta t}{\tau_i^n}(\mathcal{E}_{i,k}^n - f_{i,k}^n), \tag{2.53}$$

35

here $\mathcal{E}_{i,k}^n = \exp(\boldsymbol{\alpha}_i^n \cdot \boldsymbol{\phi}_k)$ where $\boldsymbol{\alpha}_i^n$ is the solution of

$$J(\boldsymbol{\alpha}_i^n) = \min\{\langle \exp(\boldsymbol{\beta} \cdot \boldsymbol{\phi}_k)\rangle_{\mathcal{K}} - \boldsymbol{\beta} \cdot \boldsymbol{\rho}_i^n; \quad \boldsymbol{\beta} \in R^3\}, \tag{2.54}$$

It is shown in [37] that if the initial value $f_{i,k}^0 > 0$ and the time step satisfies

$$\Delta t \left(\max_i(\frac{1}{\tau_i^n}) + \max_{k \in \mathcal{K}} \frac{|\xi_k|}{\Delta x} \right) < 1, \tag{2.55}$$

then $\{f^n\}_{n \geq 0}$ satisfies $f_{i,k}^n > 0$ and preserve the conservation laws and the entropy

inequality.

The above CFL condition on the time step requires very small Δt if τ is small.

This constraint can be removed if we consider the following implicit-explicit scheme:

$$\boldsymbol{\rho}_i^{n+1} = \boldsymbol{\rho}_i^n - \Delta t \left(D^- \langle \boldsymbol{\phi} \xi^+ f_i^n \rangle_{\mathcal{K}} + D^+ \langle \boldsymbol{\phi} \xi^- f_i^n \rangle_{\mathcal{K}} \right), \tag{2.56}$$

$$(1 + \frac{\Delta t}{\tau_i^{n+1}}) f_{i,k}^{n+1} = f_{i,k}^n - \Delta t (D^-(\xi_k^+ f_{i,k}^n) + D^+(\xi_k^- f_{i,k}^n)) + \frac{\Delta t}{\tau_i^{n+1}} \mathcal{E}_{i,k}^{n+1}, \tag{2.57}$$

here $\mathcal{E}_{i,k}^{n+1} = \exp(\boldsymbol{\alpha}_i^{n+1} \cdot \boldsymbol{\phi}_k)$ where $\boldsymbol{\alpha}_i^{n+1}$ is the solution of

$$J(\boldsymbol{\alpha}_i^{n+1}) = \min\{\langle \exp(\boldsymbol{\beta} \cdot \boldsymbol{\phi}_k)\rangle_{\mathcal{K}} - \boldsymbol{\beta} \cdot \boldsymbol{\rho}_i^{n+1}; \quad \boldsymbol{\beta} \in R^3\}, \tag{2.58}$$

Remark. The moment equations can be obtained by taking the moments of the

kinetic equation due to $\langle \boldsymbol{\phi} \mathcal{E}_{i,k}^{n+1} \rangle_{\mathcal{K}} = \boldsymbol{\rho}_i^{n+1}$.

Proposition. *If the initial value $f_{i,k}^0 > 0$ and the time step satisfies*

$$\Delta t \max_{k \in \mathcal{K}} \frac{|\xi_k|}{\Delta x} < 1, \tag{2.59}$$

36

then $\{f^n\}_{n \geq 0}$ *from the above implicit-explicit scheme satisfies* $f_{i,k}^n > 0$ *and preserve the conservation laws and the entropy inequality.*

Proof. The above scheme reads

$$\left(1 + \frac{\Delta t}{\tau_i^{n+1}}\right) f_{i,k}^{n+1} = \left(1 - \frac{\Delta t}{\Delta x}|\xi|\right) f_{i,k}^n - \frac{\Delta t}{\Delta x}\xi^- f_{i+1,k}^n + \frac{\Delta t}{\Delta x}\xi^+ f_{i-1,k}^n + \frac{\Delta t}{\tau_i^{n+1}}\mathcal{E}_{i,k}^{n+1}$$

(2.60)

Therefore

$$f_{i,k}^{n+1} = \frac{1 - \frac{\Delta t}{\Delta x}|\xi|}{1 + \frac{\Delta t}{\tau_i^{n+1}}} f_{i,k}^n - \frac{\frac{\Delta t}{\Delta x}\xi^-}{1 + \frac{\Delta t}{\tau_i^{n+1}}} f_{i+1,k}^n + \frac{\frac{\Delta t}{\Delta x}\xi^+}{1 + \frac{\Delta t}{\tau_i^{n+1}}} f_{i-1,k}^n + \frac{\frac{\Delta t}{\tau_i^{n+1}}}{1 + \frac{\Delta t}{\tau_i^{n+1}}}\mathcal{E}_{i,k}^{n+1}$$

(2.61)

If $\frac{\Delta t}{\Delta x}|\xi| < 1$, then this expression is a convex combination of $f_{i,k}^n, f_{i-1,k}^n, f_{i+1,k}^n$ and $\mathcal{E}_{i,k}^{n+1}$. Since $\mathcal{E}_{i,k}^{n+1} > 0$ we get

$$f_{i,k}^{n+1} > 0 \quad \text{when} \quad f_{i,k}^n > 0 \quad \forall i, k$$

(2.62)

The conservation laws can be easily obtained from the moment equations.

Since the function $t \log t$ is also convex, we have

$$f_{i,k}^{n+1} \log f_{i,k}^{n+1} \leq \frac{1 - \frac{\Delta t}{\Delta x}|\xi|}{1 + \frac{\Delta t}{\tau_i^{n+1}}} f_{i,k}^n \log f_{i,k}^n - \frac{\frac{\Delta t}{\Delta x}\xi^-}{1 + \frac{\Delta t}{\tau_i^{n+1}}} f_{i+1,k}^n \log f_{i+1,k}^n$$

$$+ \frac{\frac{\Delta t}{\Delta x}\xi^+}{1 + \frac{\Delta t}{\tau_i^{n+1}}} f_{i-1,k}^n \log f_{i-1,k}^n + \frac{\frac{\Delta t}{\tau_i^{n+1}}}{1 + \frac{\Delta t}{\tau_i^{n+1}}}\mathcal{E}_{i,k}^{n+1} \log \mathcal{E}_{i,k}^{n+1}$$

(2.63)

By summation over i, entropy numerical fluxes vanish, and summing over k yields

$$\sum_{i,k} f_{i,k}^{n+1} \log f_{i,k}^{n+1} \leq \sum_{i,k} \frac{1}{1 + \frac{\Delta t}{\tau_i^{n+1}}} f_{i,k}^n \log f_{i,k}^n + \sum_{i,k} \frac{\frac{\Delta t}{\tau_i^{n+1}}}{1 + \frac{\Delta t}{\tau_i^{n+1}}}\mathcal{E}_{i,k}^{n+1} \log \mathcal{E}_{i,k}^{n+1}$$

(2.64)

Since the discrete equilibrium minimizes entropy, i.e. $\sum_k \mathcal{E}_{i,k}^{n+1} \log \mathcal{E}_{i,k}^{n+1} \leq \sum_{i,k} f_{i,k}^{n+1} \log f_{i,k}^{n+1}$, then we get

$$\sum_{i,k} f_{i,k}^{n+1} \log f_{i,k}^{n+1} \leq \sum_{i,k} f_{i,k}^n \log f_{i,k}^n \tag{2.65}$$

$\square$

Remark. In the numerical computation, we may solve the minimization problem by the Newton algorithm where the initial value $\boldsymbol{\alpha}^0 = \alpha_i^{n-1}$. If we have many grid points on the velocity direction, we may take $\boldsymbol{\alpha}^0$ to be the continuous equilibrium, i.e. $\boldsymbol{\alpha} = \left(\log\left(\frac{n}{\sqrt{2\pi RT}} \right) - \frac{u^2}{2RT}, \frac{u}{2RT}, -\frac{1}{RT} \right)$.

Remark. We may use Min-Mod limiter or WENO to reconstruct the flux term $\xi_1 f$ in the above schemes to achieve the high order accuracy.

2.6   Numerical Methods to the Fluid Models

Here we will concentrate on the upwind finite difference methods to the Euler equations or Navier-Stokes equations.

Euler equations is a system of conservation laws $\partial_t \boldsymbol{\rho} + \partial_x F(\boldsymbol{\rho}) = 0$. Therefore we need to do the characteristic decomposition for the fluxes $F = F^+ + F^-$ such that the eigenvalues $\lambda^+(\lambda^-)$ of the Jacobian of $F^+(F^-)$ should be positive (negative). Then the first order finite difference scheme for the Euler equations is

$$\boldsymbol{\rho}_i^{n+1} = \boldsymbol{\rho}_i^n - \Delta t (D^+ F^- + D^- F^+), \tag{2.66}$$

2.6.1 Flux Splittings Methods to the Euler Equations

Euler equations is a system of conservation laws. In order to discretize the nonlinear convection terms by the upwind schemes, we need to split the flux into positive flux and negative flux and apply the forward or backward difference scheme respectively.

There are many different flux splittings methods. For example, the Steger-Warming splitting (SWS) in [43] is obtained by means of the property that the flux vector $F(\boldsymbol{\rho})$ is a homogeneous function of degree one. In terms of the local Mach number $M = u/c$ where $c = \sqrt{\gamma RT}$ is the sound speed, VanLeer developed a splitting [45] which is differentiable even at sonic points. The kinetic flux vector splitting (KVFS) is derived from the moment closure of a collisionless Boltzmann equation for the equilibrium gas. More kinds of flux splittings are given in [16]. Here we will mainly discuss the SWS and KVFS.

1. **Steger-Warming Splitting(SWS)**

   In the 1D case, the SWS can be explicitly expressed in terms of eigenvalues of the Jacobian of $F(\boldsymbol{\rho})$, $\lambda_1 = u, \lambda_2 = u + c$ and $\lambda_3 = u - c$ as the following

   $$F^{\pm} = \frac{\rho}{2\gamma} \begin{pmatrix} 2(\gamma - 1)\lambda_1^{\pm} + \lambda_2^{\pm} + \lambda_3^{\pm} \\ 2(\gamma - 1)\lambda_1^{\pm}u + \lambda_2^{\pm}(u + c) + \lambda_3^{\pm}(u - c) \\ (\gamma - 1)\lambda_1^{\pm}u^2 + \frac{1}{2}\lambda_2^{\pm}(u + c)^2 + \frac{1}{2}\lambda_3^{\pm}(u - c)^2 + W \end{pmatrix}, \quad (2.67)$$

   where $\lambda_i^{\pm} = \frac{1}{2}(\lambda_i \pm |\lambda_i|)$ are the eigenvalues of $(F^{\pm})'$ correspondingly and $W = \frac{(3-\gamma)(\lambda_2 + \lambda_3)c^2}{2(\gamma - 1)}$. The artificial viscosity can be introduced by simply adding

a small positive(negative) number to $\lambda_i^\pm$, i.e.

$$\tilde{\lambda}_i^\pm = \frac{\lambda_i \pm (\lambda_i^2 + \varepsilon^2)^{1/2}}{2}, \tag{2.68}$$

2. **Kinetic Flux Vector Splitting**

In [36], Deshpande and Mandel have formulated the KVFS based on the moment forms of the collisionless Boltzmann equation over the positive and negative speed of the molecules,

$$\langle \phi, \partial_t f + \xi_1 \partial_x f \rangle = 0, \tag{2.69}$$

where $f(t, x, \xi_1)$ is taken to be the local Maxwellian $\mathcal{M}$. ϕ is the collision invariants $\phi = (1, \xi_1, \xi_1^2/2)$. In the 1D physical space and 3D velocity space case, we have the splitting

$$F^\pm = \langle \xi_1^\pm \phi \mathcal{M}[\boldsymbol{\rho}] \rangle, \tag{2.70}$$

Denote the complementary error function $erfc(x) = \frac{2}{\sqrt{\pi}} \int_x^\infty e^{-t^2} dt$ and the Gaussian distribution function $G_{u,\theta} = \frac{1}{\sqrt{2\pi\theta}} \exp\left(-\frac{u^2}{2\theta}\right)$. Then we may express the kinetic flux vector splitting of Euler equation in the following:

$$F_1^\pm = \langle \xi^\pm \mathcal{M} \rangle = \pm\rho\theta G_{u,\theta} + \frac{1}{2}\rho u \ erfc\left(\mp\frac{u}{\sqrt{2\theta}}\right),$$

$$F_2^\pm = \langle \xi^\pm \xi \mathcal{M} \rangle = \pm\rho u\theta G_{u,\theta} + \frac{\rho(u^2 + \theta)}{2} \ erfc(\mp\frac{u}{\sqrt{2\theta}}),$$

$$F_3^\pm = \langle \xi^\pm \xi^2 \mathcal{M} \rangle = \pm\rho\theta\left(u^2 + \frac{\gamma+1}{\gamma-1}\theta\right) G_{u,\theta} + \rho u\left(u^2 + \frac{2\gamma}{\gamma-1}\theta\right) \ erfc\left(\mp\frac{u}{\sqrt{2\theta}}\right),$$

$$\tag{2.71}$$

2.6.2   Numerical Methods to the Navier-Stokes Equations

Compared with the Euler equations, the Navier-Stokes equations has the second order viscous terms in addition to the convection terms. In [17], Baganoff and Chou show the kinetic flux vector splitting for the Navier-Stokes equations using the collisionless Boltzmann equation again by means of the first order approximation of the C-E expansion.

For example, for the BGK model in the 1D physical space and 3D velocity space case, from expression of f_1 as (2.31) in the first order C-E expansion, we may get the splitted fluxes as

$$F^{\pm} = \langle \xi_1^{\pm} \phi f_1 \rangle, \tag{2.72}$$

The derivatives in f_1 will be discretized by center-difference scheme to get the high accuracy. If the collision frequency $\nu = \infty$, i.e. the viscosity $\mu = 0$ and the thermal conductivity $K = 0$ we will recover the KVFS for the Euler equations.

Remark. Since this flux splitting is derived from the collisionless Boltzmann equation, it is not stable when the mean free path is big, or the fluid is far from the equilibrium. It is clearly shown in the numerical tests. We know the viscous terms are dissipative and the center difference discretization are stable. Therefore the other way to solve the Navier-Stokes equations numerically is to apply the above flux splitting on the convection terms and the center-difference scheme for the dissipative viscous terms in the equations. For example, $\partial_x(\mu \partial_x v)$ can be discretized

41

in a more stable way as

$$\partial_x(\mu\partial_x v) \approx \frac{1}{\Delta x}(\mu_{j+1/2}D^+ v_j - \mu_{j-1/2}D^- v_j), \quad \text{where} \quad \mu_{j+1/2} = \frac{1}{2}(\mu_j + \mu_{j+1}), \quad (2.73)$$

Chapter 3

Multi-scale Problems and Models

In this chapter, we will propose two new multi-scale models (NSLU, ELU2) from the up-scaling strategy based on C-E expansion.

First we state what are spacial multi-scale problems based on the introduction of the local Knudsen number and why the multi-scale modeling is needed. Then it is followed by some existing multi-scale models such as domain-decomposition (DD) model, heterogeneous multi-scale (HM) model, and the first local up-scaling (ELU1) model. DD model can deal with the Euler equations or Navier-Stokes equations, but HM model and ELU1 model can only couple the Euler equations with the kinetic models. The ELU1 model is extended by the new NSLU model to couple the Navier-

Stokes equations with the kinetic models. An alternate ELU2 model is proposed to deal with the coupling of DSMC with the Euler equations where ELU1 model can not apply.

There are three general properties a good multi-scale model should hold. We give some formal discussion of these properties for each model mentioned above. In the last section we discuss the numerical schemes for these multi-scale models.

3.1 Introduction to Multi-scale Problems

From the asymptotic analysis in the previous chapter, we see that an indicator of the fluid models' validity is the Knudsen number $\kappa = \lambda/L$. This can be misleading if L is chosen to be some overall dimension of the flow. In fact, it can be specified more precisely if we define L as the scale over which the averaged quantities such as density, momentum and energy change, i.e. $L = \frac{\partial U}{\partial_x U}$, where U is the macroscopic quantities such as $\rho, \mathbf{u}$ or T. In this way we obtain the so-called local κ. When $\kappa \ll 1$, we see the collision kernel will be ≈ 0. This means the system is close to an equilibrium state and may be modeled by the macroscopic approximation, i.e. Euler equations or Navier-Stokes equations. In fact, the continuum model must be replaced by the molecular model when the local $\kappa > 0.2$, as Bird noted in his book [7]. These Knudsen number limits on the conventional mathematical formulations are shown schematically in the following table, [7]:
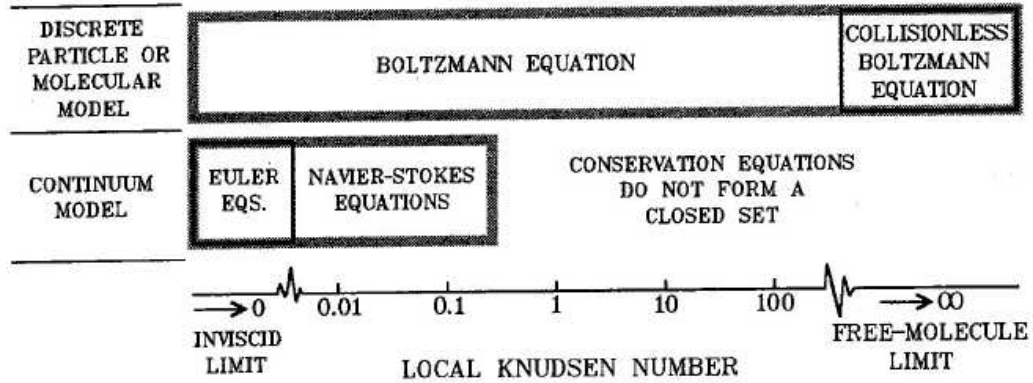
FIG. 1.1 The Knudsen number limits on the mathematical models.

Then a typical spacial multi-scale problem is that the local Knudsen number varies greatly in the whole region. Usually in most part of region κ is very small so the fluid models may be applied. For the regions where $\kappa = O(1)$, the kinetic models should be used.

In these cases, switching completely to kinetic models is not an optimal strategy not only because the kinetic models are often too complex to be dealt with, but also because they contain too much information of little interest. By means of multi-scale modeling, we want to take advantage of both the simplicity and efficiency of the fluid models as well as the accuracy of the kinetic models.

Remark. A small local Knudsen number is only a necessary condition for the validity

44

of the macroscopic models. In appendix C a velocity profile of stationary high mach number shock wave is given to show that the big difference exists between the BGK model and fluid models in the upstream region where κ is very small.

3.2 Various Multi-Scale Models

The way to couple the different levels of models brings about a variety of multi-scale models, like domain decomposition (DD) model, the heterogeneous multi-scale (HM) model, the local up-scaling models (ELU1, NSLU, ELU2), etc, and the respective numerical methods will be discussed in the following sections.

In order to be a good multi-scale model, there are three important properties it should hold:

1. Preservation of uniform flows. Because the global constant equilibrium is a true solution of both kinetic and fluid models. If the initial condition is a constant equilibrium, then it should be a solution of a good multi-scale model.

2. Asymptotic preserving. If the whole regions are fluid regions, we should recover global fluid models from the multi-scale model.

3. Conservation laws. We shall keep the basic conservation laws of the macroscopic variables on the whole region.

In the following, we take 1D1D BGK model as an example. The models can

be generalized in a straightforward way to higher dimension or other models. The demarcation of the region is as follows:

Fluid Region (ρ, u, T)   Kinetic Region f(t,x,ξ)

x=0
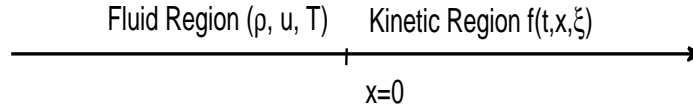
We denote the collision invariants $\phi_0 = 1, \phi_1 = \xi, \phi_2 = \frac{1}{2}\xi^2$). The conservative variable functions $\boldsymbol{\rho} = \{\rho_i\}_{i=0}^2 = \rho, \rho u, \rho(u^2 + \theta)$. $F_0(\boldsymbol{\rho}), F_1(\boldsymbol{\rho})$ and $F_2(\boldsymbol{\rho})$ are the fluxes in the Euler equations. $T_0(\boldsymbol{\rho}), T_1(\boldsymbol{\rho})$ and $T_2(\boldsymbol{\rho})$ are the viscous terms plus the heat flux in the Navier-Stokes equations. In fact for 1D1D case, $T_0 = T_1 = 0$ and T_2 is the heat flux.

3.2.1 Domain Decomposition (DD) Model

One classical model is domain decomposition model, which has been widely used in molecular dynamics problem. Recently it is applied to couple the kinetic model with the fluid model [8, 44]. The computational region is decomposed into kinetic and fluid subregions on which the kinetic models and the fluid models are used respectively.

The kinetic model is 1D1D BGK models which reads:

$$\partial_t f + \xi \partial_x f = \frac{1}{\tau}(\mathcal{M} - f), \quad \text{when } x > 0, \tag{3.1}$$

if the fluid model is Euler equations

$$\partial_t \rho_i + \partial_x F_i(\boldsymbol{\rho}) = 0, \quad \text{when } x < 0, \quad i = 0, 1, 2, \tag{3.2}$$

We need to give appropriate interface coupling condition to preserve the uniform flow, be asymptotic preserving and have the conservation laws. We may set the following interface fluxes coupling (Marshak condition):

1. the Euler equation will be solved when $x \leq 0$ whose fluxes F_i is obtained in the following way:

$$F_i = F^+(\rho_i) + \int_{\xi < 0} \xi \phi_i f d\boldsymbol{\xi}, \quad \text{where } i = 0, 1, 2, \tag{3.3}$$

where $F^+(\rho)$ will be the positive half flux from the kinetic flux splitting of Euler equations and the 2nd part is the half flux obtained from the kinetic region.

2. the inflow condition for kinetic model will be chosen as a half Maxwellian which is determined by the macro quantities, i.e. $f(t, 0, \xi) = \mathcal{M}_{\rho, u, T}$ for $\xi > 0$.

If the initial value is a constant Maxwellian $\mathcal{M}_{\rho_0^i}$, then $\rho = \rho_0^i$ and $f = \mathcal{M}_{\rho_0^i}$ is a solution of the above coupled system. Therefore DD model preserves the uniform flow.

47

If $\kappa \to 0$ in the kinetic subregion, then $f_r \approx \mathcal{M}$. Notice $F_i^\pm = \int_{\xi^\pm} \phi_i \xi \mathcal{M} d\boldsymbol{\xi}$ then DD model is asymptotic preserving.

Let $\rho_i(t, x) = \rho_i$ when $x \le 0$ and $\rho_i(t, x) = \langle \phi_i \xi f \rangle$ when $x > 0$. Since we have the flux $F_i = \langle \phi_i \xi f \rangle$ at the interface $x = 0$ so the conservation laws for ρ_i are satisfied.

Three other prevalent methods include the extrapolation of flow properties, the extrapolation of net fluxes, or the use of the asymptotic values of the solution of the linear kinetic half space problem, [25].

3.2.2   Heterogeneous Multi-Scale (HM) Model

HM model is an attempt to construct a unified framework for designing efficient simulation methods that couple the macroscopic and microscopic models. It was proposed by E and Engquist in [20] in 2003. The basic principle of HM model is that one should start with a macroscopic solver, taking into account as much as possible what is known about the macro process, and use the microscopic model to provide the missing macroscopic data that are necessary for implementing the macroscopic solver. When measuring the macroscopic data, the microscopic model should be constrained by the (local) macroscopic state of the system.

If we apply the Euler equations as the macroscopic model, it is a system of conservation laws. By taking moments of the kinetic equations, we may also get the

similar conservation laws with the unknown fluxes. These equation can be written generally as

$$\partial_t \rho_i + \partial_x \tilde{F}_i(\boldsymbol{\rho}) = 0, \quad i = 0, 1, 2, \tag{3.4}$$

The fluxes $\tilde{F}_i = F_i$ in the fluid region, i.e. $\tilde{F}_i = \langle \phi_i \xi f \rangle$ obtained from the solution of the kinetic model. At the interface of the regions, it will be the mixed flux, same as the Marshak condition.

In HM model, we don't need the boundary conditions of macro variables at the interface because the conservation laws are solved in the whole region. The inflow boundary condition for the kinetic equation is the same as the DD model, i.e. the half Maxwellian.

It is easy to see that the HM model preserves the uniform flows, i.e. constant equilibrium is a solution of HM model. If both regions are fluid regions, HM model changes to be the Euler equation, i.e. it is asymptotic preserving. Since the interface coupling is similar to DD model, the conservation laws can be obtained for ρ_i.

3.2.3 Local Up-scaling Models

Following the principle of HM model, if we already know the macroscopic model is Euler equations which describe the motion of the fluid in equilibrium state, we may start with the Euler equations and use the the kinetic model to provide the correction (up-scaling) of the fluid model which is not accurate in the kinetic region.

This is the basic idea of the local up-scaling models. In the end, we will introduce another local up-scaling model based on the Navier-Stokes equation.

3.2.3.1   First Euler Local Up-scaling (ELU1) Model

The first Euler local up-scaling model (ELU1) was introduced by Degond, Liu, and Mieussens in [19] in 2005, which solves the multi-scale problem based on the micromacro decomposition [34]. The fluid model will be solved in the whole domain together with a localized kinetic up-scaling. The up-scaling equation is solved only in the kinetic region. In order to get this model, first we need to define the micromacro decomposition of the distribution function $f(t, x, \xi)$.

We denote the five collision invariants by $\phi_i, i = 0, 1, 2$. Denote the five moments $\langle \phi_i f \rangle$ by ρ_i and the Maxwellian by $\mathcal{M}$. The decomposition is based on the decomposition of the distribution function into the macroscopic, fluid part, the local Maxwellian $\mathcal{M}(t, x, \xi)$, and the microscopic, non-fluid part $g = g(t, x, \xi)$:

$$f = \mathcal{M} + g, \text{ where } \langle \phi_i g \rangle = 0, \tag{3.5}$$

Since $\mathcal{M}$ is the zero order the C-E expansion of f, we know $g = O(\kappa)$ and $\langle \phi_i g \rangle = 0$.

The conservation laws or the fluid equations are obtained, as usual, by integrating with respect to ξ of the Boltzmann equation times the collision invariants ϕ_i:

$$\partial_t \rho_i + \partial_x F_i(\boldsymbol{\rho}) + \partial_x \langle \phi_i \xi g \rangle = 0, \text{ where } i = 0, 1, 2, \tag{3.6}$$

here $\partial_x \langle \phi_i(\xi g) \rangle$ is the up-scaling term.

Also we have the up-scaling equation for non-fluid part g as

$$\partial_t g + \xi \partial_x g = -\frac{1}{\tau} g - (\partial_t \mathcal{M} + \xi \partial_x \mathcal{M}), \tag{3.7}$$

here the term $\partial_t \mathcal{M} + \xi \partial_x \mathcal{M}$ is the down-scaling term from the macroscopic quantities.

To localize the up-scaling term, the cut-off function $h(x)$ is needed. Here $h(x) = 1(x \geq 0)$, $h(x) = 0(x < 0)$ and has a smooth transition in the fluid region. We get $g \approx hg = g_K$ because the non-fluid part $g(t, x, \xi) \approx 0$ in the fluid region. In the following, for simplicity we still use g instead of g_K to denote the localized non-fluid part. Then we get the moment equation as

$$\partial_t \rho_i + \partial_x F_i + \partial_x \langle \phi_i(\xi g) \rangle = 0, \tag{3.8}$$

where $\partial_x \langle \phi_i \xi g \rangle$ is the up-scaling term.

We may multiply the up-scaling equation by the buffer-zone function h and get the following up-scaling equation for the localized non-fluid part g:

$$\partial_t g + h\xi \partial_x g = -\frac{1}{\tau} hg - h(\partial_t \mathcal{M} + \xi \partial_x \mathcal{M}), \tag{3.9}$$

Remark. Here we only solve the up-scaling equation in the region where $h \neq 0$. Therefore we need to put the transition zone of h in the fluid region so that the computation region of the kinetic equation is a little bigger than the real kinetic region. In this way, the localized up-scaling equation is only solved in the kinetic

region plus the buffer zone since $g = 0$ in the fluid region because $h = 0$. No boundary condition is needed for solving g.

This is the local up-scaling model used in [19]. If the initial condition is a constant equilibrium, it can be easily shown $\rho = \rho^0$ and $g = 0$ is the solution of ELU1 model. This removes the constraint of the homogeneity of the Maxwellian $\mathcal{M}$, which is required to preserve the uniform flows in the method [18].

Also when both regions are macro, i.e. $\kappa \to 0$, we get $g = O(\kappa) \to 0$ so the up-scaling term in the moment equation will be zero. The model changes to be the Euler equation. The conservation laws are satisfied for the moments ρ_i from the moment equations. From the up-scaling equation, we need $\langle \phi_i g \rangle = 0$ to get the conservation laws.

3.2.3.2   Navier-Stokes Local Up-scaling (NSLU) Model

When κ is between 0.002 and 0.1, the rarefied gas can't be treated as the inviscid fluid. Therefore the Euler system may not be applied as the fluid model. Instead, it could be treated as the viscous fluid so the other fluid model-Navier-Stokes system is still valid. In this section, a new local up-scaling model (NSLU) to couple the Navier-Stokes equations with the kinetic model is derived based on the first order of Chapman-Enskog expansion.

Let's take the BGK model as the example of derivation of the NSLU model.

The first order of C-E expansion of f to get the Navier-Stokes equations is the following (1D1D case of 2.31):

$$f_1 = \mathcal{M} + \tau \left(\sum_{i=0}^{4} \partial_{\rho_i} \mathcal{M} \partial_x F_i - \xi \partial_x \mathcal{M} \right) \doteq \mathcal{M} + S, \tag{3.10}$$

Therefore we may split the distribution function f similar to the micro-macro decomposition in ELU1 model as summation of fluid part $\mathcal{M} + S$ plus non-fluid part g:

$$f = \mathcal{M} + S + g, \text{ where } g = O(\kappa^2) \text{ and } \langle \phi_i g \rangle = 0, \tag{3.11}$$

The moment equations are the following,

$$\partial_t \rho_i + \partial_x F_i + \partial_x T_i + \partial_x \langle \phi_i \xi g \rangle = 0, \quad i = 0, 1, 2, 3, 4, \tag{3.12}$$

All the terms containing g are the up-scaling terms which can be ignored in the fluid region. In the kinetic region, g should be obtained by solving the following up-scaling equation:

$$\partial_t g + \boldsymbol{\xi} \cdot \nabla_x g = -\frac{1}{\tau}(S + g) - (\partial_t f_1 + \xi \partial_x f_1), \tag{3.13}$$

In the up-scaling equation the f_1 in the down-scaling terms should be obtained from the macroscopic quantities from 3.10.

We may obtain the local up-scaling model using the transition function h again. We still use g to denote $h \cdot g$ and get the localized model as follows:

$$\partial_t \rho_i + \partial_x F_i(\boldsymbol{\rho}) + \partial_x \langle \phi_i \xi S \rangle + \partial_x \langle \phi_i \xi g \rangle = 0, \text{ where } i = 0, 1, 2, 3, 4, \tag{3.14}$$

coupled with the up-scaling equation for $g(t, x, \xi)$:

$$\partial_t g + h\xi\partial_x g = -\frac{1}{\tau}h(S + g) - h(\partial_t f_1 + \xi\partial_x f_1), \qquad (3.15)$$

If the initial condition is a constant equilibrium $\mathcal{M}_{\rho^0}$, then $\rho = \rho^0$ and $g = 0$ is the solution of the NSLU model.

If the whole region is the fluid region, we get $f \approx f_1$ so the non-fluid part $g \approx 0$. The model changes to be the Navier-Stokes equations. Therefore NSLU model is asymptotic preserving.

Due to the conservative form of the moment equations (3.14) in the NSLU model, it is easy to see the conservation laws are satisfied.

3.2.3.3 Second Euler Local Up-scaling (ELU2) Model

If we use DSMC to solve the Boltzmann equation numerically which is a particle method, it is impossible to do a micro-macro decomposition and get the up-scaling equation. In this case ELU1 model can't be used to couple the Boltzmann equation with the fluid models. This difficulty can be resolved if we still keep the original kinetic equation and rewrite the up-scaling term in the moment equation in terms of $f(t, \mathbf{x}, \boldsymbol{\xi})$ instead of non-fluid part $g(t, \mathbf{x}, \boldsymbol{\xi})$. This can easily be done for the up-scaling model of Euler equations. Here we will use the Boltzmann equation as the kinetic model. The BGK model can be dealt in the same way.

We may multiply the Boltzmann equation by the five collision invariants

54

$(1, \boldsymbol{\xi}, \frac{1}{2}|\boldsymbol{\xi}|^2)$, integrate it over the whole velocity space and also multiply all the equations by the mass of molecule, we may derive five moment equations of $\rho, \mathbf{u}, E$ which describe the conservation laws of mass, momentum, and energy:

$$
\begin{cases}
\partial_t \rho + \nabla_x \cdot (\rho \mathbf{u}) = 0, \\
\partial_t (\rho \mathbf{u}) + \nabla_x \cdot (\rho \mathbf{u} \otimes \mathbf{u}) + \nabla_x p = \nabla_x \cdot \tilde{\Sigma}, \\
\partial_t (\rho e) + \nabla_x \cdot (\rho e + p)\mathbf{u})) = \nabla_x \cdot (\tilde{\Sigma} \cdot \mathbf{u} + \tilde{\mathbf{q}})
\end{cases}
\tag{3.16}
$$

where the symmetric stress tensor Σ and heat flux vector $\mathbf{q}$ are as follows:

$$
\tilde{\Sigma} = \langle \mathbf{c} \otimes \mathbf{c} f \rangle, \quad \tilde{\mathbf{q}} = \frac{1}{2} \langle \mathbf{c} |\mathbf{c}|^2 f \rangle,
\tag{3.17}
$$

where $\mathbf{c} = \boldsymbol{\xi} - \mathbf{u}$ is the thermal velocity of the particles.

Notice $\tilde{\Sigma}$ and $\tilde{\mathbf{q}}$ play the same role as the up-scaling terms $\langle \boldsymbol{\xi} \phi_i g \rangle$ in ELU1 model. In ELU2 model, these up-scaling terms are written in terms of $f(t, \mathbf{x}, \boldsymbol{\xi})$ instead of the non-fluid part $g(t, \mathbf{x}, \boldsymbol{\xi})$, which can be obtained by solving the Boltzmann equation locally in the kinetic region, i.e.

$$
\partial_t f + \boldsymbol{\xi} \cdot \nabla_x f = Q(f, f), \quad \text{in kinetic region}
\tag{3.18}
$$

In ELU2 model, we need to supply the boundary condition for the Boltzmann equation at the interface, which may be chosen as the half Maxwellian, i.e. the diffusion boundary condition for the kinetic model.

If the initial condition is a constant equilibrium $\mathcal{M}_{\rho^0}$, then $\rho = \rho^0$ and $f = \mathcal{M}_{\rho^0}$ are the solutions of the ELUM2 model.

If the whole region is the fluid region, we get $f \approx \mathcal{M}$ so the up-scaling terms $(\tilde{\Sigma}, \tilde{\mathbf{q}})$ in the moment becomes to be zero. The model changes to be the Euler equation. This shows ELU2 model is asymptotic preserving.

Also from the conservative form of the moment equations in ELU2 model, it is easy to see the conservation laws are satisfied.

3.3 Discretization of the Multi-Scale Models

We may want to keep the three properties of the good multi-scale models in the discrete numerical schemes of these models. The preservation of the global equilibrium is true as long as the continuous model holds. Therefore we will concentrate on the other two properties: asymptotic preserving and the conservation laws.

3.3.1 Discretization of DD Model and HM Model

For DD model, we only need to choose the scheme for the kinetic model and the scheme for the Euler equations respectively, which has been discussed in 2. The coupling of the models is done through the Marshak interface condition. We may need the overlapping of several grid points of the regions to avoid the discontinuity of the solution. The asymptotic preserving of the model is obtained as long as the kinetic solver is asymptotic preserving, which is true for the upwind implicit-explicit scheme of BGK model. Also it will satisfy the conservation laws up to a small error

of order κ at the interface.

As for HM model, it can be done in the same way if we choose the upwind scheme for the kinetic model and kinetic flux splitting for the Euler equations. The inflow interface condition for the kinetic model is the half Maxwellian while half kinetic flux is needed for the conservation laws at the interface which is solved in the whole region. If the kinetic solver is asymptotic preserving, HM model is asymptotic preserving too. Because of the forms of the macroscopic solver are conservation laws, HM models keep the conservation laws.

3.3.2   Discretization of Local Up-Scaling Models

In the following, again, we consider 1D1D dimensional BGK model as an example of the kinetic model, i.e. the following dimensionless equation:

$$\partial_t f + \xi \partial_x f = \frac{1}{\tau}(\mathcal{M} - f), \tag{3.19}$$

The scheme can be generalized to apply on the Boltzmann equation or other kinetic models.

3.3.2.1   Numerical Scheme for ELU1 Model

First we derive the numerical schemes for the ELU1 model from the numerical scheme for the kinetic models.

In this case the local up-scaling equation will be

$$\partial_t g + h\xi\partial_x g = -\frac{1}{\tau}g - h(\partial_t \mathcal{M} + \xi\partial_x \mathcal{M}), \text{ with } \langle\phi_i g\rangle = 0, \qquad (3.20)$$

Let's consider the spacial and temporal discretization of the up-scaling equation. If we have a discretization of the BGK model, then we may split $f = \mathcal{M} + g$ to get the discretization of the up-scaling equation. For example, if we use the first order upwind scheme in the space and forward Euler scheme in time for the dimensionless BGK model with implicit collision term, i.e.

$$D_t^- f_j^n + \xi^+ D^- f_j^n + \xi^- D^+ f_j^n = \frac{1}{\tau_j^{n+1}}(\mathcal{M}_j^{n+1} - f_j^{n+1}), \qquad (3.21)$$

We choose the implicit-explicit scheme for BGK model since we need the scheme to be stable in the fluid region, where κ is close to 0. Here $D^+(D^-)$ is the forward(backward) difference operator defined as

$$D^+ f = \frac{1}{\Delta x}(f_{i+1} - f_i), \quad D^- f = \frac{1}{\Delta x}(f_i - f_{i-1}), \qquad (3.22)$$

Then the first order scheme for the up-scaling equation will be

$$D_t^- g_j^n + h_j(\xi^+ D^- g_j^n + \xi^- D^+ g_j^n) = -\frac{1}{\tau_j^{n+1}}h_j g_j^{n+1} - h_j(\partial_t \mathcal{M}_j^n + \xi^+ D^- \mathcal{M}_j^n + \xi^- D^+ \mathcal{M}_j^n),$$

$$(3.23)$$

We multiply the above discrete up-scaling equation with the collision invariance ϕ_i. Since $\langle\phi_i g_j^n\rangle = 0$, dividing both sides by h_j we will get the numerical scheme

for the moment equations, i.e.

$$D_t^- \rho_{i,j}^n + D^- \langle \xi^+ \phi_i \mathcal{M}_j^n \rangle + D^+ \langle \xi^- \phi_i \mathcal{M}_j^n \rangle + D^- \langle \xi^+ \phi_i g_j^n \rangle + D^+ \langle \xi^- \phi_i g_j^n \rangle = 0, \quad i = 0, 1, 2,$$

(3.24)

This implies that if we use the kinetic flux splitting for the Euler fluxes and use the above upwind scheme for the up-scaling term, the discrete up-scaling model will be consistent with the BGK model.

Proposition. *The above upwind numerical scheme for the ELU1 model is asymptotic preserving and satisfies the conservation laws for ρ_i.*

Proof. First let's show it is asymptotic preserving. Since $g = O(\kappa)$, if $\kappa \to 0$ we have

$$h_j \left((D_t^- \mathcal{M}_j^n + \xi^+ D^- \mathcal{M}_j^n + \xi^- D^+ \mathcal{M}_j^n) + \frac{1}{\tau_j^{n+1}} g_j^{n+1} \right) = 0,$$

(3.25)

Dividing both sides by the h_j because $h_j = 1$ in the kinetic region, multiplying it by the collision invariants ϕ_i and integrating them over the velocity space, we get

$$D_t^- \rho_{i,j}^n + \langle \xi^+ \phi_i D^- \mathcal{M}_j^n \rangle + \langle \xi^- \phi_i D^+ \mathcal{M}_j^n \rangle + \frac{1}{\tau_j^{n+1}} \langle \phi_i g_j^{n+1} \rangle = 0, \quad i = 0, 1, 2, \quad (3.26)$$

Assuming $\langle \phi_i g_j^{n+1} \rangle = 0 (i = 0, 1, 2)$ and noticing the first order upwind discretization operators $D^\pm$ are linear, we may switch the order of the integration and $D^\pm$ and get

$$D_t^- \rho_{i,j}^n + D^- \langle \xi^+ \phi_i \mathcal{M}_j^n \rangle + D^+ \langle \xi^- \phi_i \mathcal{M}_j^n \rangle = 0,$$

(3.27)

59

This is the first order upwind scheme of the Euler equations using the kinetic flux vector splitting. This means the numerical scheme for the up-scaling equation is asymptotic preserving.

The scheme satisfies the conservation laws because the moment equations are conservation laws which are solved in the whole region and $g = 0$ at the interface.

$\square$

Our assumption $\langle \phi_i g_j^{n+1} \rangle = 0$ is true if it is true initially for the first order upwind scheme based on the following proposition.

Proposition. *Assume we use the first order scheme for the up-scaling model and the first order scheme with kinetic flux splitting for the fluid equations, i.e. the following discretization:*

$$D_t^- \rho_{i,j}^n + D^- F_{i,j}^{+,n} + D^+ F_{i,j}^{-,n} + D^- \langle \xi^+ \phi_i g_j^n \rangle + D^+ \langle \xi^- \phi_i g_j^n \rangle = 0, \qquad (3.28)$$

$$D_t^- g_j^n + h_j(\xi^+ D^- g_j^n + \xi^- D^+ g_j^n) \qquad (3.29)$$

$$= -\frac{1}{\tau_j^{n+1}} h_j g_j^{n+1} - h_j(D_t^- \mathcal{M}_j^n + \xi^+ D^- \mathcal{M}_j^n + \xi^- D^+ \mathcal{M}_j^n), \qquad (3.30)$$

Assume $g^0 = g(x, \xi, 0)$ is the initial value, then if $\langle \phi_i g_K^0 \rangle = 0 (i = 0, 1, 2)$ initially, then $\langle \phi_i g_K^n \rangle = 0 (i = 0, 1, 2)$ for all $t > 0$.

Proof. Multiply the discrete up-scaling equation by ϕ_i and integrate it over the

60

velocity space, we get

$$D_t^- \langle \phi_i g_j^n \rangle + h_j(\langle \xi^+ \phi_i D^- g_j^n \rangle + \langle \xi^- \phi_i D^+ g_j^n \rangle) = -\frac{1}{\tau_j^{n+1}} \langle \phi_i g_j^{n+1} \rangle$$

$$- h_j(D_t^- \rho_{i,j}^n + \langle \xi^+ \phi_i D^- \mathcal{M}_j^n \rangle + \langle \xi^- \phi_i D^+ \mathcal{M}_j^n \rangle)$$

(3.31)

Thanks for the linearity of the $D^\pm$ we may switch the integration and $D^\pm$. From $F_{i,j}^\pm = \langle \xi_x^\pm \phi_i \mathcal{M}_j \rangle$ we get

$$D_t^- \langle \phi_i g_j^n \rangle = -\frac{1}{\tau_j^{n+1}} \langle \phi_i g_j^{n+1} \rangle, \qquad (3.32)$$

Then we have

$$(1 + \frac{\Delta t}{\tau_j^{n+1}}) \langle \phi_i g_j^{n+1} \rangle = \langle \phi_i g_j^n \rangle, \qquad (3.33)$$

Therefore if $\langle \phi_i g^0 \rangle = 0$, then $\langle \phi_i g_j^n \rangle = 0$ by induction. $\qquad \square$

Now we are ready to discretize the model along the ξ-direction. We may apply the finite cutoff for ξ. Since the equilibriums are Gaussians which decay very fast, we only need to keep length of the interval to be six standard deviations around the mean. For example, the x-component of the velocity's range should be $[u_{x,min} - 3\sqrt{\theta}, u_{x,max} + 3\sqrt{\theta}]$. We use the subscript k for the velocity index. Then the full upwind numerical scheme for the ELU1 model is

$$D_t^- \rho_{i,j}^n + D^- F^+(\rho^n) + D^+ F^-(\rho^n) + D^- \langle \xi_k^+ \phi_{i,k} g_{j,k}^n \rangle + D^+ \langle \xi_k^- \phi_{i,k} g_{j,k}^n \rangle = 0,$$

$$D_t^- g_{j,k}^n + h_j(\xi_k^+ D^- g_{j,k}^n + \xi_k^- D^+ g_{j,k}^n)$$

(3.34)

$$= -\frac{1}{\tau_j^{n+1}} h_j g_{j,k}^{n+1} - h_j(D_t^- \mathcal{M}_{j,k}^n + \xi_k^+ D^- \mathcal{M}_{j,k}^n + \xi_k^- D^+ \mathcal{M}_{j,k}^n),$$

61

If we ignore the consistency with the original BGK model, we may apply any existing flux splitting(SWS, etc) for the Euler fluxes, then use center differencing scheme to discretize the up-scaling term in the moment equation to get the following new discretization for the moment equation

$$D_t^- \rho_{i,j}^n + D^- F^+(\rho^n) + D^+ F^-(\rho^n) + D\langle \phi_i g_j^n \rangle = 0, \quad i = 0, 1, 2, \tag{3.35}$$

In this way, the conservation laws are satisfied because $g = 0$ on the interface.

Remark. Zero-Moment Projection of g

Since g is the non-fluid part of the distribution function f, then the moments $\langle \phi_i g \rangle = 0$, $(i = 0, 1, 2)$ at any time t. This property will not hold in the numerical computation. Therefore the equilibrium in the up-scaling equation will have an accumulated error. This will bring oscillations into the solution in the kinetic region or make the numerical solution blow up in finite time. In order to fix it, we need to imply the zero-moment projection for g^{n+1} at the end of each time step. The additional projection step from [34] needed in the numerical experiments is shown in appendix D.

3.3.2.2   Numerical Scheme for NSLU Model

We may derive a discretization of the NSLU model in the same way as the ELU1 model. Again we start from the first order upwind scheme of the BGK model:

$$D_t^- f_j^n + \xi^+ D^- f_j^n + \xi^- D^+ f_j^n = \frac{1}{\kappa_j} \nu_j (\mathcal{M}_j^{n+1} - f_j^{n+1}), \qquad (3.36)$$

Therefore we have the discretization of the up-scaling equation:

$$
\begin{aligned}
D_t^- g_j^n + h_j(\xi^+ D^- g_j^n + \xi^- D^+ g_j^n) \\
= \frac{1}{\kappa} \nu_j h_j (\mathcal{M}_j^{n+1} - f_{1,j}^{n+1} - g_j^{n+1}) - h_j(D_t^- f_{1,j}^n + \xi^+ D^- f_{1,j}^n + \xi^- D^+ f_{1,j}^n),
\end{aligned}
\qquad (3.37)
$$

Since f_1 has some spacial derivatives involved (see 2.31), we also need the discrete scheme to get those derivatives in f_1. From [17], it is done by high-order center-differencing scheme in the computation to keep the accuracy.

Because f_1 and g has no contribution to the moments ρ_i, we may get the schemes for the moment equations by taking the moments of the above equation as

$$D_t^- \rho_{i,j}^n + \langle \phi_i \xi^+ D^- f_{1,j}^n \rangle + \langle \phi_i \xi^- D^+ f_{1,j}^n \rangle + \langle \phi_i \xi^+ D^- g_j \rangle + \langle \phi_i \xi^- D^+ g_j \rangle = 0, \quad (3.38)$$

Now let's consider the asymptotic preserving property of the above numerical scheme of the NSLU model. Since $g = O(\kappa^2)$, we may ignore the up-scaling terms in the moment equations if $\kappa \ll 1$. Switching the order of the $\langle \cdot \rangle$ and $D^\pm$, we get

$$D_t^- \rho_{i,j}^n + D^- \langle \phi_i \xi^+ f_{1,j}^n \rangle + D^+ \langle \phi_i \xi^- f_{1,j}^n \rangle = 0, \quad i = 0, 1, 2, \qquad (3.39)$$

This is the first order upwind scheme of using KVFS (see [17]) for the Navier-Stokes equations. Therefore the above discretization of the up-scaling equation is asymptotic preserving.

The discretization in the velocity space will be same as the ELU1 model. Also we need the additional projection for g to keep $\langle \phi_i g \rangle = 0$.

3.3.2.3   Numerical Scheme for ELU2 Model

As for the numerical schemes for the ELUM2, the equation for f will be solved in the same way as the kinetic model. The moment equations are similar to the Navier-Stokes equation. The convection terms can be discretized by SWS or KVFS. We may apply the center-differencing scheme for the up-scaling terms in ELUM2. For example, in 1D case, we have

$$\partial_x \tilde{\Sigma} \approx D\tilde{\Sigma}, \quad \partial_x(\tilde{\Sigma}u + \tilde{q}) \approx D(\tilde{\Sigma}u + \tilde{q}), \tag{3.40}$$

where $\tilde{\Sigma}$ and $\tilde{q}$ are given in 3.17.

Chapter 4

Semiconductor Device

In this chapter, we propose the drift-diffusion local up-scaling (DrDiLU) model, which will be used to simulalate the 1D GaAs n^+-n-n^+ diode when the electric field is low.

Considering the inhomogeneities of a practical device (in particular effects due to heavily doped regions in submicron structures) a single device can not be modeled with just one single set of partial differential equations derived from kinetic model, as different magnitudes of the scaling parameters might take over in different parts of the device. This means the simulation of semiconductor device is a typical multi-scale problem.

We start with a kinetic model of semiconductor device: the relaxation-time model and scaling analysis. Similar to the rarefied gas, when the electric field is low, by means of Chapman-Enskog expansion, the drift-diffusion(DrDi) model is derived as the macroscopic model. The high-field model is derived in the case the electric field is high using Chapman-Enskog expansion under different scalings.

From this similarity to the rarefied gas, the drift-diffusion local up-scaling (DrDiLU) model is proposed to simulate the 1D GaAs n^+-n-n^+ diode when the

electric field is low. Since the distribution function for the high-field model is very complicated, the local up-scaling model can't be done when the electric field is high. We will use domain decomposition model to simulate the device.

4.1   Kinetic Model

Semiconductors are crystalline materials composed of atoms that are bound together in a periodic lattice. Because the number of atoms is very large, their common energy levels decouple into many closely spaced levels which can be treated as a continuous band. Rather than being identified with a particular shell of a particular atom, electrons in a semiconductor are characterized by the energy band in which they are found. For simplicity, here we will concentrate on the unipolar model, for example, the N-type semiconductor, in which case the charge is transported in semiconductors by the flow of electrons. For the P-type semiconductor, i.e. the charge is transported by the flow of the positive holes, it can be done similarly.

The semi-classical Boltzmann equation can also be used to describe the electron transport in semiconductor devices(see [38, 15]). In this case, we consider an electron gas, which interacts with a bath of phonons assumed to be in thermal equilibrium. In this case the semi-classical Boltzmann equation for the semiconductor device which incorporates the quantum effects of the semi-conductor crystal lattice

via the band-diagram of the material is as follows

$$\frac{\partial f}{\partial t} + \frac{1}{\hbar}\nabla_{\mathbf{k}}\varepsilon(\mathbf{k}) \cdot \nabla_{\mathbf{x}}f - \frac{e}{\hbar}\mathbf{E} \cdot \nabla_{\mathbf{k}}f = Q(f), \tag{4.1}$$

here $f(t, \mathbf{x}, \mathbf{k})$ is the electron distribution function in the phase space, which depends on time t, space coordinates $\mathbf{x}$ and specific energy band $\mathbf{k}$, which is a continuum of all the possible energy levels. $\hbar$ and e are the Planck constant divided by 2π and the positive electric charge respectively.

The electric field $\mathbf{E}$ in the equation is self-consistently produced by the electrons moving in a fixed ion background with density $\rho_d(\mathbf{x})$, called doping profile. In an impure semiconductor, the conductivity depends strongly on the impurity concentration. By doping(which means intentionally adding impurities), the semiconductor's conductivity may be greatly changed.n other words, $\mathbf{E}$ is determined by the Poisson equation

$$\epsilon\Delta\Phi = e(\rho - \rho_d), \quad \mathbf{E} = -\nabla_{\mathbf{x}}\Phi, \tag{4.2}$$

where ϵ is the permittivity of the semiconductor material. $\rho = \int_{R^3} f(t, \mathbf{x}, \boldsymbol{\xi})d\boldsymbol{\xi}$ is the density distribution in the physical space.

The expression of the particle energy $\varepsilon(\mathbf{k})$ depends on the energy band structure in the semiconductor. If the Kane model is assumed, then ε is defined as

$$\varepsilon(\mathbf{k}) = \frac{1}{1 + \sqrt{1 + 2\frac{\tilde{\alpha}}{m}\hbar^2|\mathbf{k}|^2}}\frac{\hbar^2}{m^*}|\mathbf{k}|^2, \tag{4.3}$$

67

where m is the effective mass and $\tilde{\alpha}$ is the nonparabolicity factor. A widely used parabolic energy-wave vector relationship is obtained by putting $\tilde{\alpha} = 0$. In this case, $\frac{1}{\hbar}\nabla_{\mathbf{k}}\varepsilon(\mathbf{k}) = \frac{\hbar}{m^*}\mathbf{k}$ and we will get the same relationship between energy and momentum as in the rarefied gas. Then the classical Boltzmann equation is obtained by changing variable $\boldsymbol{\xi} = \hbar\mathbf{k}/m^*$ as

$$\frac{\partial f}{\partial t} + \boldsymbol{\xi} \cdot \nabla_{\mathbf{x}} f - \frac{e}{\hbar}\mathbf{E} \cdot \nabla_{\hat{\mathbf{k}}} f = Q(f), \tag{4.4}$$

Here $\boldsymbol{\xi}$ is the electron velocity corresponding to a specific energy band $\mathbf{k}$ and $f = f(t, \mathbf{x}, \boldsymbol{\xi})$.

The collision term, which takes account of the Pauli exclusion principle, can be written as the following,

$$Q(f) = \int_{R^3} [s(\mathbf{x}, \boldsymbol{\xi}', \boldsymbol{\xi})f(t, \mathbf{x}, \boldsymbol{\xi}')(1 - f(t, \mathbf{x}, \boldsymbol{\xi})) - s(\mathbf{x}, \boldsymbol{\xi}, \boldsymbol{\xi}')f(t, \mathbf{x}, \boldsymbol{\xi})(1 - f(t, \mathbf{x}, \boldsymbol{\xi}'))]\, d\boldsymbol{\xi}',$$
$$\tag{4.5}$$

where $s(\mathbf{x}, \boldsymbol{\xi}', \boldsymbol{\xi})$ is the so-called scattering rate and $s(\mathbf{x}, \boldsymbol{\xi}', \boldsymbol{\xi})f(t, \mathbf{x}, \boldsymbol{\xi})(1 - f(t, \mathbf{x}, \boldsymbol{\xi}'))$ denotes the rate of a particle with position $\mathbf{x}$, at time t, to change its velocity $\mathbf{k}'$ into $\mathbf{k}$ due to a scattering event. The collision term is nonlocal in the momentum direction and is determined by the considered short range interaction mechanisms.

We may define the collision frequency $\lambda(\mathbf{x}, \boldsymbol{\xi})$ and the relaxation time $\tau(\mathbf{x}, \boldsymbol{\xi})$ as

$$\lambda(x, \boldsymbol{\xi}) = \int_{R^3} s(\mathbf{x}, \boldsymbol{\xi}, \boldsymbol{\xi}')\, d\boldsymbol{\xi}', \quad \tau(x, \boldsymbol{\xi}) = \frac{1}{\lambda(\mathbf{x}, \boldsymbol{\xi})}, \tag{4.6}$$

In many semiconductor device applications the electron distribution function f is small, i.e. $0 \leq f(t, \mathbf{x}, \boldsymbol{\xi}) \ll 1$ holds. Under this low density assumption, the quadratic terms in the collision term are ignored and we get

$$Q(f)(t, \mathbf{x}, \boldsymbol{\xi}) = \int_{R^3} [s(\mathbf{x}, \boldsymbol{\xi}', \boldsymbol{\xi}) f(t, \mathbf{x}, \boldsymbol{\xi}') - s(\mathbf{x}, \boldsymbol{\xi}, \boldsymbol{\xi}') f(t, \mathbf{x}, \boldsymbol{\xi})] \, d\boldsymbol{\xi}', \qquad (4.7)$$

Obviously $Q(f)$ satisfies the conservation property $\int_{R^3} Q(f) d\boldsymbol{\xi} = 0$.

The principle of detailed balance gives the local equilibrium should satisfy

$$s(\mathbf{x}, \boldsymbol{\xi}, \boldsymbol{\xi}') M(t, \mathbf{x}, \boldsymbol{\xi}') = s(\mathbf{x}, \boldsymbol{\xi}', \boldsymbol{\xi}) M(t, \mathbf{x}, \boldsymbol{\xi}), \qquad (4.8)$$

From the standard statistical mechanics, $M(t, \mathbf{x}, \boldsymbol{\xi})$ is given by the Fermi-Dirac statistics. In the context of the low density approximation, it is usually approximated by the Maxwellian distribution $M_\theta(\boldsymbol{\xi}) = \frac{1}{(\sqrt{2\pi\theta})^3} \exp\left(-\frac{|\boldsymbol{\xi}|^2}{2\theta}\right)$. Here $\theta = k_b T$ is related to the lattice temperature T and k_b is the Boltzmann constant.

It is particularly interesting to investigate whether the solutions of the Boltzmann equation converge to an equilibrium state as $t \to \infty$. When the initial data $f(t, \mathbf{x}, \boldsymbol{\xi})$ is close to a multiple of the Maxwellian, it is natural to approximate $f(t, \mathbf{x}, \boldsymbol{\xi}')$ by ρM_θ. This will give another simplification of the collision integral. In the one dimensional case, by using the definition of relaxation time $\tau(x, \xi)$, the Boltzmann equation or 1D Relaxation-Time(RT) model reads as

$$\partial_t f + \xi \partial_x f - \frac{e}{m} E \partial_\xi f = \frac{1}{\tau} (\rho M_\theta - f), \quad \text{where} \quad x \in [0, L], \quad \xi \in R, \qquad (4.9)$$

here $\rho = \int_R f(t, x, \xi) d\xi$. Notice the collision term is linear and local in the velocity.

The Poisson equation is still needed to get the electric field,

$$E(t,x) = -\partial_x \Phi, \qquad \epsilon \Phi_{xx} = e(\rho - \rho_d), \tag{4.10}$$

Again ϵ is the electric permittivity and $\rho_d = \rho_d(x)$ is the doping profile.

The RT model needs the inflow/outflow boundary conditions, like the kinetic model for the rarefied gas. As for the Poisson equation, the applied voltage is given as the boundary condition:

$$\Phi(0) = 0, \qquad \Phi(L) = V_{bias} \tag{4.11}$$

The mobility $\mu = \frac{e\tau}{m}$ and the macroscopic velocity u and the current I are define as

$$u = \int_R v f(t,x,\xi) d\xi / \rho(t,x), \quad I = \frac{e}{L} \int_0^L \rho(t,x) u(t,x) dx, \tag{4.12}$$

In fact, since the collision term preserves the number of particles, therefore ρu should be constant at steady state.

4.2   Scaling of the 1D Relaxation-Time(RT) Model

We introduce the new non-dimensional variables as

$$x = L\hat{x}, \quad t = T\hat{t}, \quad \xi = V\hat{\xi}, \quad f = F\hat{f}, \quad \Phi = [\Phi]\hat{\Phi}, \quad \tau = \tau_0 \hat{\tau}, \quad \rho_d = \rho_0 \hat{\rho}_d,$$

$$\tag{4.13}$$

Therefore $\theta = V^2 \hat{\theta}$ and we have $M = \frac{1}{V} M_{\hat{\theta}}(\hat{\xi})$. Also we get $\rho = FV\hat{\rho}(\hat{x},\hat{t}), E = \frac{[\Phi]}{L}\hat{E}(\hat{x},\hat{t})$.

70

In the following we drop the hats of the non-dimensional variables after changing the variables, and we get,

$$\begin{cases} \frac{F}{T}\partial_t f + \frac{FV}{L}\xi\partial_x f - \frac{eF[\Phi]}{mL\sqrt{\theta_0}}E\partial_\xi f = \frac{F}{\tau_0}\frac{\rho M_{\hat{\theta}}-f}{\tau}, \\ \frac{\epsilon[\Phi]}{L^2}\partial_{xx}\Phi = e(\frac{FV}{\rho_0}\rho - \rho_d), \end{cases} \tag{4.14}$$

Multiply the Boltzmann equation both sides by $\frac{L}{VF}$, and we get dimensionless equation as

$$\frac{L}{VT}\partial_t f + \xi\partial_x f - \frac{e[\Phi]}{mV^2}E\partial_\xi f = \frac{L}{V\tau_0}\frac{\rho M - f}{\tau} \tag{4.15}$$

coupled with the dimensionless Poisson equation

$$\frac{\epsilon[\Phi]}{L^2}\partial_{xx}\Phi = e\rho_0(\frac{FV}{\rho_0}\rho - \rho_d) \tag{4.16}$$

Next we consider four characteristic velocities representing different scalings:

1. Macroscopic velocity: $V_M = L/T$,

2. Thermal velocity: $V_T = \sqrt{\theta_0}$, i.e. the standard deviation of the electrons' velocities.

3. Ballistic velocity: $V_B = \sqrt{\frac{2e[\Phi]}{m}}$. This corresponds to the velocity of the electrons which transport without undergoing any collisions in the channel.

4. Drift velocity: $V_D = \tau_0\frac{e}{m}\bar{E} = \tau_0\frac{e}{m}\frac{[\Phi]}{L}$.

In terms of the characteristic velocities, we have

$$\frac{V_M}{V}\partial_t f + \xi\partial_x f - \frac{V_B^2}{2V^2}E\partial_\xi f = \frac{V_B^2}{2VV_D}\frac{\rho M - f}{\tau} \tag{4.17}$$

71

Also we define the scaled Debye length $\beta = \sqrt{\frac{\epsilon[\Phi]}{e\rho_0 L^2}}$, then the dimensionless Poisson equation will be

$$\beta^2 \Phi_{xx} = (\frac{FV}{\rho_0}\rho - \rho_d),\qquad(4.18)$$

In the following we define the scaled mean free path $\varepsilon = \frac{\tau_0\sqrt{\theta}}{L} = \frac{2V_T V_D}{V_B^2}$.

Different scalings:

1. **Low-Field (LF) Scaling:** Assume the collisions are dominate, then the drift speed is much smaller than the thermal speed. In this case, we may take $V = V_T$. Assume $\frac{V_M}{V_T} \approx \varepsilon$. In this way, $\hat{\theta} = 1$. By setting $\frac{V_B^2}{2V_T^2} = \alpha = O(1)$, we get

$$\varepsilon\partial_t f + \xi\partial_x f - \alpha E\partial_\xi f = \frac{1}{\varepsilon}\frac{\rho M_1 - f}{\tau},\qquad(4.19)$$

   We also normalize f by the doping profile and the lattice temperature, i.e. $FV_T = \rho_0$ and we get the Poisson equation

$$\beta^2 \Phi_{xx} = (\rho - \rho_d),\qquad(4.20)$$

2. **Drift-Collision Balance (DCB) Scaling:** The collisions continue to be dominant but the force field is higher and now the drift speed is of the order of the thermal speed. In this sense this scaling appears for higher potential drops than the LFS. We may still take $V = V_T$ and set $\gamma = \frac{V_D}{V_T} \approx \frac{V_M}{V_T} = O(1)$ to get

$$\gamma\partial_t f + \xi\partial_x f - \frac{\gamma}{\varepsilon}E\partial_\xi f = \frac{1}{\varepsilon}\frac{\rho M_1 - f}{\tau},\qquad(4.21)$$

and take the normalization for f as $FV_D = \rho_0$. Then the Poisson equation is

$$\beta^2 \Phi_{xx} = (\gamma^{-1}\rho - \rho_d), \tag{4.22}$$

3. **Ballistic Scaling:** Here we consider the potential is significantly higher than that in previous cases and the drift speed is of the order of the ballistic speed and much larger than the thermal speed. This time we take $V = V_B$. Set $\nu = \frac{V_B}{V_T} \rightarrow 0$, $\alpha = \frac{V_D}{V_B} = O(1)$ and $\frac{V_M}{V_D} = 1$ and we get

$$\eta\partial_t f + \xi\partial_x f - \frac{1}{2}E\partial_x f = \frac{1}{2\alpha}\frac{\rho M_{\nu^2} - f}{\tau}, \tag{4.23}$$

We normalize f by $FV_B = \rho_0$, then the Poisson equation is

$$\beta^2 \Phi_{xx} = (\rho - \rho_0), \tag{4.24}$$

Remark. For LF or DCB scaling, macroscopic models (drift-diffusion model, high-field model) are derived by means of Chapman-Enskog expansions when $\varepsilon \rightarrow 0$. So far, as I know, there is no asymptotic expansion available for ballistic scaling when $\nu \rightarrow 0$.

4.3   Drift-Diffusion (DrDi) Model

Assume the electric field is low or the device is not very small, we may recall that the low-field scaling dimensionless 1D RT model of the semiconductor equation as

$$\varepsilon\partial_t f + \xi\partial_x f - \alpha E\partial_\xi f = \frac{1}{\varepsilon}\frac{\rho M_1 - f}{\tau}, \tag{4.25}$$

73

with the coupled Poisson equation $\beta^2 \Phi_{xx} = (\rho - \rho_d)$. Give $\alpha = O(1), \beta = O(1)$, we

only need to consider the approximation of the Boltzmann equation when $\varepsilon \to 0$.

This is a similar case to the rarefied gas with an extra force term. We may apply

the first order Chapman-Enskop expansion on the LF scaling dimensionless 1-d

relaxation-time model, i.e. we take the distribution function f as

$$f \approx \rho M_1 - \varepsilon\tau(\xi\partial_x(\rho M_1) + \partial_x\Phi\partial_\xi(\rho M_1)),$$

$$\approx \rho M_1 - \varepsilon\tau(\xi M_1(\partial_x\rho + E\rho)),$$

(4.26)

Notice the second term doesn't have contribution to the zeroth order moment of f.

Plug it into the above equation and integrate it over the velocity space, we get

$$\partial_t\rho + \partial_x(J_{vis} + J_{hyp}) = 0,$$

(4.27)

where

$$J_{vis} = -\varepsilon\tau\partial_x\rho, \quad J_{hyp} = \varepsilon\tau\rho\partial_x\Phi = -\varepsilon\tau\rho E,$$

(4.28)

Therefore the dimensional drift-diffusion model for the 1-d semiconductor device is

$$\partial_t\rho + \partial_x(J_{vis} + J_{hyp}) = 0,$$

(4.29)

where

$$J_{vis} = -\tau\theta\partial_x\rho, \quad J_{hyp} = \mu\rho\partial_x\Phi = -\mu\rho E, \quad \text{where} \quad \mu = e/m\tau,$$

(4.30)

here θ is the lattice temperature which is a constant. The coupled Poisson equation

74

is

$$\epsilon \Phi_{xx} = e(\rho - \rho_d), \tag{4.31}$$

4.4   High Field (HF) Model

If there is a strong electric force field, we need to apply the drift-collision balancing scaling for the model. Here the dimensionless Boltzmann equation is

$$\gamma \partial_t f + v \partial_x f - \frac{\gamma}{\varepsilon} E \partial_\xi f = \frac{1}{\varepsilon} \frac{\rho M_1 - f}{\tau} \tag{4.32}$$

with the coupled Poisson equation $\beta^2 \Phi_{xx} = (\gamma^{-1} \rho - \rho_d)$. Here we assume $\gamma = O(1), \beta = O(1)$ and let $\varepsilon \to 0$. In [14], the authors derived the high-field model from the first order Chapman-Enskog expansion in the following way.

Assume the distribution function $f = f(\rho, E, v)$, i.e. f depends on t, x through the function ρ, E. Then we get

$$\partial_t f = \frac{\partial f}{\partial \rho} \partial_t \rho + \frac{\partial f}{\partial E} \partial_t E, \tag{4.33}$$

Notice $\partial_t \rho + \partial_x \langle v f \rangle = 0$ so we may eliminate the time derivative of ρ. As for $\partial_t E$, we differentiate the Poisson equation with respect to t and get

$$\beta^2 \partial_t \Phi_{xx} = \gamma^{-1} \partial_t \rho = -\gamma^{-1} \partial_x \langle v f \rangle, \quad E = -\partial_x \Phi, \tag{4.34}$$

thus $\partial_t E = \frac{1}{\beta^2 \gamma}(\langle v f \rangle + w)$ where w is a constant. In this way, we get

$$\partial_t f = -\frac{\partial f}{\partial \rho} \partial_x \langle v f \rangle + \frac{1}{\beta^2 \gamma} \frac{\partial f}{\partial E}(\langle v f \rangle + w), \tag{4.35}$$

75

and we may express the dimensionless Boltzmann equation as

$$-\frac{\partial f}{\partial \rho}\partial_x \langle vf \rangle + \frac{1}{\beta^2\gamma}\frac{\partial f}{\partial E}\left(\langle vf \rangle + w\right) + v\partial_x f - \frac{\gamma}{\varepsilon}E\partial_\xi f = \frac{1}{\varepsilon}\frac{\rho M_1 - f}{\tau}, \qquad (4.36)$$

We take the first C-E expansion of f in terms of ε, i.e.

$$f \approx f_0 + \varepsilon f_1, \quad \langle f \rangle = \langle f_0 \rangle \qquad (4.37)$$

Then we get the following equations for f_0 and f_1 by balancing the order of each ε term:

$$-\gamma E\partial_\xi f_0 = \frac{1}{\tau}(\rho M_1 - f_0) \qquad (4.38)$$

and

$$-\frac{\partial f_0}{\partial \rho}\partial_x \langle vf_0 \rangle + \frac{1}{\beta^2\gamma}\frac{\partial f_0}{\partial E}\left(\langle vf_0 \rangle + w\right) + v\partial_x f_0 - \gamma E\partial_\xi f_1 = -\frac{f_1}{\tau}, \qquad (4.39)$$

We may obtain

$$\langle vf_0 \rangle = -\tau E\rho, \quad \langle vf_1 \rangle = -\tau(1+2\tau^2 E^2)\rho + \tau^2 E\partial_x(\tau E\rho) + \frac{\tau^2}{\gamma\beta^2}\rho(-\tau E\rho + w), \quad (4.40)$$

Therefore the dimensionless equation of the density function ρ will be

$$\partial_t \rho + \partial_x \langle vf \rangle = \partial_t \rho + \partial_x J = 0, \qquad (4.41)$$

where $J = J_{hyp} + J_{vis}$ and

$$J_{hyp} = -\tau E\rho + \varepsilon\frac{\tau^2}{\gamma\beta^2}\rho(-\tau E\rho + w), \quad J_{vis} = -\varepsilon\tau\partial_x((1 + 2\tau^2 E^2)\rho) + \varepsilon\tau^2 E\partial_x(\tau E\rho),$$

$$(4.42)$$

Taking $\gamma = \varepsilon = 1, \beta^2 = \epsilon/e$ and changing M_1 to be M_θ, we get the dimensional equations for the high field model reads:

$$\partial_t \rho + \partial_x J = 0, \tag{4.43}$$

where $J = J_{hyp} + J_{vis}$ and

$$J_{hyp} = -\mu E \rho + \frac{e\tau\mu}{\epsilon}\rho(-\mu E \rho + w), \quad J_{vis} = -\tau\partial_x((\theta + 2\mu^2 E^2)\rho) + \tau\mu E \partial_x(\mu E \rho), \tag{4.44}$$

with the coupled Poisson equation $\epsilon\Phi_{xx} = q(\rho - \rho_d)$.

Notice we need to give the expression of the constant w. For the steady problem, we finally get $\partial_t E = 0$. Therefore we should have $\langle vf_0 \rangle + w = -\mu E \rho + w \approx 0$ which is used to obtain the constant w in the high field model. In this case, the constant w is set to be $(\mu E \rho)|_{x=0}$ if we assume $x = 0$ is the left end point of the interval.

Remark. From 4.38, it shows that the explicit form of f_0 and f_1 can't be obtained. This implies the up-scaling model for the HF model can't be obtained. We will use DD model to simulate the diode for the DCBS.

4.5 Numerical Methods

Here we will concentrate on the upwind schemes of finite difference methods for the above models.

4.5.1 Numerical Methods to the 1D RT Model

First we consider the Boltzmann equation in the 1-D RT model of the semiconductor device. It is similar to the BGK model of the rarefied gas with the additional convection term $E\partial_\xi f$. The tempal derivative and the transport term will be discretized in the same way as the BGK model. For the additional convection term $E\partial_\xi f$, we will apply the forward/backward difference scheme based on the sign of E. To avoid unphysical boundary condition on the ξ direction, we will apply one-sided derivative at the ξ boundary. For the source term, we will apply the implicit scheme as we did for the BGK model.

A uniform grid in ξ-direction will be used in the numerical computation. For LF scaling, the cut-off of the velocity will be $[-4\sqrt{\theta}, 4\sqrt{\theta}]$, i.e. four standard deviations. In the case of the higher eletric field or larger mobility, we need to use bigger domain of ξ.

To solve the Poisson equation in the model, we discretize the derivative using the standard center-difference scheme and solve the system of the linear equations to get the electric potential.

The first order numerical scheme with the implicit relaxation term is as follows:

$$D_t^- \rho_j^n + \sum_k (D_x^- \xi_k^+ f_{j,k}^n)\Delta\xi + \sum_k (D_x^+ \xi_k^- f_{j,k}^n)\Delta\xi = 0,$$

$$\epsilon \tilde{D}^2 \Phi_j^{n+1} = e(\rho_j^{n+1} - \rho_{d,j}), \quad E_j^{n+1} = -D\Phi_j^{n+1},$$

$$D_t^- f_{j,k}^n + D_x^- (\xi_k^+ f_j^n) + D_x^+ (\xi_k^- f_{j,k}^n) - D_\xi^- (\frac{e}{m} E_j^{-,n} f_{j,k}^n) - D_\xi^+ (\frac{e}{m} E_j^{+,n} f_{j,k}^n)$$

$$= \frac{1}{\tau_j^{n+1}} (\rho_j^{n+1} M_k - f_{j,k}^{n+1}),$$

$$(4.45)$$

here $\tilde{D}^2$ is the standard short stencil center-difference scheme for the second derivative and $E^+ = \max(E,0), \quad E^- = \min(E,0)$.

Remark. Notice in the moment equation, we switch the $\sum_k$ and D_x^-. This will make no difference for the first order scheme, but it will make the solution long time stable for the high order schemes due to the consistence with the discretization of the relaxation time equation, i.e. the third equation.

4.5.2 Numerical Methods to the DrDi Model

For the flux in DrDi model $J = -\tau\theta\partial_x\rho - \mu E\rho$, if we apply the KVFS method similar to the Navier-Stokes equation's case, we will get $J^+ = J^- = \frac{1}{2}J$ due to the zero mean of lattice Maxwellian. Then

$$\partial_x J = (D^- J^+ + D^+ J^-) = DJ \qquad (4.46)$$

79

where D is the standard center-differencing operator. Here the derivative $\partial_x \rho$ in J will be obtained by

$$\partial_x \rho \approx \frac{1}{2}(D^+ \rho^- + D^- \rho^+) \doteq \hat{D}\rho, \tag{4.47}$$

where $\rho^{\pm}$ is the fifth order WENO reconstruction for ρ to introduce some numerical viscosity and keep the accuracy.

Remark. If we insist to use $\partial_x \rho \approx D\rho$ in the expression of J, which turns out to be long stencil center differencing scheme for the fluxes and not stable in the computation because of the large gradient of ρ.

The numerical scheme for the dimensional DrDi model is as follows

$$\begin{aligned} D_t^- \rho_j^n - D(\tau_j^n(\theta \hat{D}\rho_j^n + \frac{e}{m} E_j^n \rho_j^n)) &= 0, \\ \epsilon \tilde{D}^2 \Phi_j^n = e(\rho_j^n - \rho_{d,j}), \quad \text{with} E_j^n &= -D\Phi_j^n, \end{aligned} \tag{4.48}$$

4.5.3   Numerical Methods to the HF Model

For the viscous flux in the HF model, we apply center-differencing scheme. And for the hyperbolic flux in the HF model, we apply the upwind scheme. Therefore we

get the following numerical scheme for the dimensional HF model:

$$D_t^- \rho_j^n - \hat{D}(J_{vis})_j^n - D^-((F_j^n)^+ \rho_j^n) - D^+((F_j^n)^- \rho_j^n) = 0,$$

$$\text{where} \quad F^\pm = \frac{1}{2}\left(-\mu E + \frac{\epsilon\tau\mu}{q}(-\mu E\rho + w) \pm |-\mu E + \frac{\epsilon\tau\mu}{q}(-\mu E\rho + w)|\right),$$

$$\text{with} \quad w = (\mu E\rho)|_{j=0}^n,$$

$$\text{and} \quad \hat{D}(J_{vis}) = \frac{1}{\Delta x}(\tau_{j+1/2}D^+[(\theta + 2\mu^2 E^2)\rho]_j - \tau_{j-1/2}D^-[(\theta + 2\mu^2 E^2)\rho]_j)$$

$$- \frac{1}{\Delta x}((\tau\mu E)_{j+1/2}D^+[\mu E\rho]_j - (\tau\mu E)_{j-1/2}D^-[\mu E\rho]_j),$$

$$\epsilon\tilde{D}^2\Phi_j^n = q(\rho_j^n - \rho_{d,j}), \quad \text{with} E_j^n = -D\Phi_j^n,$$

$$\tag{4.49}$$

4.6   Drift-Diffusion Local Up-scaling(DrDiLU) Model

Similar to the NSLU model for the rarefied gas, we set

$$f = \rho M_1 - \varepsilon\tau(\xi\partial_x(\rho M_1) + \partial_x\Phi\partial_\xi(\rho M_1)) + g = \rho M_\theta - \tau(\partial_x\rho + \frac{e}{m\theta}E\rho))\xi M_\theta + g, \tag{4.50}$$

Denote $S = -\tau(\partial_x\rho + \frac{e}{m\theta}E\rho))\xi M_\theta$, then the up-scaling model is as follows:

$$\partial_t\rho - \partial_x(\tau\theta\partial_x\rho + \frac{e}{m}\tau E\rho) + \partial_x\langle\xi g\rangle = 0,$$

$$\epsilon\Phi_{xx} = e(\rho - \rho_d), \tag{4.51}$$

$$\partial_t g + \xi\partial_x g - \frac{e}{m}E\partial_\xi g = \frac{1}{\tau}(S + g) - (\partial_t + \xi\partial_x - \frac{e}{m}E\partial_\xi)(\rho M_\theta - \tau S),$$

By means of the smooth transition fuction h which $= 1$ in the kinetic region, $= 0$ in the drift-diffusion region and notice $h\partial_\xi g = \partial_\xi(hg)$, we get the DrDiLU model as

follows:

$$\partial_t \rho - \partial_x(\tau\theta\partial_x\rho + \frac{e}{m}\tau E\rho) + \partial_x\langle\xi g\rangle = 0,$$

$$\epsilon\Phi_{xx} = e(\rho - \rho_d), \tag{4.52}$$

$$\partial_t g + h\xi\partial_x g - \frac{e}{m}E\partial_\xi g = -\frac{h}{\tau}(S + g) - h\left(\partial_t + \xi\partial_x - \frac{e}{m}E\partial_\xi\right)[\rho M_\theta - \tau S],$$

The first order numerical scheme for DrDiLU model using KFVS will be

$$D_t^-\rho_j^{n+1} - D\left(\tau_j^n(\theta\hat{D}\rho_j^n + \frac{e}{m}E_j^n\rho_j^n)\right)$$

$$+ \sum_k \left(D_x^-\xi_k^+ g_{j,k}^n\right)\Delta\xi + \sum_k \left(D_x^+\xi_k^- g_{j,k}^n\right)\Delta\xi = 0,$$

$$\epsilon\tilde{D}^2\Phi_j^n = e(\rho_j^n - \rho_{d,j}), \quad \text{with } E_j^n = -D\Phi_j^n,$$

$$D_t^- g_{j,k}^n + h_j\left(D_x^-(\xi_k^+ g_j^n) + D_x^+(\xi_k^- g_{j,k}^n)\right) - \frac{e}{m}\left(D_\xi^-(E_j^{-,n}g_{j,k}^n) - D_\xi^+(E_j^{+,n}g_{j,k}^n)\right)$$

$$= -\frac{h_j}{\tau_j^{n+1}}(S_{j,k}^{n+1} + g_{j,k}^{n+1})$$

$$- h_j\left(D_t^- + D_x^-\xi_k^+ + D_x^+\xi_k^- - \frac{e}{m}(D_\xi^- E_j^{-,n} + D_\xi^+ E_j^{+,n})\right)\left[\rho_j^n(\mathcal{M}_\theta)_k - S_{j,k}^n\right],$$

$$\text{where } S_{j,k}^l = -\tau_j^l(\hat{D}\rho_j^l + \frac{e}{m\theta}E_j^l\rho_j^l)(\xi\mathcal{M}_\theta)_k, \quad l = n, n+1$$

$$(4.53)$$

Recall $\hat{D}\rho = \frac{1}{2}(D^-\rho^+ + D^-\rho^+)$ where $\rho^\pm$ is the fifth order WENO reconstruction

for ρ to introduce some numerical viscosity and keep the accuracy.

In fact the above scheme is not stable due to the large gradient of the doping

profile. Instead we should use the following scheme for the density equation:

$$D_t^- \rho_j^{n+1} - \nu(D^-\rho - D^+\rho)) - D\left(\tau_j^n(\theta\hat{D}\rho_j^n + \frac{e}{m}E_j^n\rho_j^n)\right)$$
$$+ \sum_k \left(D_x^- \xi_k^+ g_{j,k}^n\right)\Delta\xi + \sum_k \left(D_x^+ \xi_k^- g_{j,k}^n\right)\Delta\xi = 0, \tag{4.54}$$

where $\nu = \sum \xi_k^+(\mathcal{M}_\theta)_k \Delta\xi$. The extra term comes from the kinetic flux splitting of $\langle \xi\rho\mathcal{M}_\theta \rangle$ to ensure the consistency of the upscaling equation with the density equation and plays a role as an artificial viscosity.

4.7   High-Field Domain Decomposition(HFDD) Model

Although the high field model is derived from the 1D RT model, the up-scaling model cannot be derived due to the fact that the distribution function f to get the high-field model can't be explicitly obtained (see 4.38). In order to couple the 1D RT model with the high-field model, we may apply the DD model. Here we can't apply the Marshak condition due to the unknown distribution function f. To couple the HF model with the 1D RT model, on the interface we simply set the inflow boundary condition for RT model is $f = \rho\mathcal{M}_\theta$. Numerical results shows this coupling is good only when the electric field is not very high.

Chapter 5

Numerical Examples

In this last chapter, we will do some numerical tests to compare the results from different models for the multi-scale problems.

We begin with an artificial multi-scale problem obtained from the Jin-Xin relaxation model for the inviscid Burger's equation. The ELU1 and NSLU models will be used to compute a traveling shock problem.

Then it is followed by the BGK models for the rarefied gas. We will consider an initial-value problem for 1D-1D case and a stationary shock problem for 1D-3D case. The ELU1, ELU2 and NSLU models will be used in the computation.

We will also do a diode simulation for the semiconductor using the DrDiLU model when the electric field is low. When electric field is high, we apply DD model to couple the high-field model with the relaxation-time model.

In the last part, we will do a simulation of 2D plannar Couette flow using ELU2 model based on the DSMC for the Boltzmann equation.

5.1 Jin-Xin Relaxation Model for the Inviscid Burger's Equation

The well-known inviscid Burger's equation is given by the 1D scalar conservation law as

$$\partial_t \rho + \partial_x F(\rho) = 0, \quad \forall x \in R \tag{5.1}$$

where the flux is $F(\rho) = \frac{1}{2}\rho^2$.

Here we consider a Riemann problem for this equation, i.e. the initial condition for ρ is given as $\rho(0, x) = \rho^0(x))$ where $\rho^0(x) = 1$ for $x < 0$ and $\rho^0(x) = \frac{1}{2}$ if $x \geq 0$.

The solution of the inviscid Burger's equation with the above initial condition is a traveling shock wave $\rho(t, x) = \rho^0(x - st)$, whose speed s is determined by Rankine-Hugoniot condition

$$s = \frac{F(\rho_r) - F(\rho_l)}{\rho_r - \rho_l}, \tag{5.2}$$

where ρ_r and ρ_l are the $\rho(x)$'s values evaluated around the discontinuity. In our case, $\rho_r = \frac{1}{2}$ and $\rho_l = 1$. Therefore $s = \frac{3}{4}$.

In numerical computation, the domain is limited to be $x \in [-0.5, 0.5]$. Therefore we need to apply inflow boundary condition as $\rho(t, -0.5) = 1$ because the shock is traveling from the left to the right.

The Jin-Xin relaxation model for the 1D scalar conservation law is as follows:

$$\partial_t \rho + \partial_x v = 0,$$
$$\partial_t v + \partial_x \rho = \frac{1}{\tau}(F(\rho) - v), \tag{5.3}$$

here $F(\rho) = \frac{1}{2}\rho^2$ for the inviscid Burger's equation. The τ is the constant relaxation rate. This model was introduced by Jin and Xin in [29] in order to introduce the relaxation schemes for the system of conservation laws.

The relaxation system is a hyperbolic system plus a stiff term. In order to impose appropriate boundary conditions, first we need to diagonalize the system.

Denote $f_1 = \frac{1}{2}(\rho + v)$, $f_2 = \frac{1}{2}(\rho - v)$, then we get the following BGK form of Jin-Xin relaxation model:

$$\begin{aligned}
\partial_t f_1 + \partial_x f_1 &= \frac{1}{\tau}(M_1 - f_1), \\
\partial_t f_2 - \partial_x f_2 &= \frac{1}{\tau}(M_2 - f_2),
\end{aligned} \tag{5.4}$$

where $M_i(\rho) = \frac{1}{2}(\rho \pm F(\rho)) = \frac{1}{2}((f_1 + f_2) \pm \frac{1}{2}(f_1 + f_2)^2)$, $i = 1, 2$.

The initial condition of v should be consistent with ρ to avoid the initial layer. Since $v = F(\rho) + O(\tau) \approx \frac{1}{2}\rho^2$, we may impose $v(0, x) = \frac{1}{2}\rho_0^2$ as the initial condition, where ρ_0 is the initial condition for the inviscid Burger's equation. No initial layer is observed in the numerical tests.

As for the boundary conditions, we need to apply the following inflow and outflow boundary conditions for the traveling shock problem:

$$f_1(t, -0.5) = M_1(\rho(t, -0.5)) = \frac{3}{4}, \quad f_2(t, 0.5) = M_2(\rho(t, 0.5)) = \frac{3}{16}, \tag{5.5}$$

In the BGK form, we may treat the Jin-Xin model as an simple kinetic model with discrete velocity $\xi = \pm 1$. $\rho = f_1 + f_2$ is the zero-order moment of the distribu-

tion function. M_i are the local Maxwellian evaluated at ± 1. The relaxation rate τ plays the same role as the Knudsen number and the collision frequency $\nu = 1$.

To apply the zeroth C-E expansion, we set $f_i \approx M_i$. Notice $F(\rho) = \rho^2/2 = M_1 - M_2$ so we get the inviscid Burger's equation as the fluid model.

To apply the first order Chapman-Enskog expansion with respect to τ, we set

$$f_i \approx M_i \mp \frac{1}{2}\tau(1 - \rho^2)\partial_x\rho, \tag{5.6}$$

The resulting fluid model turns out to be the Burger's equation with a viscosity term.

$$\partial_t\rho + \partial_x F(\rho) = \partial_x(\tau(1 - \rho^2)\partial_x\rho), \tag{5.7}$$

Notice $\tau > 0$. Then this equation is dissipative if the sub-characteristic condition $|\rho| \leq 1$ is satisfied, which serves as a stability criterion for the system, [29].

This model has been studied by T.-P. Liu, [33] for the case that $\tau = \tau(\rho)$. If τ is a constant, it has been show the solution will converge to the solution of inviscid Burger's equation when $\tau \to 0$, [41].

In the following, we set $\tau = \tau(x)$ so τ can vary significantly in space to add the multi-scale effect. We choose $\tau = \tau(x)$ to be piecewise linear, i.e. $\tau = 0.01(0.05)$ in $[-0.5, 0.05]$ and $\tau = 1$ in $[0.1, 0.5]$ and is linear between these two intervals. Here $\tau = 0.01(0.05)$ is small enough to apply the inviscid(viscous) Burger's equation as the fluid model. It will be considered as the kinetic region where $\tau = 1$.

5.1.1   ELU1 Model for Jin-Xin Model

By means of the transition function $h(x)$ the local up-scaling model will be:

$$\partial_t \rho + \partial_x(\rho^2/2)) + \partial_x(g_1 - g_2) = 0,$$

$$\partial_t g_1 + h\partial_x g_1 = -\frac{1}{\tau}hg_1 - h\left(\partial_t M_1 + \partial_x M_1\right), \qquad (5.8)$$

$$\partial_t g_2 - h\partial_x g_2 = -\frac{1}{\tau}hg_2 - h\left(\partial_t M_2 - \partial_x M_2\right),$$

We choose 100 points to solve the kinetic model in the entire domain and 100 points for the numerical approximation of the coupling model. The transition function $h(x)$ is defined to be piecewise linear and continuous : 0 for $x \leq a$ and 1 for $x \geq b$, and linear between a and b. From the comparison of the results of the BGK model and inviscid Burger's equation's result given the above profile of $0.01 \leq \tau(x \leq 1)$ when $t = 0.2$, these two solutions will be distinct when $x \geq 0.02$. We will use the buffer-zones: $a = -0.05$ and $b = 0.02$ so the buffering zone entirely lies in the fluid region. The time step is chosen to satisfy the CFL condition, i.e. $\frac{\Delta t}{\Delta x} \leq 1$. In the computation, we use $\frac{\Delta t}{\Delta x} \leq \frac{1}{2}$ instead. All the results are obtained when $t = 0.2$.

For the boundary conditions, the Dirichlet boundary is applied for the moment equation. We also apply the inflow boundary conditions for the up-scaling equations. As we know, since $h = 0$ at the interface between the buffering zone and the fluid region, g_1's equation doesn't need the boundary condition. From the boundary condition for the relaxation model, we assume the right boundary always keeps

equilibrium so $g_2(0.5, t) = 0$. No boundary layer is observed in the numerical results.

The first order numerical scheme using KVFS will be:

$$D_t^- \rho_j^n + D^- M_{1,j}^n + D^+ M_{2,j}^n + D^- g_{1,j}^n - D^+ g_{2,j}^n = 0,$$

$$D_t^- g_{1,j}^n + h_j D^- g_{1,j}^n = -\frac{1}{\tau_j} h_j g_{1,j}^{n+1} - h_j \left(D_t^- M_{1,j}^n + D^- M_{1,j}^n \right),$$

$$D_t^- g_{2,j}^n - h_j D^+ g_{2,j}^n = -\frac{1}{\tau_j} h_j g_{2,j}^{n+1} - h_j \left(D_t^- M_{2,j}^n - D^+ M_{2,j}^n \right),$$

$$\text{where } M_{1,j}^k = \frac{1}{2}(\rho_j^k + (\rho_j^k)^2), \ M_{2,j}^k = \frac{1}{2}(\rho_j^k - (\rho_j^k)^2), \ k = n, n+1,$$

(5.9)

The relaxation model is discretized by the explicit-implicit scheme since we need it to be stable when τ is close to zero. The inviscid Burger's equation is solved by the upwind scheme using kinetic flux vector splitting. The 2nd order scheme is obtained by means of the standard 2nd order Min-Mod limiter reconstruction to replace $D^\pm$, see figure 5.1.

The vertical lines show the position of the buffer-zone. The numerical solution of the inviscid Burger's equation is not a sharp shock in the first plot because of the numerical viscosity. It is much sharper in the second plot.

From the accuracy test, we see the numerical solution of the ELU model approximates the BGK model's solution very well in both fluid region($\tau = 0.01$) and kinetic region($\tau = 1$). There is no oscillation observed here which is mentioned in the model, [18].

The solution of ELU1 model is almost independent of the buffering function $h(x)$. For example, in the degenerate case we may set $h(x)$ as a step function, i.e.

(a) 1st order   (b) 2nd order
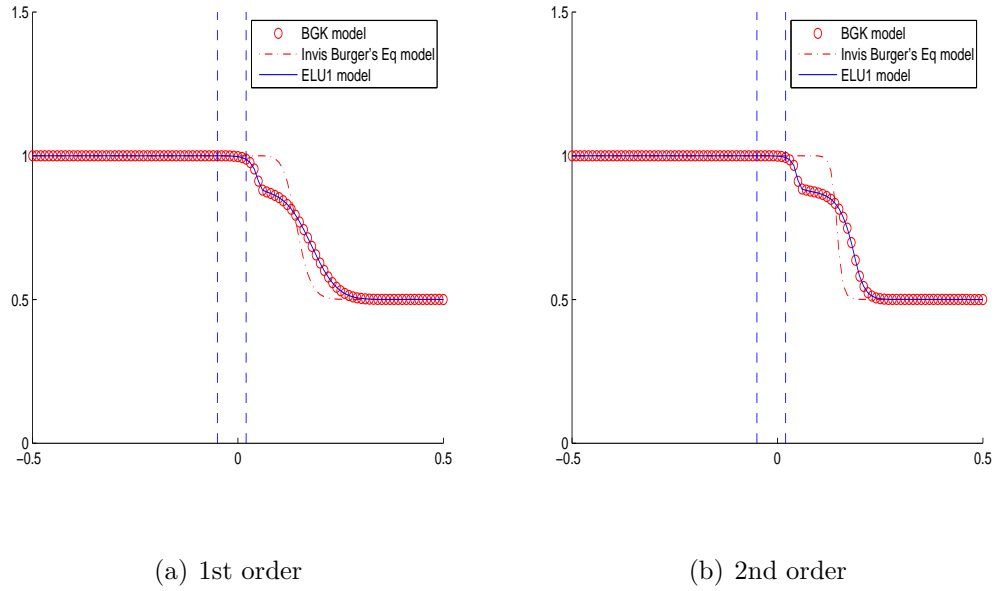
Figure 5.1: Accuracy of ELU1 with KFVS: $t = 0.2$

$a = b = 0.02$ and obtain the Figure 5.2.

It shows there is no big change for the ELU1 model's result. The ELU1 model is still a very good approximation to the BGK model.

Next we choose $\tau = 0.01$ in the whole region to test the asymptotic preserving property of the ELU1 model, Figure 5.3.

From Figure 5.2 - 5.3 we see that the three solutions of inviscid Burger's equation, ELU1 model and BGK model are very close in both plots. This shows the ELU1 model is the asymptotic preserving.

Remark. Zero-Moment Preservation of $g_1 + g_2$:

Here we only have two discrete velocity $\xi = \pm 1$. If we add up these two up-
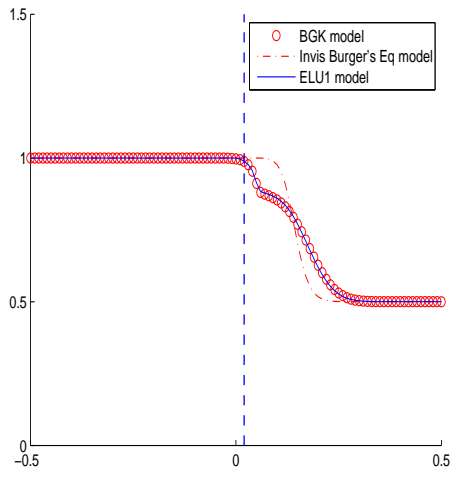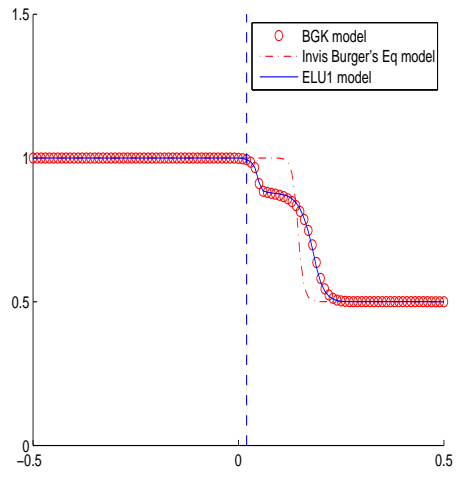
(a) 1st order   (b) 2nd order

Figure 5.2: Accuracy of ELU1 for JX with KFVS: $t = 0.2$
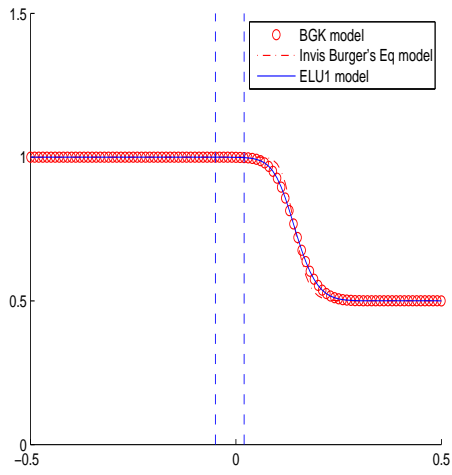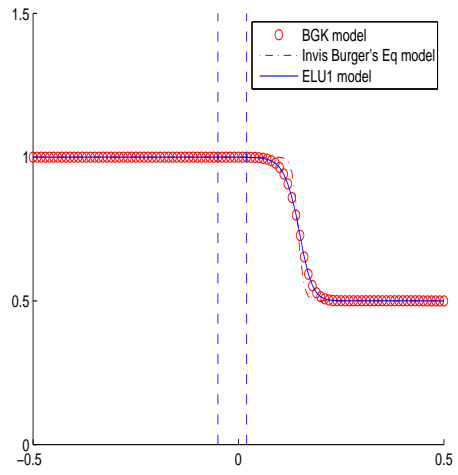
(a) 1st order   (b) 2nd order

Figure 5.3: Asymptotics test of ELU1 for JX with KFVS: $t = 0.2$

scaling equations, noticing $D_t^- \rho_j^n = D_t^- (M_{1,j}^n + M_{2,j}^n)$ since time derivative is linear, we will get

$$D_t^- (g_{1,j}^n + g_{2,j}^n) + h_j (D^- g_{1,j}^n - D^+ g_{2,j}^n) = -\frac{1}{\tau_j} h_j (g_{1,j}^{n+1} + g_{2,j}^{n+1})$$

$$- h_j \left(D_t^- \rho_{1,j}^n + D^- M_{1,j}^n - D^+ M_{2,j}^n \right)$$
(5.10)

By means of the fluid equation, we will get

$$D_t^- (g_{1,j}^n + g_{2,j}^n) = -\frac{1}{\tau_j} h_j (g_{1,j}^{n+1} + g_{2,j}^{n+1}),$$
(5.11)

This shows $g^1 + g^2 = 0$ holds if initially it holds no matter the operator $D^{\pm}$ is linear or not. No zero-moment projection is needed in this case.

Since $\rho > 0$, we may use the upwind scheme for $\partial_x (\rho^2/2)$ as $D^-(\rho^2)/2$ in the conservative form directly. Then we get the following modified upwind scheme for the up-scaling model:

$$D_t^- \rho_j^n + D^- ((\rho_j^n)^2/2) + D^- g_{1,j}^n - D^+ g_{2,j}^n = 0,$$

$$D_t^- g_{1,j}^n + h_j D^- g_{1,j}^n = -\frac{1}{\tau_j} h_j g_{1,j}^{n+1} - h_j \left(D_t^- M_{1,j}^n + D^- M_{1,j}^n \right),$$
(5.12)

$$D_t^- g_{2,j}^n - h_j D^+ g_{2,j}^n = -\frac{1}{\tau_j} h_j g_{2,j}^{n+1} - h_j \left(D_t^- M_{2,j}^n - D^+ M_{2,j}^n \right),$$

The result is show in Figure 5.4.

Notice that the first order result has big oscillations in the kinetic region. It is a little improved in the second order result. This is because the moment equation is solved in a way other than KVFS, from the previous remark, we can see the

(a) 1st order

(b) 2nd order
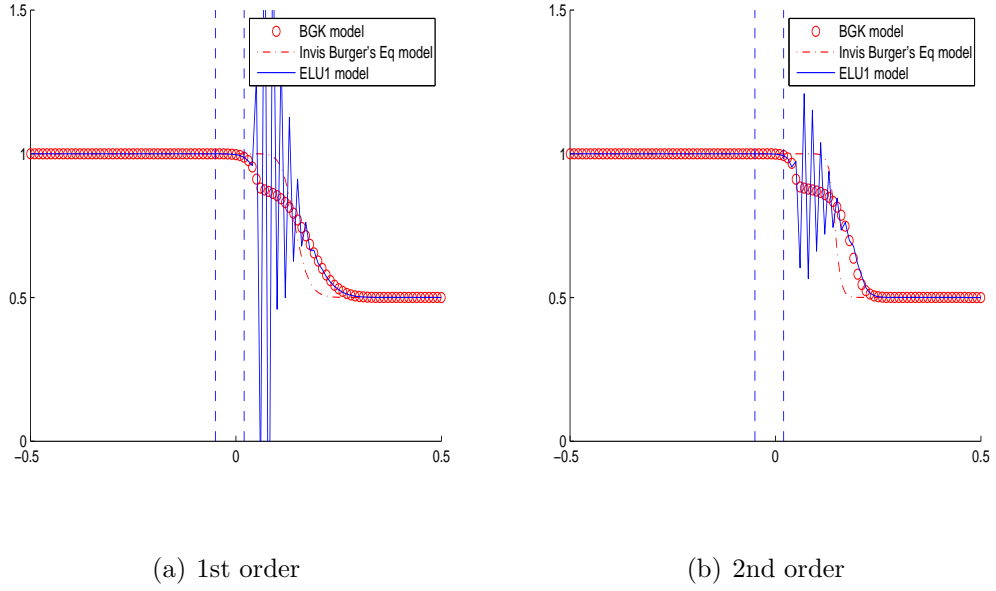
Figure 5.4: ELU1 for JX with modified upwind, No Proj: $t = 0.2$

zero-moment preservation can't hold in the modified scheme. This can be remedied if an additional zero-moment projection is applied at the end of each time step, i.e.

$$\tilde{g}_1^{n+1} = g_1^{n+1} - (g_1^{n+1} + g_2^{n+1})/2, \quad \tilde{g}_2^{n+1} = g_2^{n+1} - (g_1^{n+1} + g_2^{n+1})/2, \tag{5.13}$$

where $\tilde{g}_1^{n+1}(\tilde{g}_2^{n+1})$ will be used as $g_1^n(g_2^n)$ at the next step. This shows a big improvement in the numerical results. Here is the comparison of the results (figure: 5.5) for the second order scheme with or without projection.

(a) 1st order   (b) 2nd order
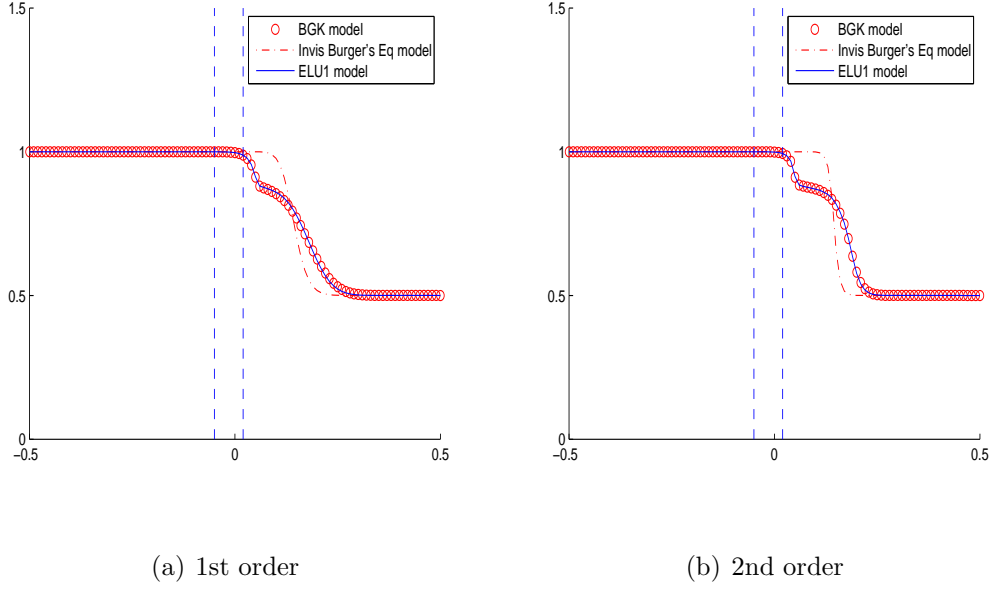
Figure 5.5: ELU1 for JX with modified Upwind + Proj: $t = 0.2$

5.1.2 NSLU Model for Jin-Xin Model

Denote $S = \frac{1}{2}(1 - F'(\rho)^2)\partial_x\rho,$, by means of the transition function h, we get the

local up-scaling model:

$$\partial_t\rho + \partial_x\left(M_1 - \tau S - (M_2 + \tau S)\right) + \partial_x(g_1 - g_2) = 0,$$

$$\partial_t g_1 + h\partial_x g_1 = h(S - \frac{1}{\tau}g_1) - h(\partial_t + \partial_x)(M_1 - \tau S), \qquad (5.14)$$

$$\partial_t g_2 - h\partial_x g_2 = -h(S + \frac{1}{\tau}g_2) - h(\partial_t - \partial_x)(M_2 + \tau S),$$

According to the kinetic flux vector splitting for the N-S equation, we use

center-difference scheme to get S, then we have the following 1st order scheme:

$$D_t^- \rho_j^n + D^-(M_{1,j}^n - \tau_j S_j^n) - D^+(M_{2,j}^n + \tau_j S_j^n) + D^- g_{1,j}^n - D^+ g_{2,j}^n = 0,$$

$$D_t^- g_{1,j}^n + h_j D^- g_{1,j}^n = h_j[-S_j^{n+1} - \frac{1}{\tau_j} g_{1,j}^{n+1} - D_t^-(M_{1,j}^n - \tau_j S_j^n) - D^-(M_{1,j}^n - \tau_j S_j^n)],$$

$$D_t^- g_{2,j}^n - h_j D^+ g_{2,j}^n = h_j[S_j^{n+1} - \frac{1}{\tau_j} g_{2,j}^{n+1} - D_t^-(M_{2,j}^n + \tau_j S_j^n) + D^+(M_{2,j}^n + \tau_j S_j^n)],$$

$$\text{where } S_j^k = (1 - (\rho_j^k)^2)D\rho_j^k, \quad k = n, n+1,$$

$$(5.15)$$

Remark. In this scheme, we may again add the two up-scaling equations to get the following by means of the moment equation:

$$D_t^-(g_{1,j}^n + g_{2,j}^n) = -\frac{1}{\tau_j} h_j(g_{1,j}^{n+1} + g_{2,j}^{n+1}), \tag{5.16}$$

It shows the zero-moment preservation of the $g_1 + g_2$. Therefore we may any discretization for $\partial_x \rho$ in S and high order nonlinear upwind operators to take the place of $D^\pm$, the $g_1 + g_2 = 0$ always holds if initially it is true.

Now we are ready to do the accuracy test for this scheme. We will take $\tau = 0.05$ as the index for the fluid region and $\tau = 1$ to denote the kinetic region and again we choose the buffer zone as $[-0.05, 0.02]$, as shown in Figure 5.6.

Here we use KVFS scheme for the viscous Burger's equation whose result shows some oscillations in the solution of the fluid model in the kinetic region. This is not unexpected since the scheme may not stable when τ is big. In fact, in the first order scheme, the kinetic scheme of the viscous Burger's equation is equivalent to the

(a) 1st order   (b) 2nd order
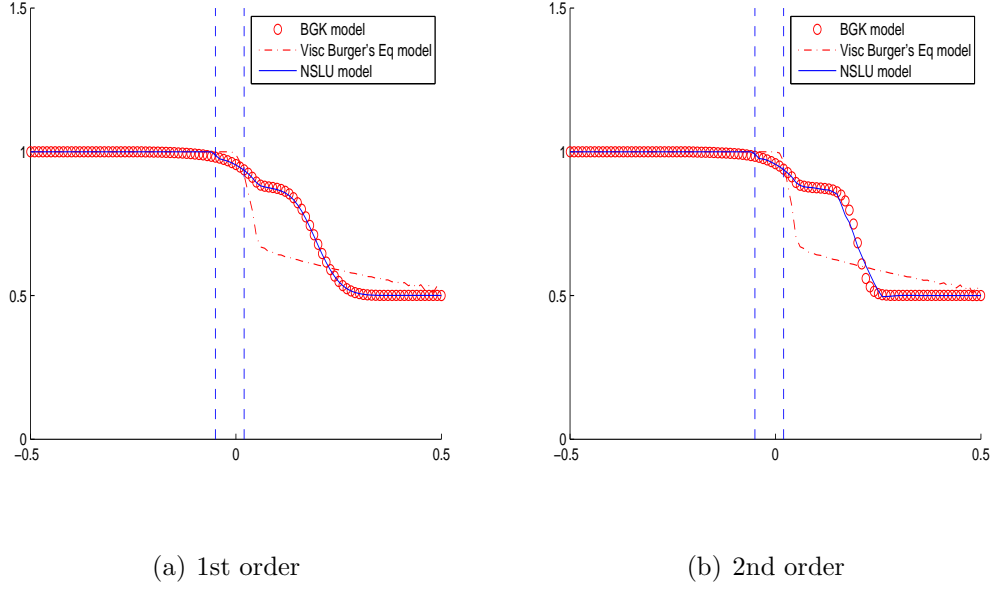
Figure 5.6: Accuracy of NSLU for JX with KFVS: $t = 0.2$

KVFS scheme of the inviscid Burger's equation plus the long-stencil discretization of the viscosity term. Since the NSLU model becomes to be the kinetic model in the kinetic region where τ is big, so it is not a problem for NSLU model and we see the solution of NSLU model is smooth.

Also we set $\tau = 0.05$ in the whole region to do the asymptotic preserving test. In this case, the inviscid Burger's equation can't be used as the fluid model. Instead we need to apply viscous Burger's equation, Figure 5.7.

Notice if we remove the up-scaling term in the fluid equation, we may get a discretization of the viscous Burger's equation:

$$D_t^- \rho_j^n + D^-(M_{1,j}^n - \tau_j S_j^n) - D^+(M_{2,j}^n + \tau_j S_j^n) = 0, \tag{5.17}$$

96

(a) 1st order   (b) 2nd order
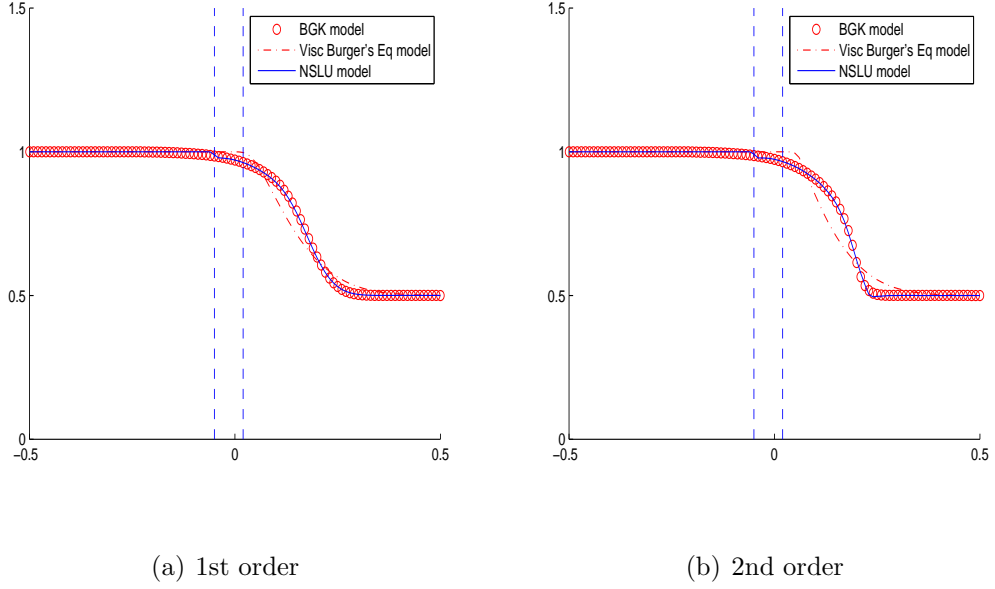
Figure 5.7: Asymtptoics of NSLU for JX with KFVS: $t = 0.2$

here the discretization of the viscosity term is as follows

$$D^-(\tau_j S_j^n) + D^+(\tau_j S_j^n) = \frac{\tau_{j+1}(1 - F'(\rho_{j+1}^n)^2)D\rho_{j+1}^n - \tau_{j-1}(1 - F'(\rho_{j-1}^n)^2)D\rho_{j-1}^n}{2},$$

(5.18)

i.e. the 2nd order center-difference scheme for the viscosity term using the long stencils. This explains that we get some oscillations in the fluid model result and they disappear when we refine the grid.

Since the viscosity term $\partial_x(\tau(1 - F'(\rho)^2)\partial_x\rho) = 2\partial_x(\tau S)$ can be discretized in a more stable and standard way:

$$2\partial_x(\tau S) \approx 2\tilde{D}(\tau_j S_j) = [\tau(1 - F'(\rho)^2)]_{j+\frac{1}{2}}D^+\rho_j - [\tau(1 - F'(\rho)^2)]_{j-\frac{1}{2}}D^+\rho_{j-1} \quad (5.19)$$

97

where the subscript$_{j+\frac{1}{2}}$ means the average of $_{j+1}$ + $_j$. Together with $D^-(\rho^2/2)$ we may consider the following discretization of the density equation in NSLU model:

$$D_t^- \rho_j^n + D^-((\rho_j^n)^2/2) + D^- g_{1,j}^n - D^+ g_{2,j}^n = 2\tilde{D}(\tau_j S_j^n) \qquad (5.20)$$

The upscaling equation is discretized the same way as before, 5.15. The result is as Figure 5.8 shows.

(a) 1st order   (b) 2nd order
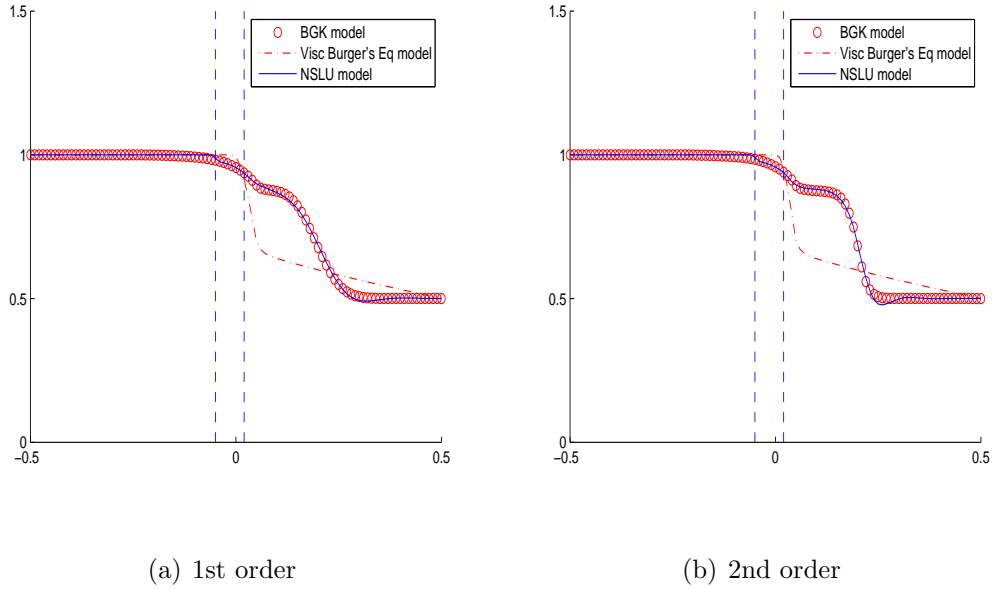
Figure 5.8: Modified scheme of NSLU for JX, No Proj: $t = 0.2$

The viscous Burger's equation's profile is smooth due to that the more stable scheme is applied. We notice there is a small bump in the plot of NSLU model due to the discontinuous initial condition for ρ and large variation of τ, which becomes more obvious in the 2nd order's result. It can't be improved by the zero-moment

projection but it will become smaller if more grid points are used. Here is the result
of 200 points. (Figure 5.9)
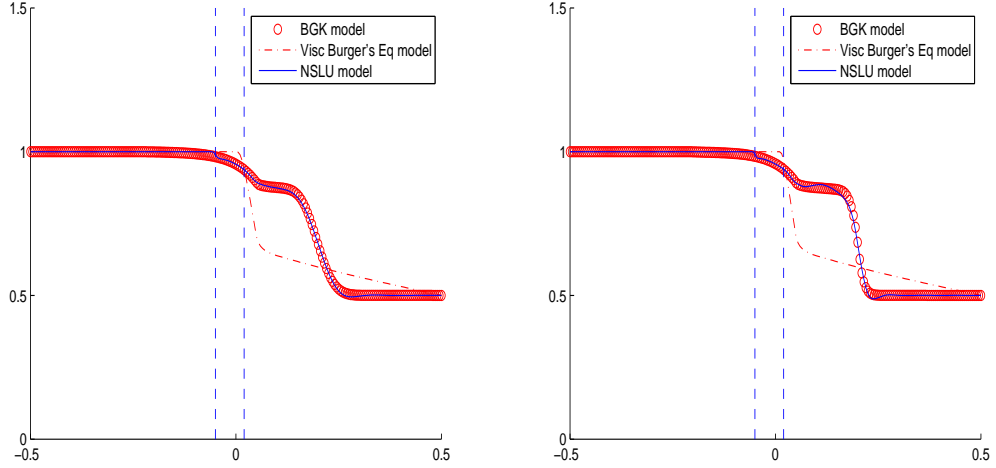
(a) 1st order (b) 2nd order

Figure 5.9: Modified scheme of NSLU for JX, No proj (200 pts): $t = 0.2$

5.2 1D1D BGK Model of Rarefied Gas Dynamics

In this example, let's consider an initial-value problem for the 1-d physical space(x)
and 1-d velocity (ξ) dimensionless BGK model for the rarefied gas

$$\partial_t f + \xi \partial_x f = \frac{1}{\kappa} \nu (\mathcal{M} - f),$$

where ρ_i are the conservative variables: the number density $\rho_1 = \rho = \langle f \rangle$, the
moment $\rho_2 = m = \langle \xi f \rangle$, and the energy density $\rho_3 = e = \frac{1}{2} \langle \xi^2 f \rangle$.

The local Maxwellian $\mathcal{M} = \frac{\rho}{\sqrt{2\pi\theta}} \exp\left(-\frac{(u-\xi)^2}{2\theta}\right)$, where ρ, u, θ are primitive variables such that $m = \rho u$ and $e = \frac{1}{2}\rho(u^2 + \theta)$.

In this example we take the collision frequency $\nu = 1$. We take $\kappa = \kappa(x)$ to incorporate the multi-scale effects. In this example, we choose $\kappa(x)$ is piecewise smooth, i.e. $\kappa = 0.001(0.01)$ in $[0, 0.6]$ and $\kappa = 1$ in $[0.65, 1]$ and is linear in $[0.6, 0.65]$.

The initial set-up of ρ, u, θ is taken as a uniform flow plus a perturbation , as follows:

$$\rho_0 = 1 + \frac{0.1}{\sqrt{0.002\pi}} \exp\left(-\frac{(x - 0.5)^2}{0.002}\right), \quad u_0 = 0, \quad \theta_0 = 1,$$

Then f_0 is set to be the equilibrium determined by ρ_0, u_0, θ_0.

In the numerical test, we choose the computational domain as $[0, 1]$ which is big enough to avoid boundary effects.

The kinetic model will be solved using the implicit-explicit scheme to make sure it is stable at the region where $\kappa(x)$ is small.

A simpler Euler equations for this 1D1D BGK model from C-E expansion will be:

$$\partial_t U + \partial_x F(U) = 0, \qquad U = \begin{bmatrix} \rho \\ m \\ E \end{bmatrix}, \qquad F = \begin{bmatrix} m \\ nu^2 + p \\ u(E + p) \end{bmatrix}, \qquad (5.21)$$

where the $m = \rho u$ is the momentum and $E = \rho e$ is the total energy. In this case

100

$\gamma = 3$ so $e = \frac{1}{2}(u^2 + RT)$.

5.2.1   ELU1 Model for 1D1D BGK Model

Apply the zero-order C-E expansion, we get the compressible Euler equation with $\gamma = 3$, i.e.

$$\partial_t \rho + \partial_x F_1 = \partial_t \rho + \partial_x(\rho u) = 0,$$

$$\partial_t(\rho u) + \partial_x F_2 = \partial_t(\rho u) + \partial_x(\rho(u^2 + \theta)) = 0, \qquad (5.22)$$

$$\partial_t(\rho(u^2 + \theta)) + \partial_x F_3 = \partial_t(\rho(u^2 + \theta)) + \partial_x(\rho u(u^2 + 3\theta)) = 0,$$

Here $F_i(\rho, u, \theta)$ are the fluxes in the above equations. Using the flux splitting method (e.g. SWS or KVFS), we get the first order numerical scheme for the compressible Euler equation:

$$D_t^- \rho_j^n + D^- F_{1,j}^{+;n} + D^+ F_{1,j}^{-;n} = 0,$$

$$D_t^- (\rho_j^n u_j^n) + D^- F_{2,j}^{+;n} + D^+ F_{2,j}^{-;n} = 0, \qquad (5.23)$$

$$D^- (\rho_j^n((u_j^n)^2 + \theta_j^n)) + D^- F_{3,j}^{+;n} + D^+ F_{3,j}^{-;n} = 0,$$

By means of the smooth transition function $h(x)$ we get the ELU1 model as the following:

$$\partial_t \rho + \partial_x F_1 = 0, \quad \partial_t(\rho u) + \partial_x F_2 = 0,$$

$$\partial_t(\rho(u^2 + \theta)) + \partial_x F_3 + \partial_x \langle \xi^3 g_K \rangle = 0, \qquad (5.24)$$

$$\partial_t g + h\xi \partial_x g = -\frac{1}{\kappa}hg - h(\partial_t \mathcal{M} + \xi \partial_x \mathcal{M}),$$

101

Notice the 1st and 2nd equations don't have the up-scaling term due to the zero-moments of the non-fluid part g.

The first order upwind scheme with flux splitting is as follows:

$$D_t^- \rho_j^n + D^- F_{1,j}^{+;n} + D^+ F_{1,j}^{-;n} = 0, \quad D_t^- (\rho_j^n u_j^n) + D^- F_{2,j}^{+;n} + D^+ F_{2,j}^{-;n} = 0,$$

$$D_t^- (\rho_j^n ((u_j^n)^2 + \theta_j^n)) + D^- F_{3,j}^{+;n} + D^+ F_{3,j}^{-;n} + D^- \langle \xi_k^+ \xi_k^2 g_{j,k}^n \rangle + D^+ \langle \xi_k^- \xi_k^2 g_{j,k}^n \rangle = 0,$$

$$D_t^- g_{j,k}^n + h_j (D^- (\xi_k^+ g_{j,k}^n) + D^+ (\xi_k^- g_{j,k}^n)) = -\frac{1}{\tau_j} h_j g_{j,k}^{n+1}$$

$$- h_j \left(D_t^- \mathcal{M}_{j,k}^n + D^- (\xi_k^+ \mathcal{M}_{j,k}^n) + D^+ (\xi_k^- \mathcal{M}_{j,k}^n) \right),$$

$$(5.25)$$

We choose $\kappa(x) = 0.001$ in the fluid region ($[0, 0.6]$), which is small enough so the Euler equation is valid approximation to the BGK model.

The buffer zone is chosen as $[0.50, 0.55]$. We choose 100 points in x-direction and 50 points in ξ-direction with the velocity range $[-5, 5]$, which means ξ will be within 5 standard deviations initially. The Δt is taken to satisfy the CFL condition, i.e. $\Delta t / \Delta x \leq 1/5$. For the numerical scheme of BGK model, we use the explicit-implicit scheme which is stable when τ is small.

We will use KVFS introduced in chapter 1 to split the fluxes in the fluid equation. Here are results of the first and second order schemes. The top left figure shows the profiles of the Knudsen number $\kappa(x)$ and the buffer-zone function $h(x)$. The the top right, bottom left and bottom right figures are the profiles of ρ, u, θ accordingly, as the Figure 5.10 shows.
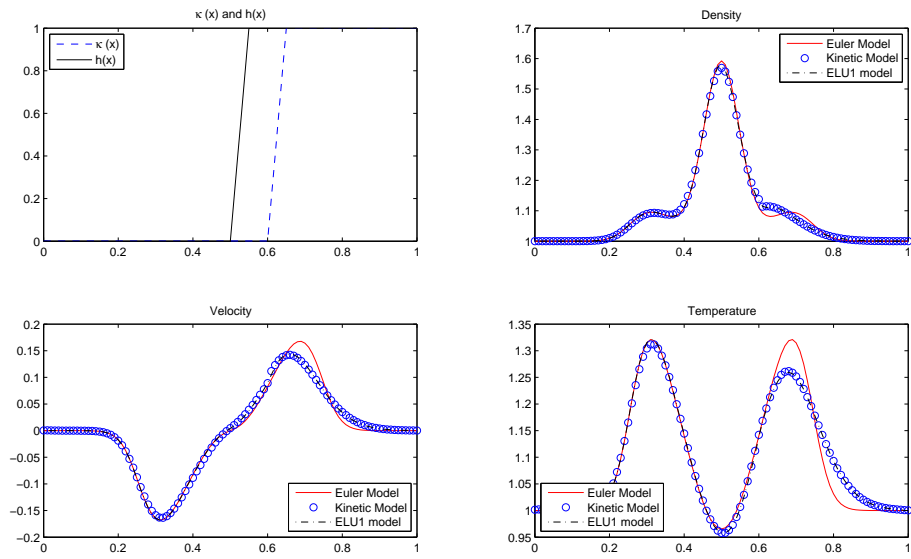
(a) 1st order
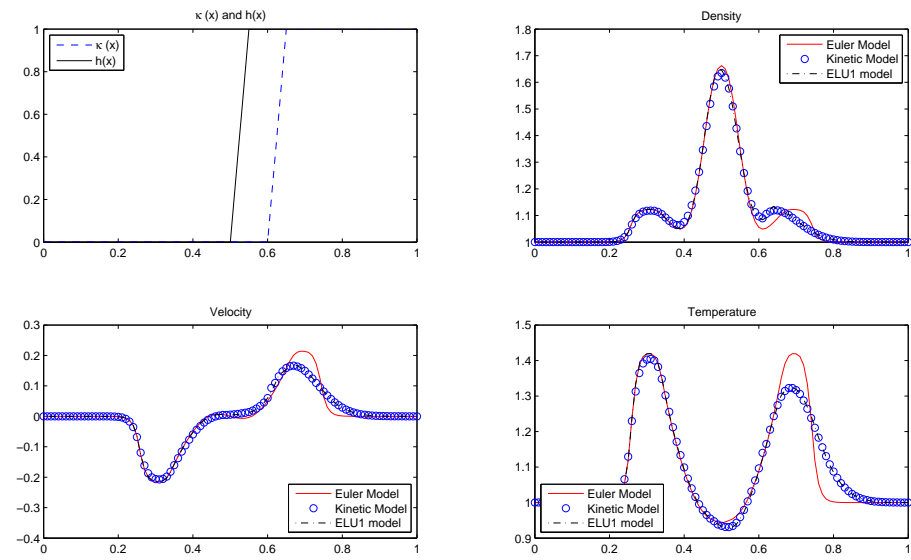
(b) 2nd order

Figure 5.10: Accuracy of ELU1 for 1D1DBGK,KFVS,$t = 0.1$

We choose $\kappa(x) = 0.001$ in the whole region to do the asymptotic preserving test. It is shown in Figure 5.11.

From these results, we see the up-scaling solution approximates the BGK's solution very well in the whole region in both accuracy test and asymptotic preserving test.

We may also use the Steger-Warming splitting(SWS) in chapter 1.6.1 for the fluid equations in ELU1 model. Set the artificial viscosity $\varepsilon = 0.02$ and get Figure 5.12.

The Euler model's result is sharper than the previous result due to a smaller artificial viscosity. Like the Jin-Xin model, some oscillations occur around the interface between the fluid region and the kinetic region. By means of the zero-moment projection, these oscillations will disappear, as Figure 5.13 shows.

Remark. the different behavior of the zero-moment preservation for KVFS and SWS

We consider the zero-moments preservation of the non-fluid part g. Here the zero-moment of g can't be preserved due to the error of numerical integral. In other words, because $\sum \xi_k^i \mathcal{M}_k \neq \rho^i$, $i = 0, 1, 2$ and similar reason for the fluxes, we can't get the preservation of $\sum_j \xi^i g_j$, $i = 0, 1, 2$ even if we try the KVFS and the minimization method in [37]. This is different from Jin-Xin model.

On the other hand, it is well-known that the trapezoid rule for numerical quadrature has spectral accuracy if the integrated function is periodic and C^∞ in
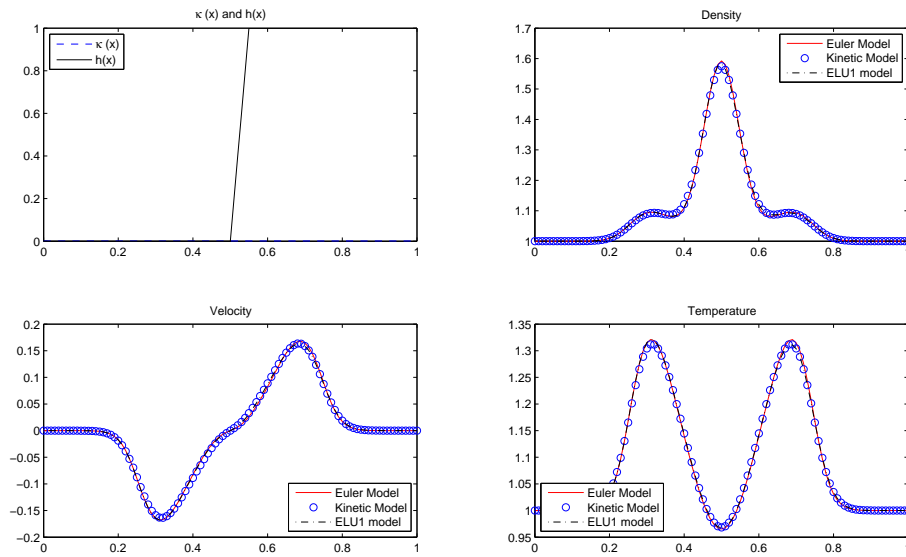
(a) 1st order
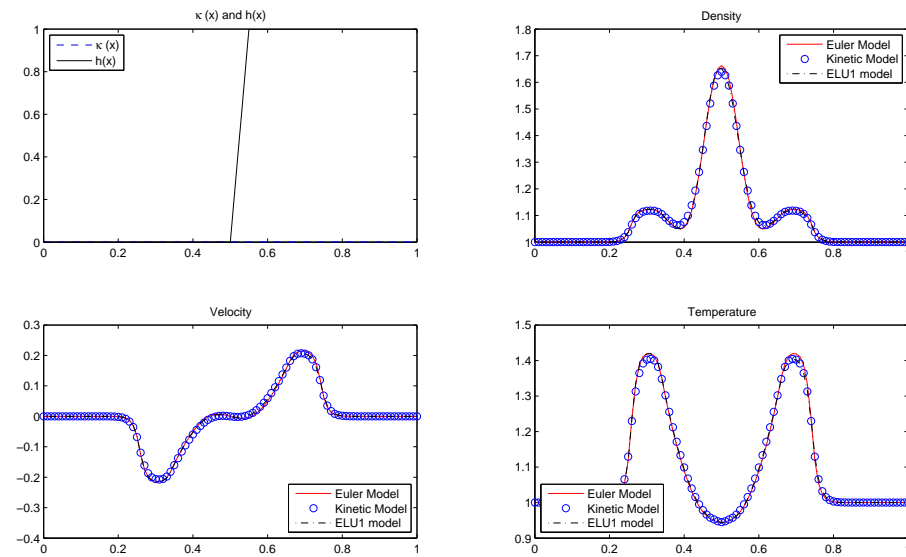
(b) 2nd order

Figure 5.11: Asymptotic of ELU1 for 1D1DBGK,KFVS,$t = 0.1.\kappa = 0.001$
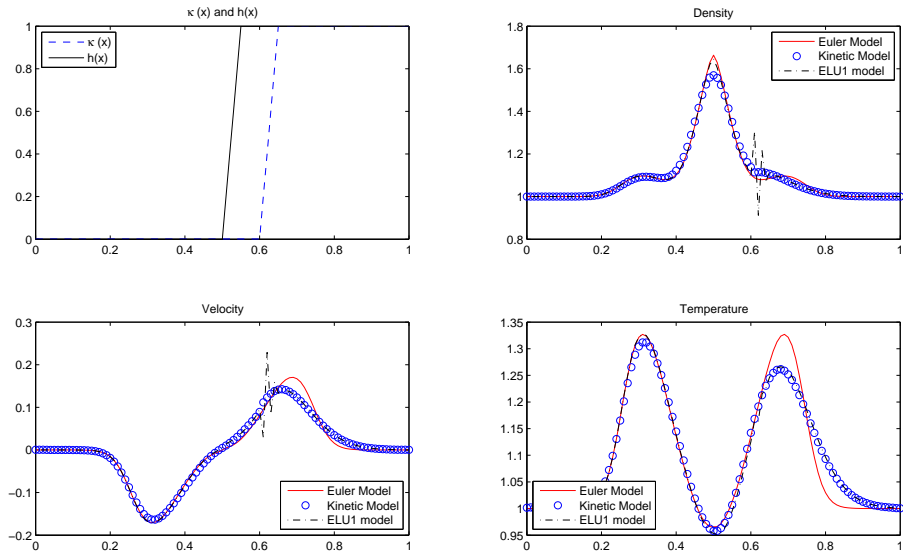
(a) 1st order
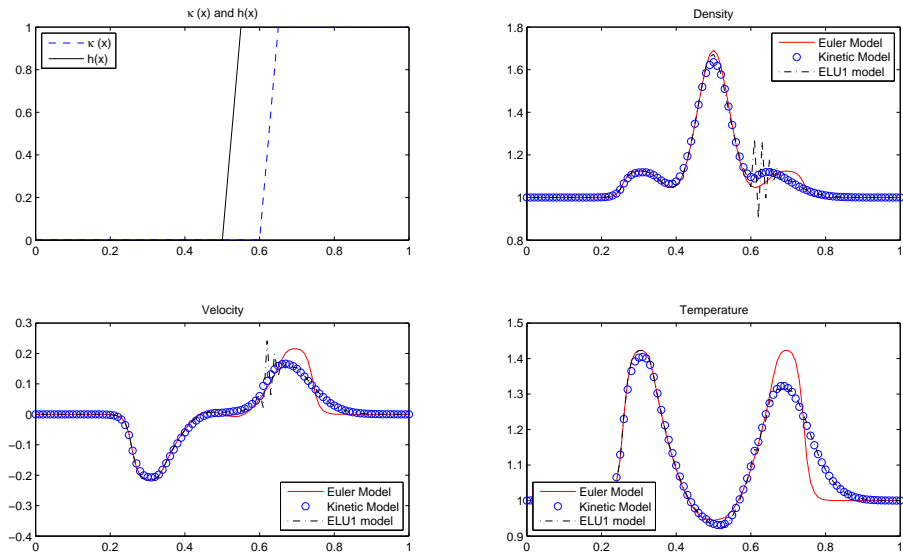
(b) 2nd order

Figure 5.12: Accuracy of ELU1 for 1D1DBGK, SWS: $t = 0.1$
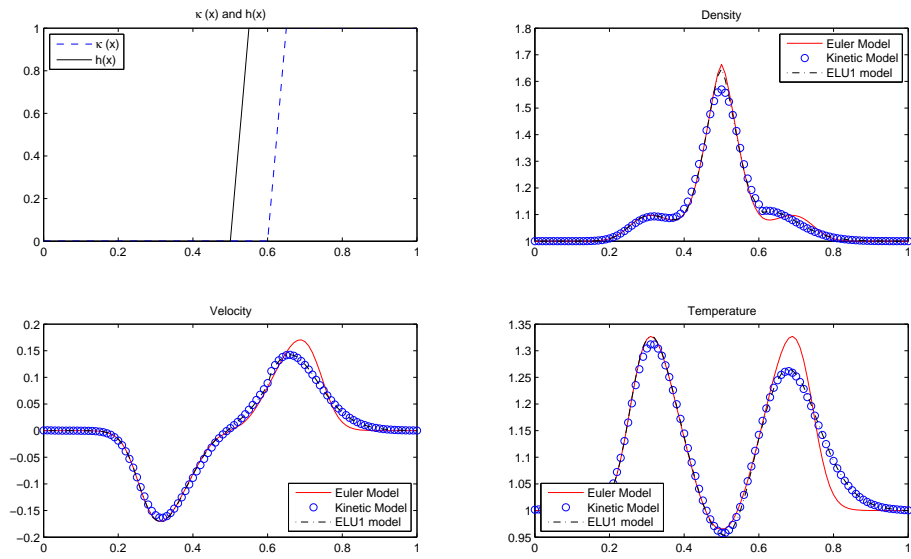
(a) 1st order
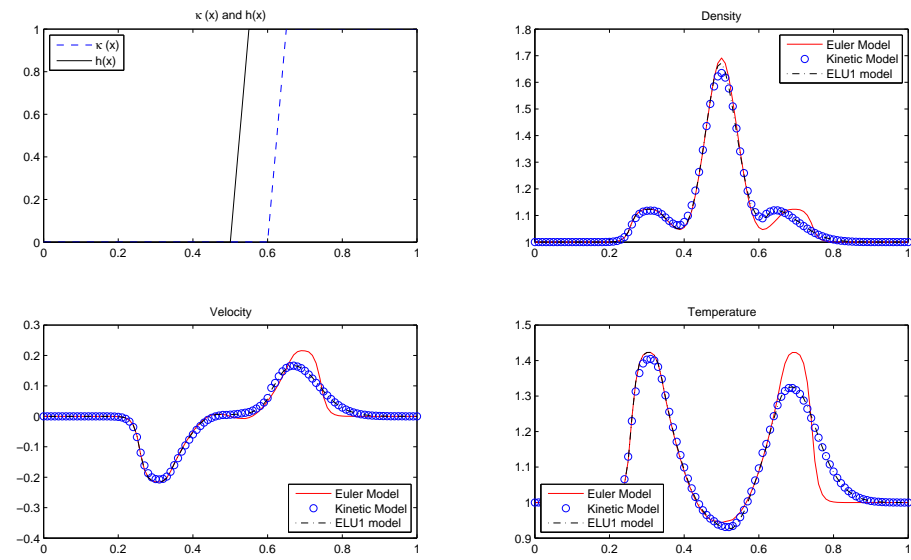
(b) 2nd order

Figure 5.13: Accuracy of ELU1 for 1D1DBGK, SWS + Proj: $t = 0.1$

107

the region. Here the Maxwellian $\mathcal{M}(\xi)$ is a smooth function and decays exponentially when ξ approaches infinity. If we select a big range for ξ like three standard deviations away from the mean so $\mathcal{M}(\xi)$ can be approximately treated as a periodic function in this interval. Also we choose uniform grid with many points($= 50$) to discretize ξ and the summation becomes to be the trapezoid rule for the integral. In this way, the numerical integral should have spectral accuracy and the error could be ignored. Then the zero-moment of g will be approximately preserved in the KVFS scheme ($\langle g \rangle, \langle \xi g \rangle, \langle \xi^2 g \rangle \approx 0.02$). See Figure 5.14.

For the ELU1 model with SWS, the zero-moment of g can't be preserved at all even ignoring the numerical integration error(≈ 0.2) as the Figure 5.15 shows.

5.2.2   ELU2 Model for 1D1D BGK Model

Notice $\langle \xi^3 g \rangle = \langle (\xi - u)^3 f \rangle$. As already discussed in the Chapter 2.2.3.2, the ELU2 model is the following:

$$\partial_t \rho + \partial_x F_1 = 0, \quad \partial_t(\rho u) + \partial_x F_2 = 0,$$

$$\partial_t(\rho(u^2 + \theta)) + \partial_x F_3 + h\partial_x \langle (\xi - u)^3 f \rangle = 0, \tag{5.26}$$

$$\partial_t f + \xi \partial_x f = \frac{1}{\tau}(\mathcal{M} - f),$$

Here three moment equations will be solved in the whole region $[0, 1]$, while f is solved only in the kinetic region $[0.5, 1]$ In order to get a smooth transition, we multiply the up-scaling term $\partial_x \langle (\xi - u)^3 f \rangle$ by a artificial transition function $h(x)$,

108
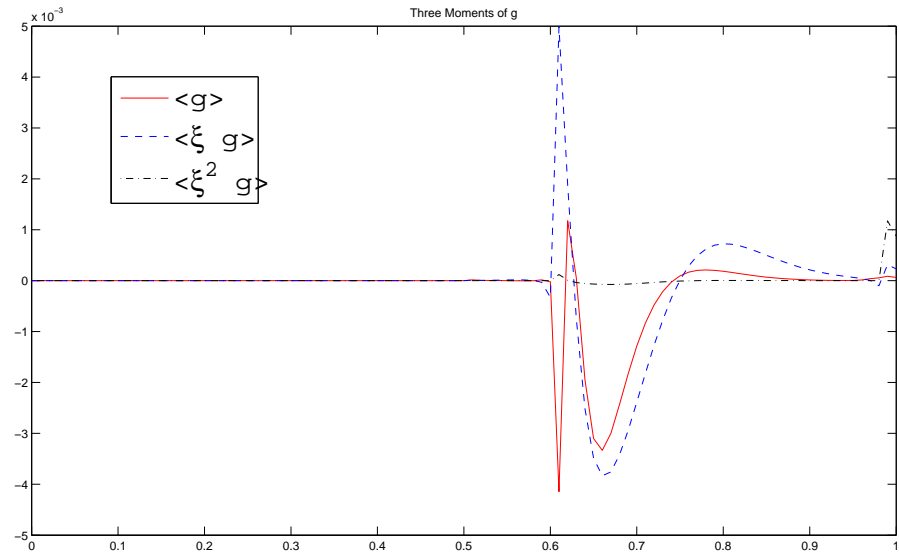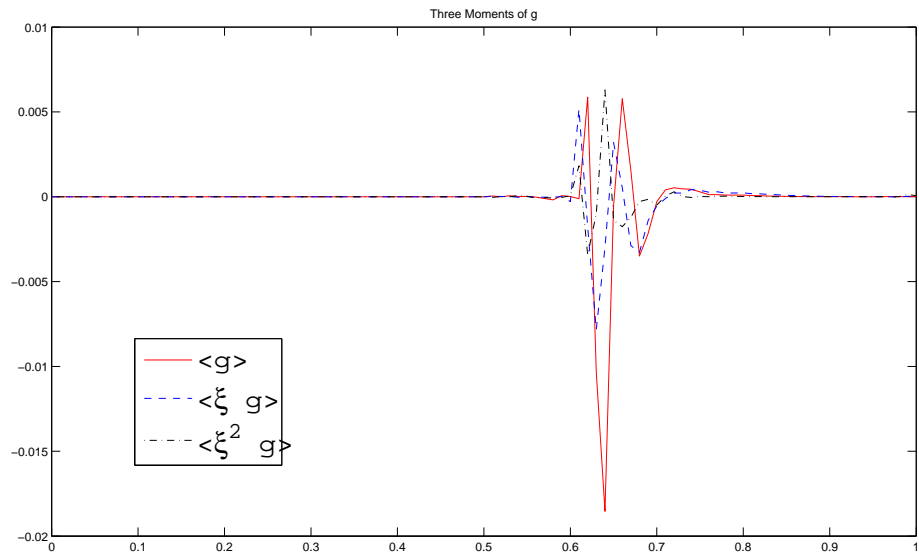
(a) 1st order

(b) 2nd order

Figure 5.14: Three moments of g of ELU1 for 1D1DBGK, KFVS:$t = 0.1$
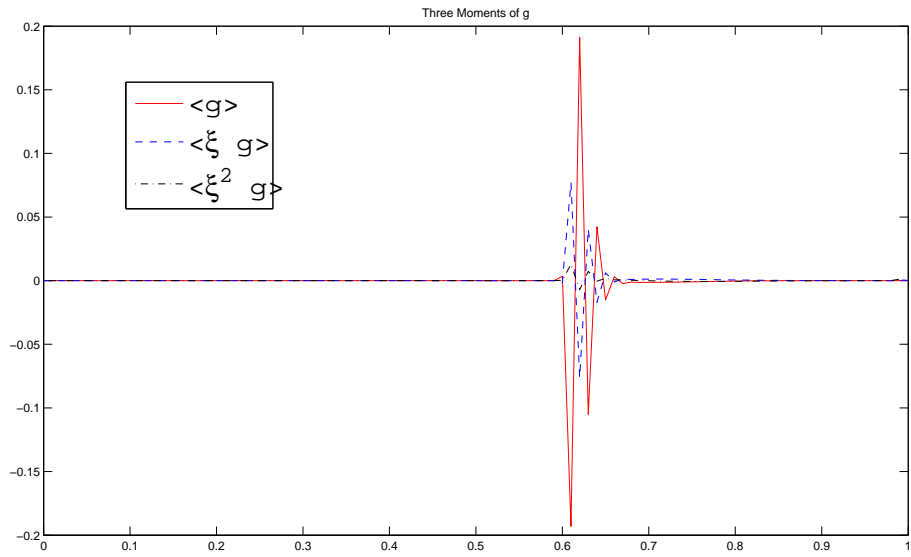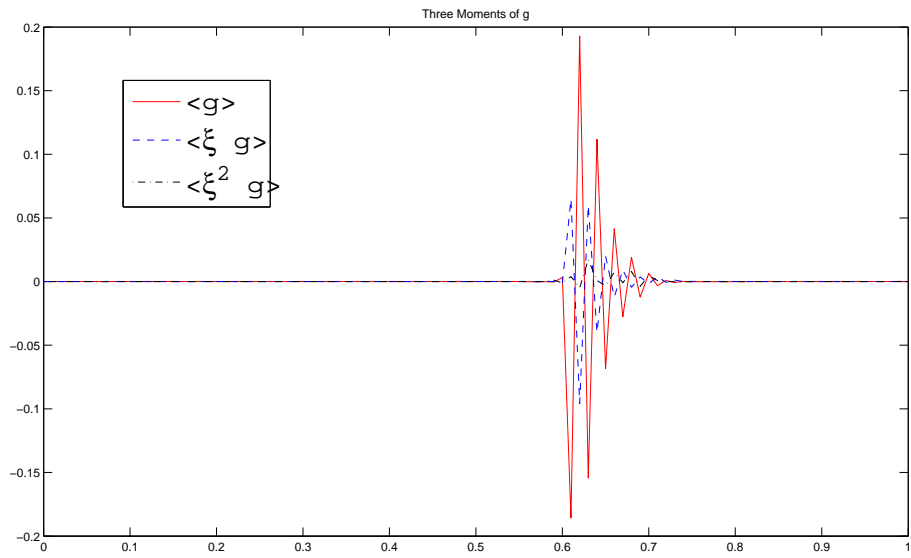
(a) 1st order

(b) 2nd order

Figure 5.15: Three moments of g of ELU1 for 1D1DBGK, SWS: $t = 0.1$

which works the same way as the buffer-zone function.

The first order upwind scheme with flux splitting is as follows:

$$D_t^- \rho_j^n + D^- F_{1,j}^{+;n} + D^+ F_{1,j}^{-;n} = 0, \quad D_t^- (\rho_j^n u_j^n) + D^- F_{2,j}^{+;n} + D^+ F_{2,j}^{-;n} = 0,$$

$$D_t^- (\rho_j^n ((u_j^n)^2 + \theta_j^n)) + D^- F_{3,j}^{+;n} + D^+ F_{3,j}^{-;n} + h_j D \left(\sum_k (\xi_k - u)^3 f_{j,k}^n \right) = 0,$$

$$D_t^- f_{j,k}^n + D^- (\xi_k^+ f_{j,k}^n) + D^+ (\xi_k^- f_{j,k}^n) = \frac{1}{\tau_j} \left(\mathcal{M}_{j,k}^{n+1} - f_{j,k}^{n+1} \right),$$

The interface is set at $x = 0.5$. Therefore the inflow boundary condition on the interface for f is the half Maxwellian, i.e. $f(t, 0.5, \xi) = \mathcal{M}(t, 0.5, \xi)$ for $\xi > 0$. Boundary condition at $x = 1$ is the same as BGK model. The initial condition will be the same as the BGK model. Figure 5.16 is the numerical result using KVFS as the flux splitting method.

Also we may try SWS instead to get the result in Figure 5.17. Notice there is no oscillation in the result. No projection is needed for ELU2 model.

5.2.3   NSLU Model for 1D1D BGK Model

We apply the first order C-E expansion of the distribution function and get

$$f_1 = \left(1 + \kappa \left[\frac{(u - \xi)^3 - 3(u - \xi)\theta}{2\theta^2} \partial_x \theta \right] \right) \mathcal{M} = \mathcal{M} + \kappa S, \qquad (5.27)$$

here the $S = \left(\frac{(u-\xi)((u-\xi)^2 - 3\theta)}{2\theta^2} \partial_x \theta \right) \mathcal{M}$ is the Navier-Stokes non-equilibrium part.

By taking the moments, i.e. plug the expression of f into the BGK equation, multiply its both sides with the collision invariants $1, \xi, \frac{1}{2}\xi^2$ respectively and integrate
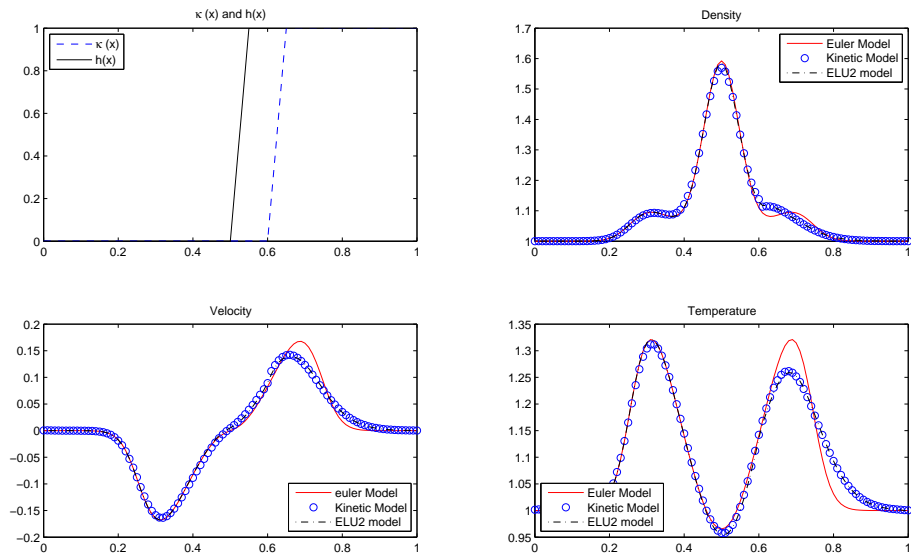
(a) 1st order
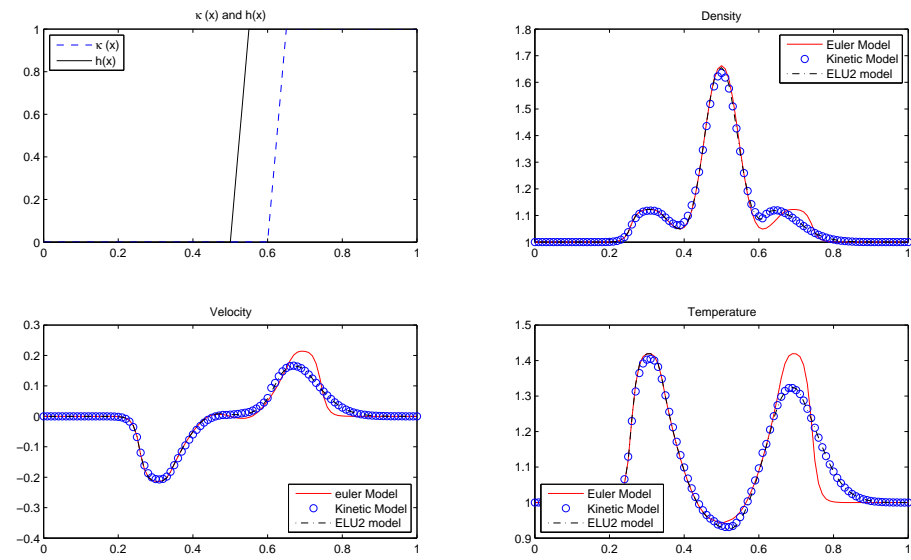
(b) 2nd order

Figure 5.16: Accuracy of ELU2 for 1D1DBGK, KFVS: $t = 0.1$
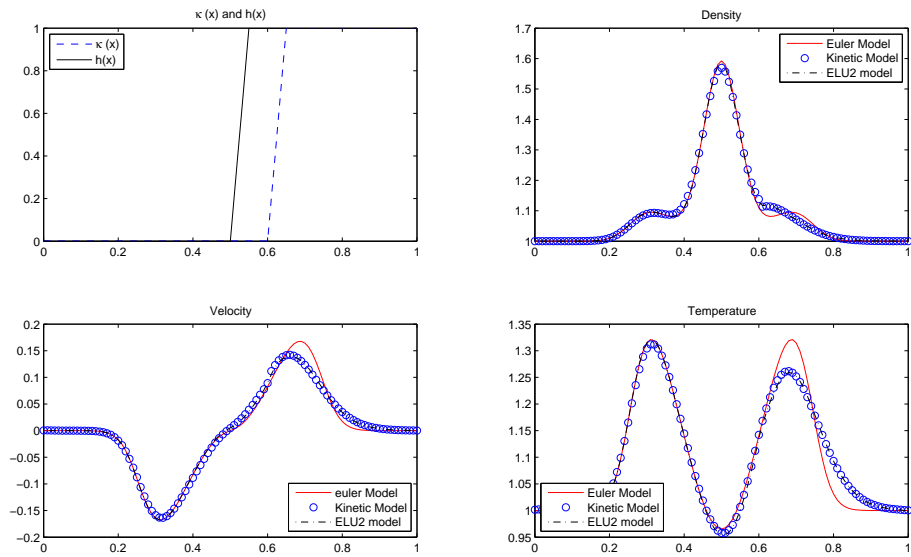
(a) 1st order
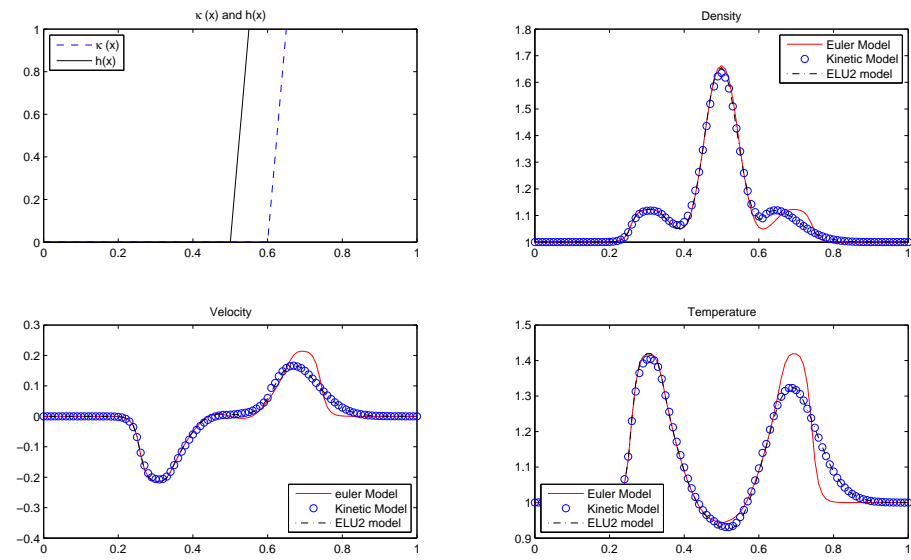
(b) 2nd order

Figure 5.17: Accuracy of ELU2 for 1D1DBGK, SWS: $t = 0.1$

113

them over the velocity space, we get the Navier-Stokes equation:

$$\partial_t \rho + \partial_x (F_1 + \kappa T_1) = 0,$$

$$\partial_t (\rho u) + \partial_x (F_2 + \kappa T_2) = 0, \tag{5.28}$$

$$\partial_t (\rho(u^2 + \theta)) + \partial_x (F_3 + \kappa T_3) = 0,$$

Here the $F_i (i = 1, 2, 3)$ are the fluxes of the Euler equations. $T_i = \langle \xi^i S \rangle (i = 1, 2, 3)$ are the viscosity terms. In fact $T_1 = T_2 = 0$ and $T_3 = -3\rho\theta\partial_x\theta$. Therefore this system is an Euler system plus a heat flux.

For the KVFS, we get $F_i^{\pm}(i = 1, 2, 3)$ is same as the Euler equations. The heat flux

$$T_3^{\pm} = \langle \xi^{\pm} \xi^2 S \rangle = -\frac{3}{2}\rho\theta \text{ erfc}\left(\mp\frac{u}{\sqrt{2\theta}}\right)\partial_x\theta, \tag{5.29}$$

The partial derivative $\partial_x \theta$ in T_3 will be discretized using the center-difference scheme, i.e.

$$T_{3,j}^{n,\pm} = -\frac{3}{2}\rho_j^n \theta_j^n \text{ erfc}\left(\mp\frac{u_j^n}{\sqrt{2\theta_j^n}}\right)D\theta_j^n, \tag{5.30}$$

Therefore the 1st order up-wind scheme based on the flux splittings of the Navier-Stokes equation is as follows:

$$D_t^- \rho_j^n + D^- F_{1,j}^{+;n} + D^+ F_{1,j}^{-;n} = 0,$$

$$D_t^- (\rho_j^n u_j^n) + D^- F_{2,j}^{+;n} + D^+ F_{2,j}^{-;n} = 0, \tag{5.31}$$

$$D^- (\rho_j^n((u_j^n)^2 + \theta_j^n)) + D^- (F_{3,j}^{+;n} + \kappa_j T_{3,j}^{+;n}) + D^+ (F_{3,j}^{-;n} + \kappa_j T_{3,j}^{-;n}) = 0,$$

where $F_i^{\pm}(i = 1, 2, 3)$ is same as the Euler equations. Since the KVFS is obtained from the collision-less Boltzmann equation, it can only be applied if the Knudsen

114

number is small. This explains the instability of the scheme in the kinetic region. In the numerical test, we will use center-difference scheme to discretize the viscosity term instead of upwind scheme to improve the stability. In other words, we use the following scheme for the 3rd equation:

$$D^-(\rho_j^n((u_j^n)^2 + \theta_j^n)) + D^- F_{3,j}^{+,n} + D^+ F_{3,j}^{-,n} + \tilde{D}T_{3,j}^n = 0,$$

$$\text{where } \tilde{D}T_{3,j}^n = D^-([-3\rho\theta]_{j+1/2}^n D^+\theta_j^n),$$

(5.32)

Again, by means of the transition function $h(x)$ we get the NSLU model for

$$\partial_t\rho + \partial_x F_1 = 0, \quad \partial_t(\rho u) + \partial_x F_2 = 0,$$

$$\partial_t(\rho(u^2 + \theta)) + \partial_x(F_3 + \kappa T_3) + \partial_x\langle \xi^3 g\rangle = 0,$$

$$\partial_t g + h\partial_x(\xi g) = -hS - \frac{1}{\kappa}hg - h(\partial_t + \partial_x\xi)f_1,$$

$$\text{where} \quad f_1 = \mathcal{M} + \kappa S,$$

(5.33)

The 1st order upwind scheme is as follows:

$$D_t^- \rho_j^n + D^- F_{1,j}^{+,n} + D^+ F_{1,j}^{-,n} = 0,$$

$$D_t^- (\rho_j^n u_j^n) + D^- F_{2,j}^{+,n} + D^+ F_{2,j}^{-,n} = 0,$$

$$D_t^- (\rho_j^n ((u_j^n)^2 + \theta_j^n)) + D^- (F_{3,j}^{+,n} + \kappa_j T_{3,j}^{+,n}) + D^+ (F_{3,j}^{-,n} + \kappa_j T_{3,j}^{-,n}) +$$

$$D^- \sum_k (\xi^+ \xi_k^2 g_{k,j}^n)) + D^+ \sum_k (\xi^- \xi_k^2 g_{K,j}^n)) = 0, \tag{5.34}$$

$$D_t^- g_{K,j}^n + h_j D^- (\xi_k^+ g_{k,j}^n) + h_j D^+ (\xi_k^- g_{k,j}^n) = -h_j S_j^{n+1} - \frac{1}{\kappa_j} h_j g_{K,j}^{n+1}$$

$$- h_j (D_t^- + D^- \xi_k^+ + D^+ \xi_k^-)(\mathcal{M}_j^n + \kappa_j S_j^n),$$

$$\text{where } S_j^k = \left(\frac{(u_j^k - \xi)^3 - 3(u_j^k - \xi)\theta_j^k}{2(\theta_j^k)^2} D\theta_j^k \right) \mathcal{M}_j^k, \quad k = n, n+1,$$

In order to see the difference between the ELU1 model and NSLU model. We choose a bigger Knudsen number $\kappa = 0.005$ in $[0, 0.6]$ and $\kappa = 1$ in $[0.65, 1]$ and is linear in $[0.6, 0.65]$. We choose 100 points in x-direction and 50 points in ξ-direction with the velocity range $[-5, 5]$. The Δt is taken to satisfy the CFL conditions. We may try the ELU1 model with KVFS first. Here is the numerical result for the comparison of the compressible Euler equation and BGK model. From the first plot in Figure 5.18, we can tell the big difference between these two models even in the fluid region $[0, 0.5]$.

Now that κ is much bigger in the fluid region so the Euler model is not a good fluid model to the BGK model. We can easily tell this by comparing the graphs in the fluid region. The Navier-Stokes equations has a much better fitness with the

116
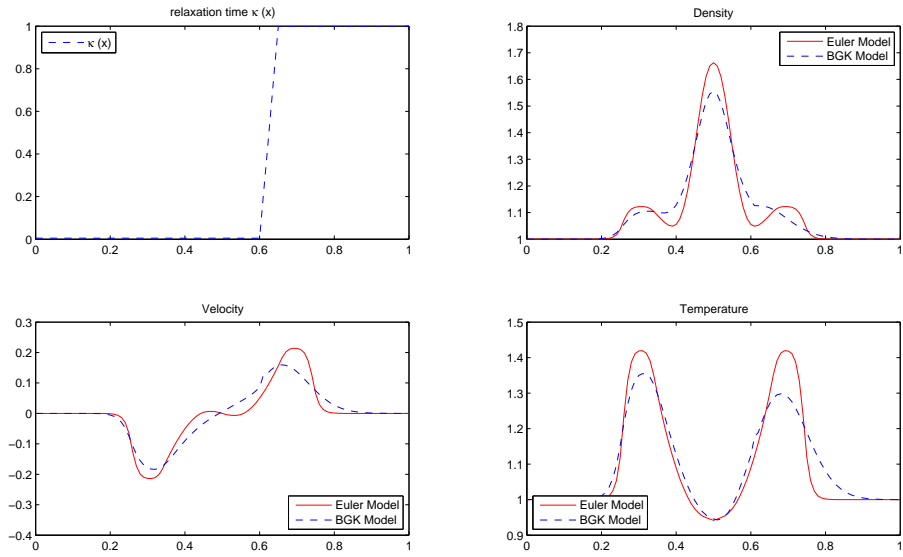
(a) Euler and BGK
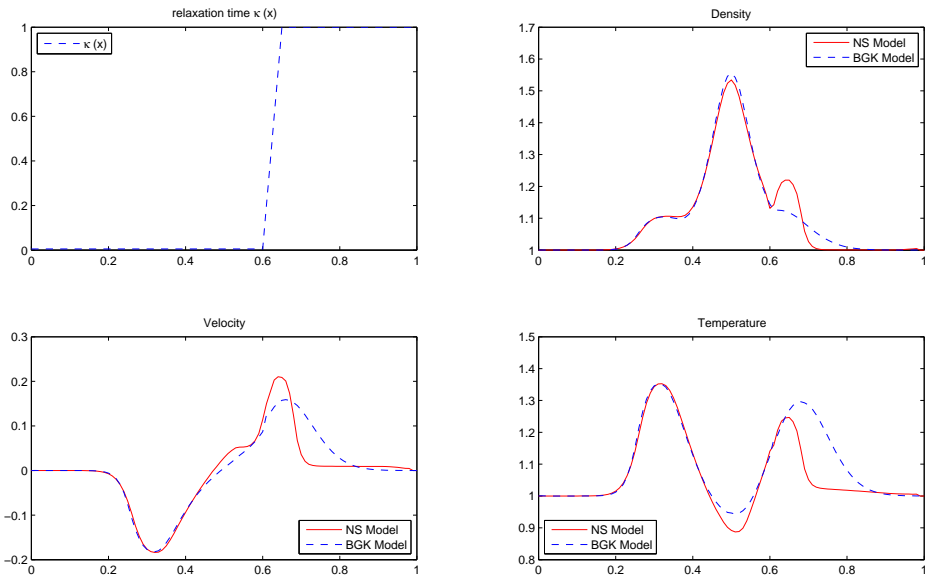
(b) NS and BGK

Figure 5.18: Comparison of Euler/BGK & NS/BGK, $\kappa = 0.005$(fluid) : $t = 0.1$

117

BGK model in the fluid region (second plot in Figure 5.18). In this case, we should apply NSLU model to approximate the BGK model instead of ELU1 (ELU2) model.

From the figure 5.19, we may observe small oscillations in the first order plot, which become bigger in the second order plot. If we take a look at the three moments of g in NSLU model (Figure 5.20), we will see the moments of g are not preserved very well in this case. (≈ 0.08 for second order plot)

The reason is that in ELU1 model the moments we need are up to third order to get the moments' equation for g, but in NSLU model we need the fifth order moments due to the existence of S. Therefore the numerical integrations' error can't be ignored any more. The result can be improved by means of the zero-moment projection for g (Figure 5.21. Please refer the appendix for the formula of the projection.

If we apply SWS for the Euler fluxes and center-differencing for the viscosity
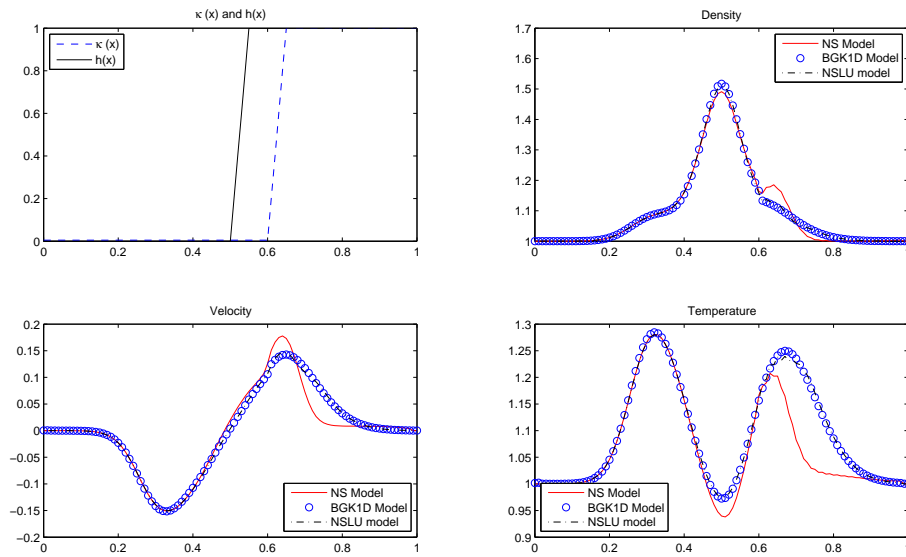
(a) 1st order
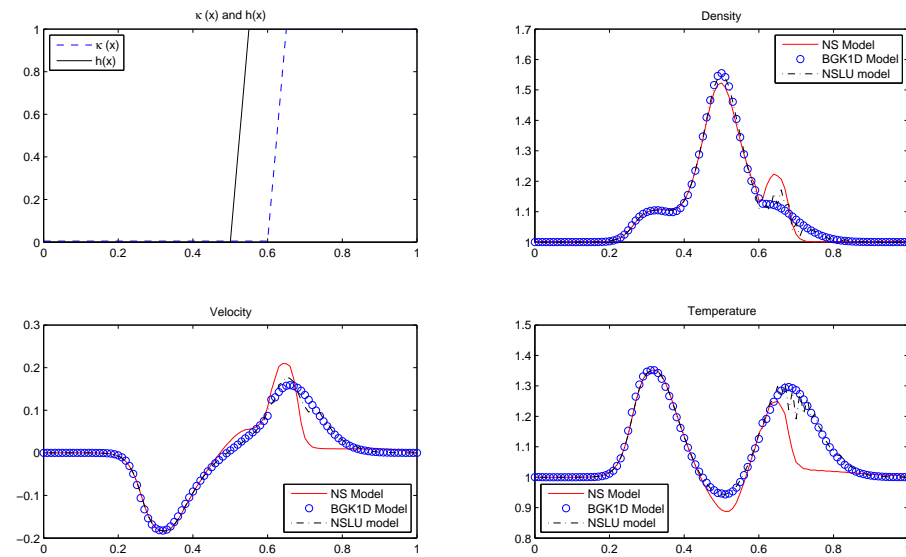
(b) 2nd order

Figure 5.19: Accuracy of NSLU for 1D1DBGK, KFVS, No Proj: $t = 0.1$
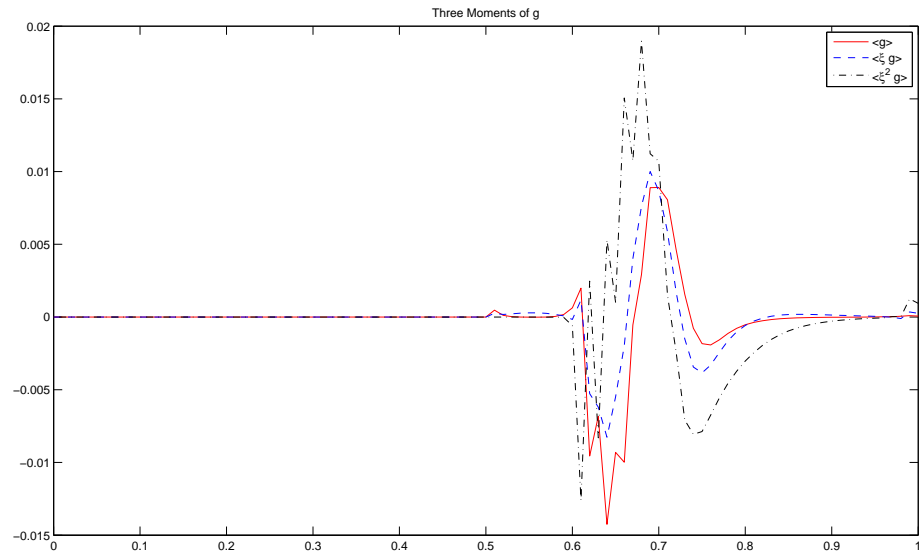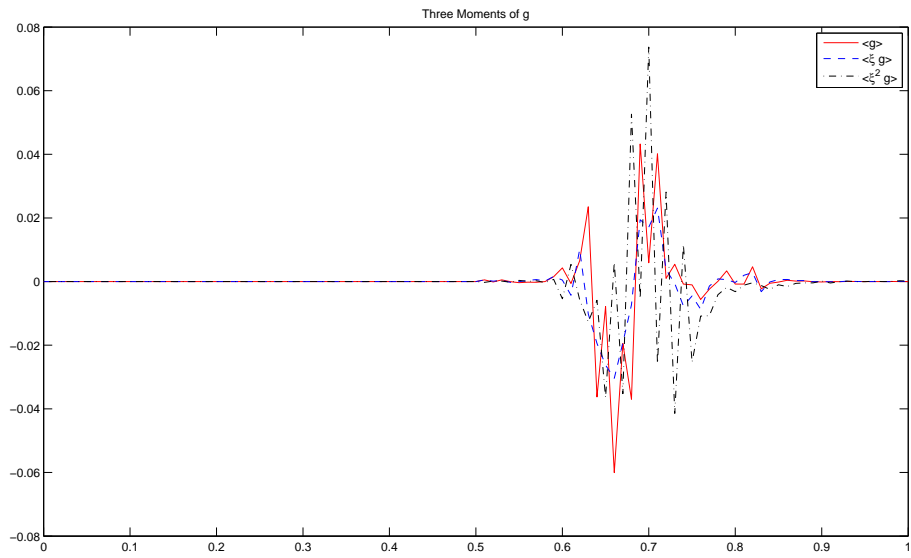
(a) 1st order

(b) 2nd order

Figure 5.20: Three moments of g of NSLU for 1D1DBGK,KFVS,No proj:$t = 0.1$
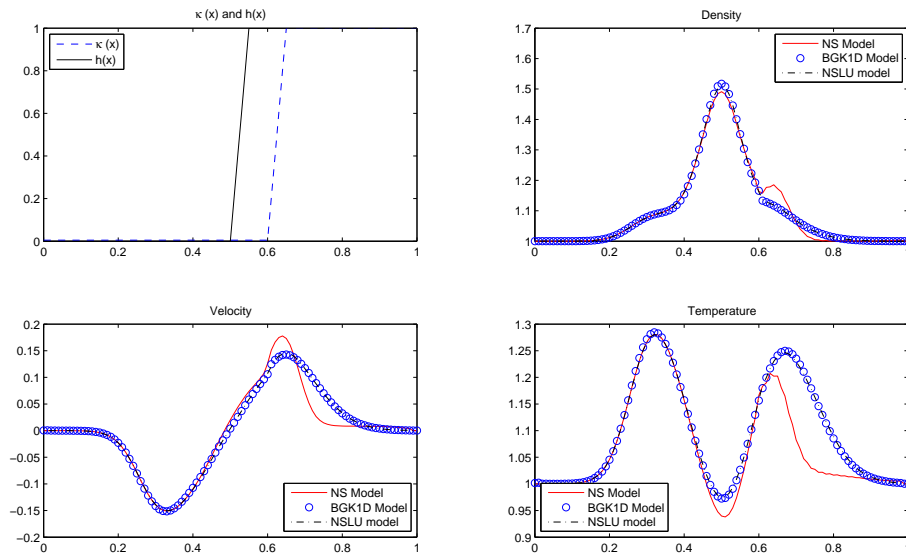
(a) 1st order
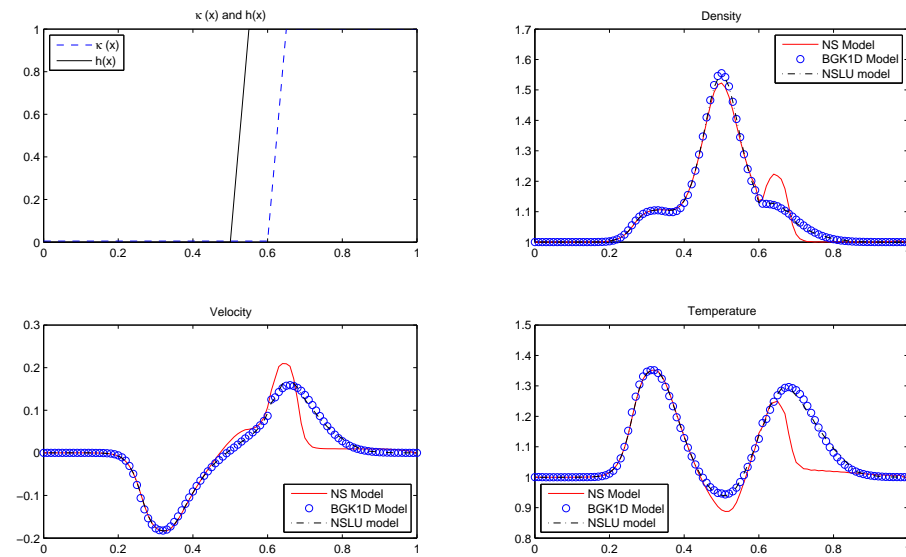
(b) 2nd order

Figure 5.21: Accuracy of NSLU for 1D1DBGK, KFVS with proj: $t = 0.1$

terms, we get the following numerical scheme:

$$D_t^- \rho_j^n + D^- F_{1,j}^{+;n} + D^+ F_{1,j}^{-;n} = 0,$$

$$D_t^- (\rho_j^n u_j^n) + D^- F_{2,j}^{+;n} + D^+ F_{2,j}^{-;n} = 0,$$

$$D_t^- (\rho_j^n ((u_j^n)^2 + \theta_j^n)) + D^- F_{3,j}^{+;n} + D^+ F_{3,j}^{-;n} + \tilde{D}(\kappa_j T_{3,j}^n) + D^- \sum_k \xi_k^+ \xi_k^2 g_{k,j}^n$$

$$+ D^+ \sum_k \xi_k^- \xi_k^2 g_{k,j}^n = 0, \quad \text{where } \tilde{D}(\kappa_j T_{3,j}^n) = D^- ([-3\kappa\rho\theta]_{j+1/2}^n D^+ \theta_j^n),$$

$$D_t^- g_{k,j}^n + h_j D^- (\xi_k^+ g_{k,j}^n) + h_j D^+ (\xi_k^- g_{k,j}^n) = -h_j S_j^{n+1} - \frac{1}{\kappa_j} h_j g_{k,j}^{n+1}$$

$$- h_j (D_t^- + D^- \xi_k^+ + D^+ \xi_k^-)(\mathcal{M}_j^n + \kappa_j S_j^n),$$

$$\text{where } S_j^k = \left(\frac{(u_j^k - \xi)^3 - 3(u_j^k - \xi)\theta_j^k}{2(\theta_j^k)^2} D\theta_j^k \right) \mathcal{M}_j^k, \quad k = n, n+1,$$

(5.35)

In the numerical computation, this scheme is unstable if no zero-moment projection is applied. With zero-moment projection, the first and second order results are shown in the figure 5.22.

We observe the big difference around the interface $x = 0.65$ between the BGK model and the NSLU model. Since in the up-scaling equation the viscous term is discretized in an upwind way which is inconsistent with the short stencil center-differencing scheme in the fluid equation. This inconsistence will cause $O(1)$ error due to the large gradient of $\kappa(x)$ across the interface. If we only change the Euler flux splitting to be SWS and keep the upwind discretization of the viscous terms in the fluid equation, the results with the projection applied are shown in figure 5.23.
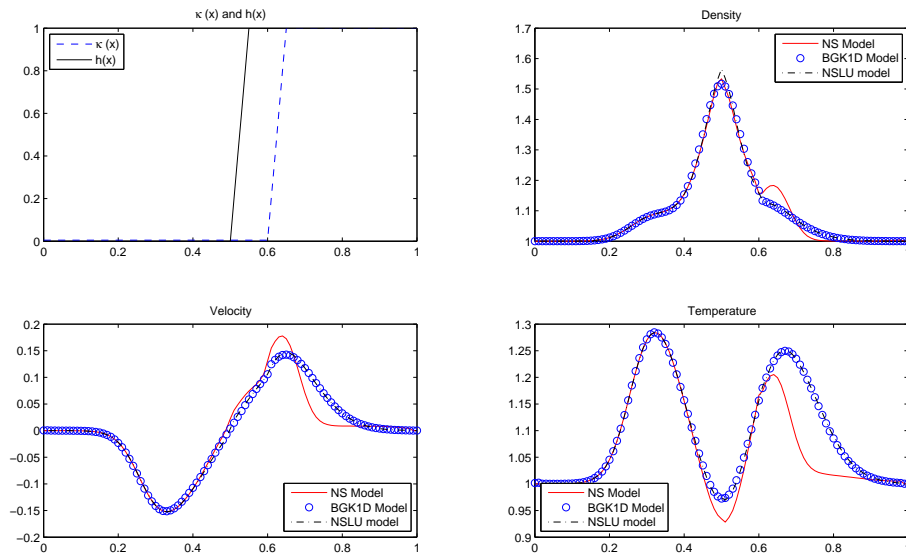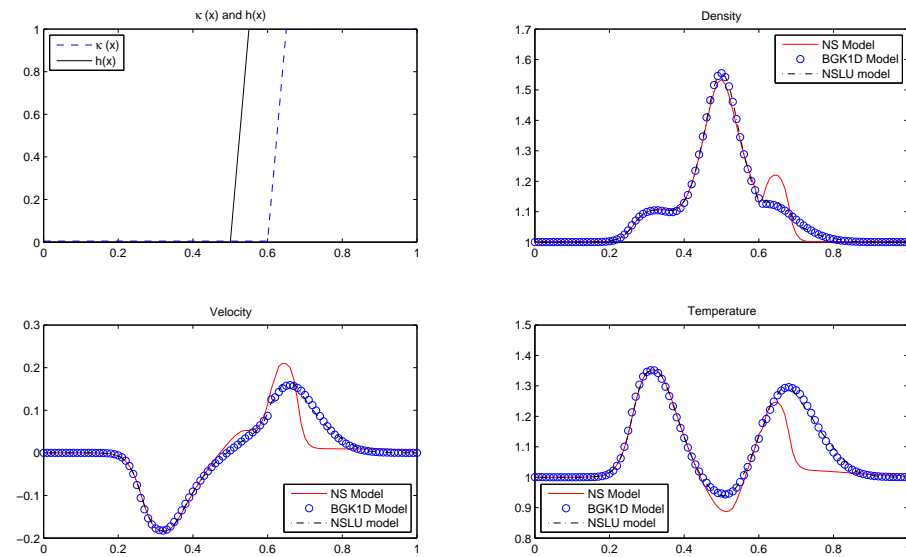
122
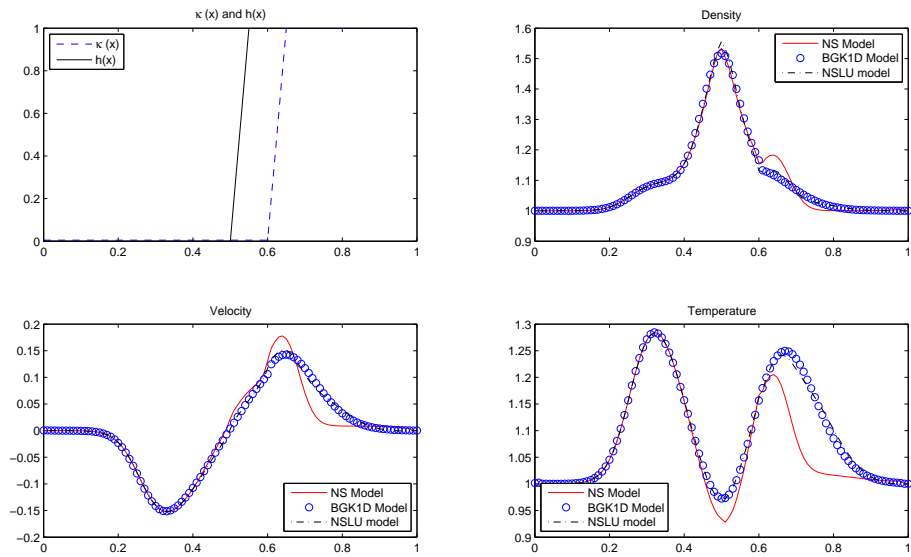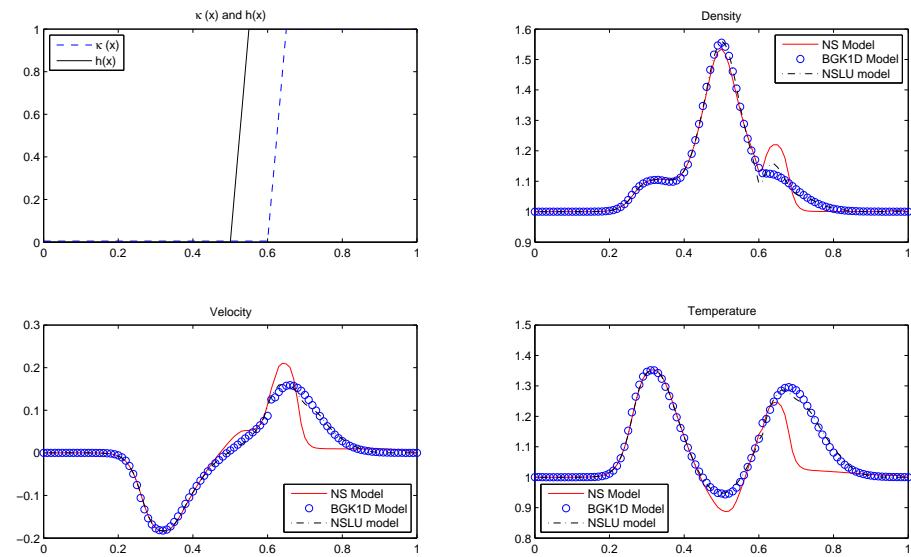
(a) 1st order

(b) 2nd order

Figure 5.22: Accuracy of NSLU for 1D1D BGK, SWS + Proj: $t = 0.1$

(a) 1st order

(b) 2nd order

Figure 5.23: Accuracy of NSLU for 1D1D BGK, modified SWS + Proj: $t = 0.1$

5.3 1D3D BGK Model of Rarefied Gas Dynamics

Considering the space of the velocity is 3D, i.e. $\boldsymbol{\xi} = (\xi_1, \xi_2, \xi_3)$, but the physical space is still 1D. Assuming the distribution function $f = f(x, \boldsymbol{\xi}, t)$, the dimensional BGK model of the rarefied gas is

$$\partial_t f + \xi_1 \partial_x f = \frac{1}{\tau}(\mathcal{M}_3 - f), \tag{5.36}$$

The equilibrium $\mathcal{M}_3$ is the local Maxwellian in $3D$ velocity space:

$$\mathcal{M}_3 = \frac{\rho}{(2\pi\theta)^{3/2}} \exp\{-\frac{(u - \xi_1)^2 + \xi_2^2 + \xi_3^2}{2\theta}\}, \tag{5.37}$$

where ρ is mass density, u is the macroscopic velocity in the x direction and θ is the temperature. These quantities are related to the moments of the distribution function $f(x, \boldsymbol{\xi}, t)$ in the following way:

$$\rho = \int_{R^3} f d\boldsymbol{\xi}, \quad m = \rho u = \int_{R^3} \xi_1 f d\boldsymbol{\xi}, \quad 2e = \rho(u^2 + 3\theta) = \int_{R^3} |\boldsymbol{\xi}|^2 f d\boldsymbol{\xi}, \tag{5.38}$$

The dimensional relaxation time $\tau = \mu/p$ where $p = \rho\theta$ is the pressure and $\mu = CT^\omega$ is the viscosity. For hydrogen, $C = 1.99 \times 10^{-3}$ and $\omega = 0.81$.

Next we use the standard reduction technique in [26] to simplify the system to be 1D1D BGK system by means of the symmetry in the y, z axes.

Denote $\tilde{f}(x, \xi_1, t) = \int_{R^2} f d\xi_2 \xi_3$, $\hat{f}(x, \xi_1, t) = \int_{R^2} (\xi_2^2 + \xi_3^2) f d\xi_2 d\xi_3$, then $\tilde{f}$ and $\hat{f}$ satisfy the following system:

$$\partial_t \begin{pmatrix} \tilde{f} \\ \hat{f} \end{pmatrix} + \xi_1 \partial_x \begin{pmatrix} \tilde{f} \\ \hat{f} \end{pmatrix} = \frac{1}{\tau} \begin{pmatrix} \mathcal{M}[\rho] - \tilde{f} \\ 2\theta\mathcal{M}[\rho] - \hat{f} \end{pmatrix}, \tag{5.39}$$

where the 1D Maxwellian $\mathcal{M} = \frac{\rho}{\sqrt{2\pi\theta}} \exp\{-\frac{(u-\xi_1)^2}{2\theta}\}$. Here the macroscopic quantities in $\mathcal{M}$ are obtained by

$$\rho = \int_R \tilde{f} d\xi_1, \quad m = \rho u = \int_R \xi_1 \tilde{f} d\xi_1, \quad 2e = \rho(u^2 + 3\theta) = \int_R \xi_1^2 \tilde{f} + \hat{f} d\xi_1, \quad (5.40)$$

Therefore the first component of the heat flux term

$$\frac{1}{2} \langle c_1 |\mathbf{c}|^2 f \rangle = \frac{1}{2} \left(\langle c_1^3 \tilde{f} \rangle + \langle c_1 \hat{f} \rangle \right) \tag{5.41}$$

where $c_1 = \xi_1 - u_1$.

We take the stationary normal shock problem as an example. The quantities of the upstream flow's are set to be:

$$\rho_l = 6.63 \times 10^{-6} \ kg \cdot m^{-3}, \quad u_l = 637.8 \ m \cdot s^{-1}, \tag{5.42}$$

$$\theta_l = RT_l = 208.24 \times 293 = 6.1014 \times 10^4 m^2 \cdot s^{-2}, \tag{5.43}$$

This yields a shock whose Mach number is $M = u_l/\sqrt{\gamma\theta_l} = 2$ where $\gamma = 5/3$. From the R-H condition with the shock speed $s = 0$ we get the following relations:

$$\rho_r u_r = \rho_l u_l, \quad \rho_r(u_r^2 + \theta_r) = \rho_l(u_l^2 + \theta_l), \quad \rho_r u_r(u_r^2 + 5\theta_r) = \rho_l u_l(u_l^2 + 5\theta_l), \quad (5.44)$$

Therefore

$$u_r = \frac{1}{4} u_l + \frac{5\theta_l}{4u_l}, \ \theta_r = \theta_l + \frac{1}{5}(u_l^2 - u_r^2), \ \rho_r = \frac{\rho_l u_l}{u_r}, \tag{5.45}$$

we get $\rho_r = 25.33 \times 10^{-6}$, $u_r = 667.65$, $\theta_r = 1.2734 \times 10^6$.

The local Knudsen number is defined as $\kappa = \frac{\lambda}{Q} \left| \frac{\partial Q}{\partial x} \right|$, where λ is the local mean free path and Q is a flow property (density or temperature). The profiles of

κ are shown in figure 5.24. In order to apply ELU1(ELU2) model, we choose the transition function $h(x) = 1$ in the region $(-0.15 \le x \le 0.1)$) between the solid vertical lines to get $\kappa < 0.001$ on the outside region. To apply NSLU model, we will set $h(x) = 1$ in the region $(-0.1 \le x \le 0.05)$) between the dotted vertical lines to get $\kappa < 0.01$ on the outside region.

In the discretization of the velocity, we choose length of the interval to be 3 times the standard deviation, which is big enough to represent the Maxwellian well. We use 50 points in ξ direction and choose the time long enough so the stationary solution is obtained. As usual for this test case, we use a stabilization technique to prevent the shock from moving to the right. Namely, after each time step, the solution is shifted so that the mean density point x (defined by the relation $n(x) = \frac{n_l + n_r}{2}$, [39]) is equal to 0.

5.3.1 ELU1 Model for 1D3D BGK Model

In the following, we use the notation ξ to replace ξ_1. Assuming $f = \mathcal{M}_3$ (i.e. $F = \mathcal{M}$, $G = \theta \mathcal{M}$, the zero-order C-E expansion), we get:

$$\partial_t \rho + \partial_x \langle \xi \mathcal{M}_3 \rangle = \partial_t \rho + \partial_x F_1 = 0,$$

$$\partial_t(\rho u) + \partial_x \langle \xi^2 \mathcal{M}_3 \rangle = \partial_t(\rho u) + \partial_x F_2 = 0, \qquad (5.46)$$

$$\partial_t(\rho(u^2 + 3\theta)) + \partial_x \langle \xi |\boldsymbol{\xi}|^2 \mathcal{M}_3 \rangle = \partial_t(\rho(u^2 + 3\theta)) + \partial_x F_3 = 0,$$

where F_i are the fluxes:

$$F_1 = \langle \xi \mathcal{M}_3 \rangle = \rho u, \quad F_2 = \langle \xi^2 \mathcal{M}_3 \rangle = \rho(u^2 + 3\theta), \quad F_3 = \langle \xi |\boldsymbol{\xi}|^2 \mathcal{M}_3 \rangle = \rho u(u^2 + 5\theta),$$

$$(5.47)$$

This is the Euler system for the compressible gas with $\gamma = \frac{5}{3}$.

Therefore the first order numerical scheme for the compressible Euler equations using flux splittings will be

$$D_t^- \rho_j^n + D^- F_{1,j}^{+;n} + D^+ F_{1,j}^{-;n} = 0,$$

$$D_t^- (\rho_j^n u_j^n) + D^- F_{2,j}^{+;n} + D^+ F_{2,j}^{-;n} = 0, \qquad (5.48)$$

$$D^- (\rho_j^n ((u_j^n)^2 + 3\theta_j^n)) + D^- F_{3,j}^{+;n} + D^+ F_{3,j}^{-;n} = 0,$$

The boundary conditions for the Euler equations need to be given carefully because this is a hyperbolic system. As for the left boundary, since the sound speed $c_l = \sqrt{\gamma \theta_l} = 318.9 < u_l$, we need the boundary conditions for all the three equations. For the right boundary, the sound speed $c_r = \sqrt{\gamma \theta_r} = 1458 > u_r > 0$. Therefore we need to give the boundary condition for ρ, but not (u, θ), [24].

By means of the transition function,$h(x)$ and take $\tilde{f} = \mathcal{M} + \tilde{g}, \hat{f} = 2\theta \mathcal{M} + \hat{g},$

we may get the up-scaling model of the reduced system as

$$\partial_t \rho + \partial_x F_1 = 0, \quad \partial_t(\rho u) + \partial_x F_2 + \partial_x \langle \xi^2 p \rangle = 0,$$

$$\partial_t(\rho(u^2 + 3\theta)) + \partial_x F_3 + \partial_x \langle \xi^3 \tilde{g} \rangle + \partial_x \langle \xi \hat{g} \rangle = 0,$$

$$\partial_t \tilde{g} + h \partial_x(\xi \tilde{g}) = -\frac{1}{\tau} h \tilde{g} - h(\partial_t + \xi \partial_x)\mathcal{M},$$

$$\partial_t \hat{g} + h \partial_x(\xi \hat{g}) = -\frac{1}{\tau} h \hat{g} - h(\partial_t + \xi \partial_x)(2\theta \mathcal{M}),$$

(5.49)

The first order upwind numerical scheme is the following:

$$D_t^- \rho_j^n + D^- F_{1,j}^{+;n} + D^+ F_{1,j}^{-;n} = 0,$$

$$D_t^-(\rho_j^n u_j^n) + D^- F_{2,j}^{+;n} + D^+ F_{2,j}^{-;n} + D^- \sum_k \xi_k^+ \xi_k \tilde{g}_{k,j}^n + D^+ \sum_k \xi_k^- \xi_k \tilde{g}_{k,j}^n = 0,$$

$$D_t^-(\rho_j^n((u_j^n)^2 + 3\theta_j^n)) + D^- F_{3,j}^{+;n} + D^+ F_{3,j}^{-;n} + D^- \sum_k \xi_k^+ \xi_k^2 \tilde{g}_{k,j}^n$$

$$+ D^+ \sum_k \xi_k^- \xi_k^2 \tilde{g}_{k,j}^n + D^- \sum_k \xi_k^+ \hat{g}_{k,j}^n + D^+ \sum_k \xi_k^- \hat{g}_{k,j}^n = 0,$$

$$D_t^- \tilde{g}_{k,j}^n + h_j(D^- \xi_k^+ + D^+ \xi_k^-)\tilde{g}_{k,j}^n = -\frac{1}{\tau_j^{n+1}} h_j \tilde{g}_{k,j}^{n+1} - h_j\left(D_t^- + D^- \xi_k^+ + D^+ \xi_k^-\right)\mathcal{M}_{k,j}^n,$$

$$D_t^- \hat{g}_{k,j}^n + h_j(D^- \xi_k^+ + D^+ \xi_k^-)\hat{g}_{k,j}^n =$$

$$-\frac{1}{\tau_j^{n+1}} h_j \hat{g}_{k,j}^{n+1} - h_j\left(D_t^- + D^- \xi_k^+ + D^+ \xi_k^-\right)(2\theta_j^n \mathcal{M}_{k,j}^n),$$

(5.50)

The heat flux is obtained by

$$\frac{1}{2}\left(\langle(\xi - u)^3 \tilde{g}\rangle + \langle(\xi - u)\hat{g}\rangle\right) \approx \frac{1}{2}\sum_k\left((\xi_k - u)^3 \tilde{g}_{k,j}^n + (\xi_k - u)\hat{g}_{k,j}^n\right)\Delta\xi \quad (5.51)$$

Based on the profile of the Knudsen number, figure 5.24, we choose the buffer-zone

function $h(x) = 1$ in $[-0.15, 0.1]$ and $h(x) = 0$ in $[-0.5, -0.18]$ and $[0.13, 0.5]$, and

linear between these intervals. Therefore the two buffer zones will be $[-0.18, -0.15]$ and $[0.1, 0.13]$.

We may also choose KVFS scheme to split the fluxes in the moments' equation and get the results in figure 5.25.
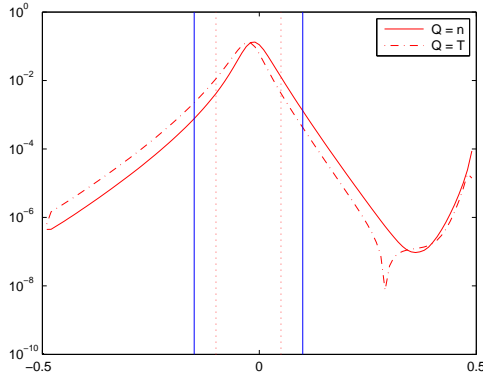

Figure 5.24: Steady Shock: $\kappa = \left| \frac{\lambda}{Q} \frac{\partial Q}{\partial x} \right|$

The top-left plot shows the Knudsen number $\kappa = \frac{\lambda |\rho_x|}{\rho}$ and the positions of the two buffer zones. The other three plots show the profiles of the macroscopic quantities ρ, u and T. All these quantities are normalized so their values are between 0 and 1. The region outside of the two vertical lines in these plots show the regions where $h = 0$. In other words, the compressible Euler equations will be solved in these regions without the up-scaling correction. The macroscopic quantities' agreement of the ELU model and the BGK model are very well in both first order and second order tests.

It is hardly to tell the difference for the macroscopic quantities's profiles if the zero-moment projection is applied.(See appendix for the formula of projection). If we take a close look at the heat flux, a smoother and better-fitting heat flux is obtained if the zero-moment projection is applied. See the results in Figure 5.26 (1st order) and Figure 5.27 (2nd order).

The results with projection applied show a smoother and better profile of heat flux than the results without projection in the kinetic region, esp. in the 2nd order result.

If we apply the SWS scheme, the scheme is not stable if no zero-moment projection is applied. The result in Figure 5.28 is obtained using 1st and 2nd order scheme with zero-moment projection.

Heat flux's profiles is shown in Figure 5.29. We see that both the macroscopic quantities and the heat flux fit the result from the BGK model very well.

5.3.2   NSLU Model for 1D3D BGK Model

Apply the first order of C-E expansion and we will get

$$
f_1 = \mathcal{M}_3 \left(1 + \tau\left(\frac{-2(\xi - u)^2 + \xi_2^2 + \xi_3^2}{3\theta}\partial_x u + \frac{u - \xi}{2\theta^2}((u - \xi)^2 + \xi_2^2 + \xi_3^2 - 5\theta)\partial_x \theta)\right) \right),
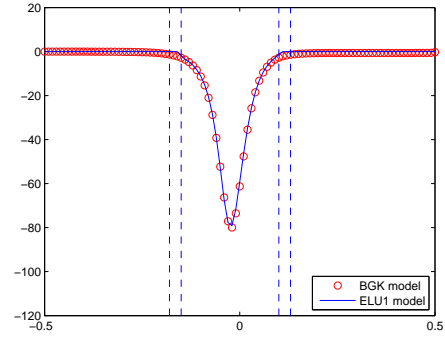$$

$$(5.52)$$
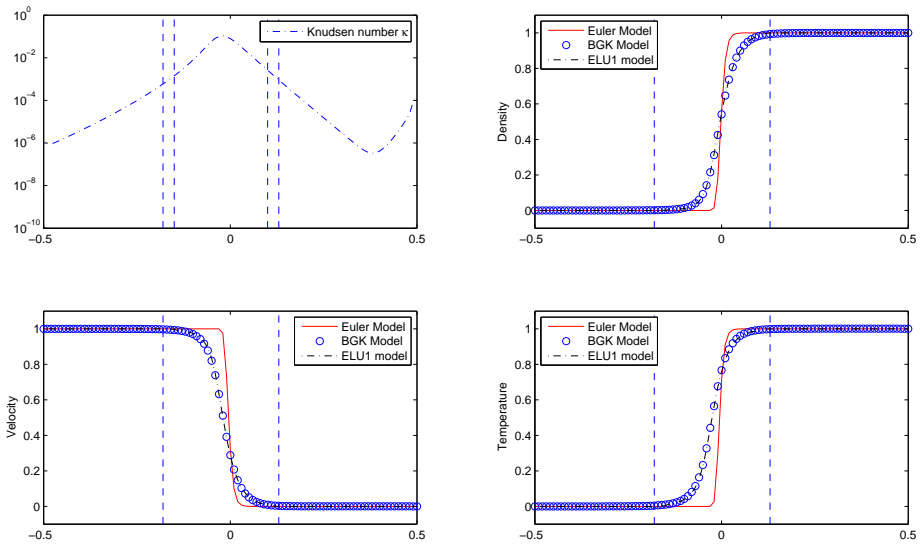
(a) 1st order
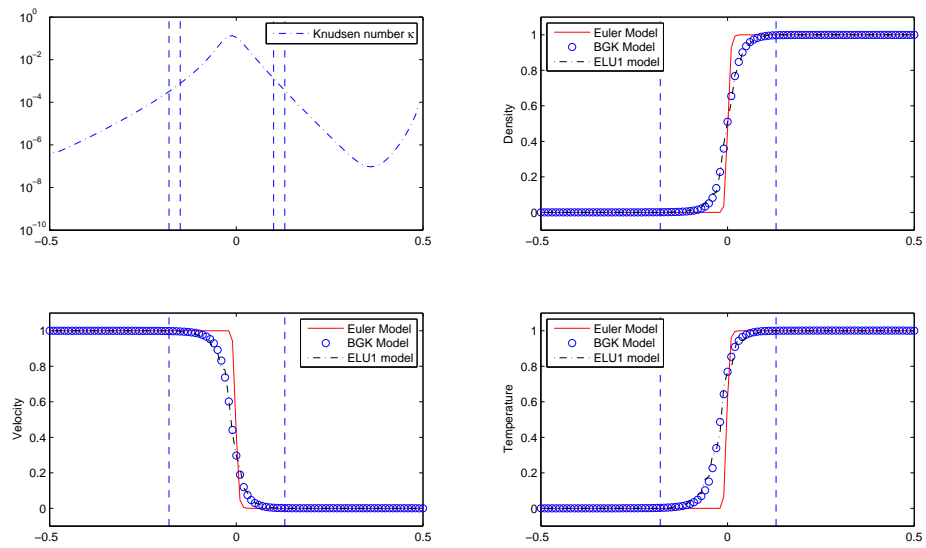
(b) 2nd order

Figure 5.25: Accuracy of ELU1 for 1D3D BGK with KFVS
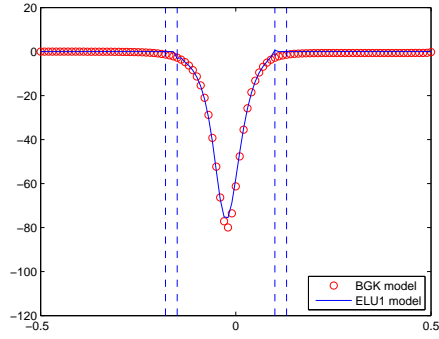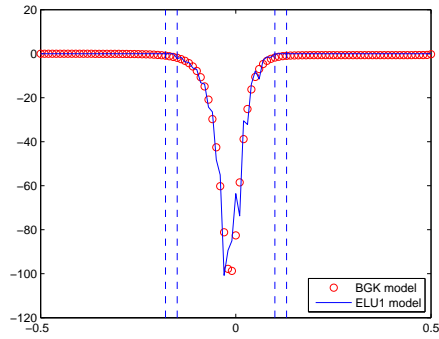
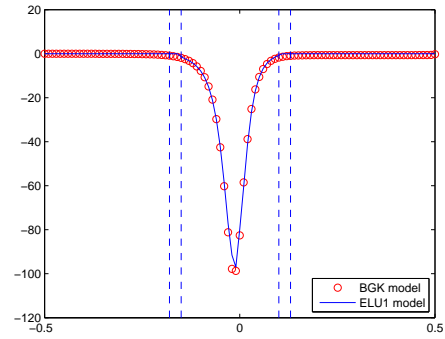(a) No projection   (b) With projection

Figure 5.26: Heat flux of ELU1 for 1D3D BGK with KFVS, 1st order
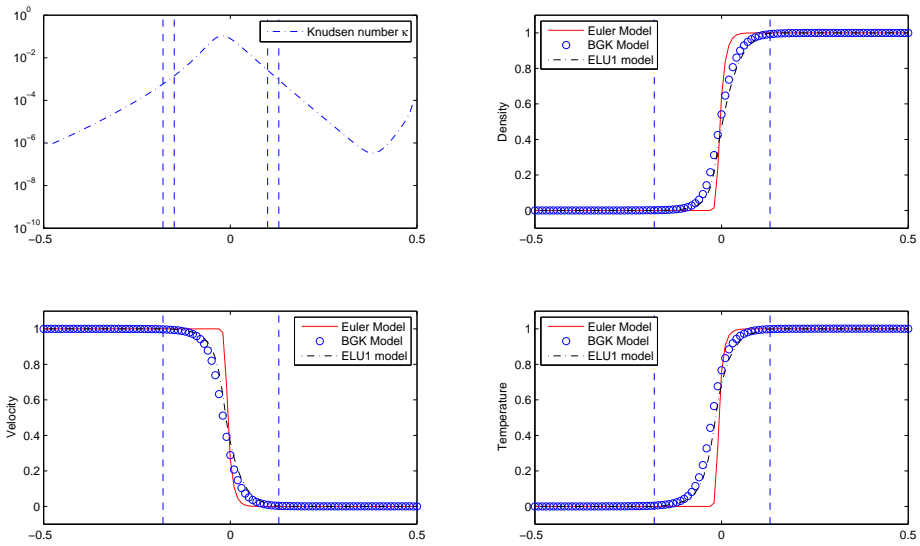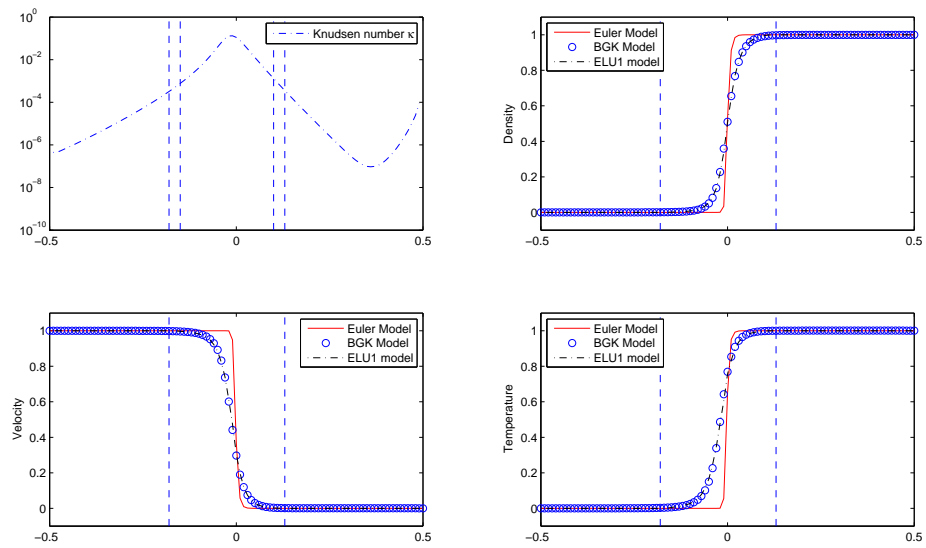

(a) No projection   (b) With projection

Figure 5.27: Heat flux of ELU1 for 1D3D BGK with KFVS, 2nd order

(a) 1st order

(b) 2nd order

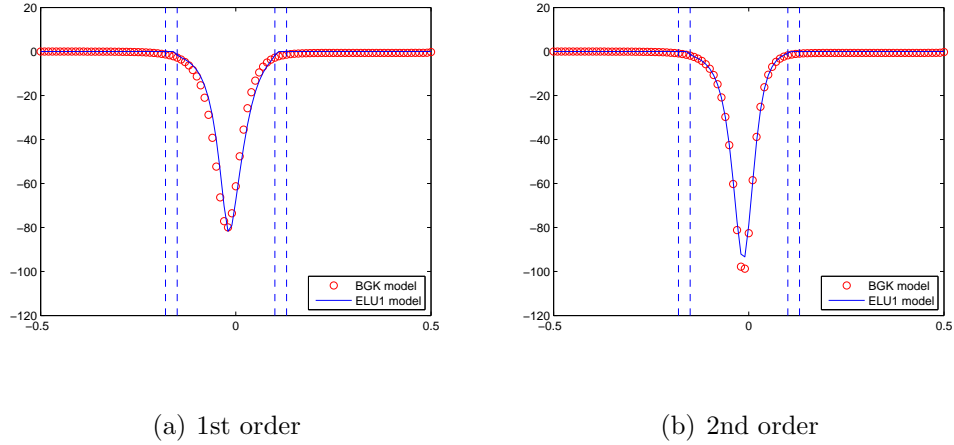Figure 5.28: ELU1 for 1D3D BGK with SWS + Proj

(a) 1st order (b) 2nd order

Figure 5.29: Heat flux of ELU1 for 1D3D BGK with SWS + Proj

Denote the Navier-Stokes non-equilibrium part:

$$S = \left(\frac{-2(\xi - u)^2 + \xi_2^2 + \xi_3^2}{3\theta} \partial_x u + \frac{u - \xi}{2\theta^2}((u - \xi)^2 + \xi_2^2 + \xi_3^2 - 5\theta)\partial_x \theta \right) \mathcal{M}_3, \quad (5.53)$$

Plug f_1 into the Boltzmann equation and take moments, we get the following Navier-Stokes equations:

$$\partial_t \rho + \partial_x (F_1 + \tau T_1) = 0,$$

$$\partial_t (\rho u) + \partial_x (F_2 + \tau T_2) = 0, \quad (5.54)$$

$$\partial_t (\rho(u^2 + 3\theta)) + \partial_x (F_3 + \tau T_3) = 0,$$

Here the $F_i (i = 1, 2, 3)$ are the fluxes of the Euler equations. And the viscosity terms

$$T_1 = \langle \xi S \rangle, \quad T_2 = \langle \xi^2 S \rangle, \quad T_3 = \langle \xi |\boldsymbol{\xi}|^2 S \rangle, \quad (5.55)$$

135

In this case it can be shown

$$T_1 = 0, \quad T_2 = -\frac{4}{3}\rho\theta\partial_x u, \quad T_3 = -\frac{8}{3}\rho u\theta\partial_x u - 5\rho\theta\partial_x\theta, \qquad (5.56)$$

The foregoing equations become identical to the 1D Navier-Stokes equations we discussed in chapter 2 if we set the dynamic viscosity coefficient $\mu = \tau\rho\theta/R$ (R : the ordinary gas constant) and the thermal conductivity $k = \frac{5}{2}\kappa\rho\theta$. Then the Prandtl number $Pr = c_p\mu/k = 1$ since the specific heat at constant pressure $c_p = \frac{5}{2}R$.

Let $\mathcal{G} = \frac{1}{2\pi\theta}\exp\{-\frac{u^2}{2\theta}\}$, then the kinetic flux vector splitting for the viscosity terms T_2, T_3 is as follows

$$T_2^\pm = \langle\xi^\pm\xi S\rangle = \rho\theta\left(-\frac{2}{3}\ \mathrm{erfc}(\mp\frac{u^2}{2\theta})\partial_x u \mp \mathcal{G}_{u,\theta}\partial_x\theta\right),$$

$$T_3^\pm = \langle\xi^\pm|\boldsymbol{\xi}|^2 S\rangle = \rho\theta\left((\mp4\theta\mathcal{G}_{u,\theta} - \frac{4}{3}u\ \mathrm{erfc}(\mp\frac{u^2}{2\theta}))\partial_x u + (\pm u\mathcal{G}_{u,\theta} - \frac{5}{2}\ \mathrm{erfc}(\mp\frac{u^2}{2\theta}))\partial_x\theta\right),$$

$$(5.57)$$

The first order up-wind scheme based on the flux splitting of the Navier-Stokes equation is as follows:

$$D_t^-\rho_j^n + D^- F_{1,j}^{+;n} + D^+ F_{1,j}^{-;n} = 0,$$

$$D_t^-(\rho_j^n u_j^n) + D^-(F_{2,j}^{+;n} + \tau_j^n T_{2,j}^{+;n}) + D^+(F_{2,j}^{-;n} + \tau_j^n T_{2,j}^{-;n}) = 0, \qquad (5.58)$$

$$D^-(\rho_j^n((u_j^n)^2 + \theta_j^n)) + D^-(F_{3,j}^{+;n} + \tau_j^n T_{3,j}^{+;n}) + D^+(F_{3,j}^{-;n} + \tau_j^n T_{3,j}^{-;n}) = 0,$$

where $F_i^\pm(i = 1, 2, 3)$ is same as the Euler equations. In the numerical test, we will use center-difference scheme to discretize the viscosity term instead of upwind

scheme to improve the stability.

$$D_t^- \rho_j^n + D^- F_{1,j}^{+;n} + D^+ F_{1,j}^{-;n} = 0,$$

$$D_t^-(\rho_j^n u_j^n) + D^- F_{2,j}^{+;n} + D^+ F_{2,j}^{-;n} + \tilde{D}(\tau_j^n T_{2,j}^n) = 0, \qquad (5.59)$$

$$D^-(\rho_j^n((u_j^n)^2 + \theta_j^n)) + D^- F_{3,j}^{+;n} + D^+ F_{3,j}^{-;n} + \tilde{D}(\tau_j^n T_{3,j}^n) = 0,$$

Since $f_1 = \mathcal{M}_3 + \tau S$, we get the Navier-Stokes distribution functions in the reduced dimension are

$$\tilde{f}_1 = \int_{R^2} f_1 d\xi_2 d\xi_3 = \mathcal{M} + \tau \tilde{S}, \qquad (5.60)$$

where

$$\tilde{S} = \left(-\frac{2((u-\xi)^2 - \theta)}{3\theta} \partial_x u + \frac{(u-\xi)((u-\xi)^2 - 3\theta)}{2\theta^2} \partial_x \theta \right) \mathcal{M}, \qquad (5.61)$$

and

$$\hat{f}_1 = \int_{R^2} \frac{1}{2}(\xi_2^2 + \xi_3^2) f_1 d\xi_2 d\xi_3 = \theta \mathcal{M} + \tau \hat{S}, \qquad (5.62)$$

where

$$\hat{S} = \left(-\frac{2}{3}((u-\xi)^2 - 2\theta) \partial_x u + \frac{u-\xi}{2\theta}((u-\xi)^2 - \theta) \partial_x \theta \right) \mathcal{M}, \qquad (5.63)$$

In the numerical scheme, the derivatives in $\tilde{S}$ and $\hat{S}$ will be obtained by center difference scheme.

Let $\tilde{f} = \tilde{f}_1 + \tilde{g}$ and $\hat{f} = \hat{f}_1 + \hat{g}$, by means of the transition function $h(x)$ we

get the NSLU model as

$$\partial_t \rho + \partial_x F_1 = 0,$$

$$\partial_t(\rho u) + \partial_x(F_2 + \tau T_2) + \partial_x\langle \xi^2 \tilde{f}\rangle = 0,$$

$$\partial_t(\rho(u^2 + \theta)) + \partial_x(F_3 + \tau T_3) + \partial_x\langle \xi^3 \tilde{g}\rangle + \partial_x\langle \xi \hat{g}\rangle = 0, \qquad (5.64)$$

$$\partial_t \tilde{g} + \partial_x(\xi \tilde{g}) = -h\tilde{S} - \frac{1}{\tau}h\tilde{g} - h(\partial_t + \xi\partial_x)\tilde{g}_{NS},$$

$$\partial_t \hat{g} + \partial_x(\xi \hat{g}) = -h\hat{S} - \frac{1}{\tau}h\hat{g} - h(\partial_t + \xi\partial_x)\hat{g}_{NS},$$

The first order upwind numerical scheme of the NSLU model is the following:

$$D_t^- \rho_j^n + D^- F_{1,j}^{+;n} + D^+ F_{1,j}^{-;n} = 0,$$

$$D_t^-(\rho_j^n u_j^n) + D^-(F_{2,j}^{+;n} + \tau_j^n T_{2,j}^{+;n}) + D^+(F_{2,j}^{-;n} + \tau_j^n T_{2,j}^{-;n})$$

$$+ D^- \sum_k \xi_k^+ \xi_k \hat{g}_{k,j}^n + D^+ \sum_k \xi_k^- \xi_k \hat{g}_{k,j}^n = 0,$$

$$D_t^-(\rho_j^n((u_j^n)^2 + \theta_j^n)) + D^-(F_{3,j}^{+;n} + \tau_j^n T_{3,j}^{+;n}) + D^+(F_{3,j}^{-;n} + \tau_j^n T_{3,j}^{-;n})$$

$$+ D^- \sum_k \xi_k^+ \xi_k^2 \tilde{g}_{k,j}^n + D^- \sum_k \xi_k^+ \hat{g}_{k,j}^n + D^+ \sum_k \xi_k^- \xi^2 p_{k,j}^n + D^+ \sum_k \xi_k^- \hat{g}_{k,j}^n = 0,$$

$$D_t^- \tilde{g}_{k,j}^n + h_j(D^-\xi_k^+ + D^+\xi_k^-)\tilde{g}_{k,j}^n = -h_j \tilde{S}_{k,j}^{n+1} - \frac{1}{\tau_j^{n+1}} h_j \tilde{g}_{k,j}^{n+1}$$

$$- h_j(D_t^- + D^-\xi_k^+ + D^+\xi_k^-)(\mathcal{M}_{k,j}^n + \tau_j^n \tilde{S}_{k,j}^n),$$

$$D_t^- \hat{g}_{k,j}^n + h_j(D^-\xi_k^+ + D^+\xi_k^-)\hat{g}_{k,j}^n = -h_j \hat{S}_{k,j}^{n+1} - \frac{1}{\tau_j^{n+1}} h_j \hat{g}_{k,j}^{n+1}$$

$$- h_j(D_t^- + D^-\xi_k^+ + D^+\xi_k^-)(\theta\mathcal{M}_{k,j}^n + \tau_j^n \hat{S}_{k,j}^n),$$

$$(5.65)$$

138
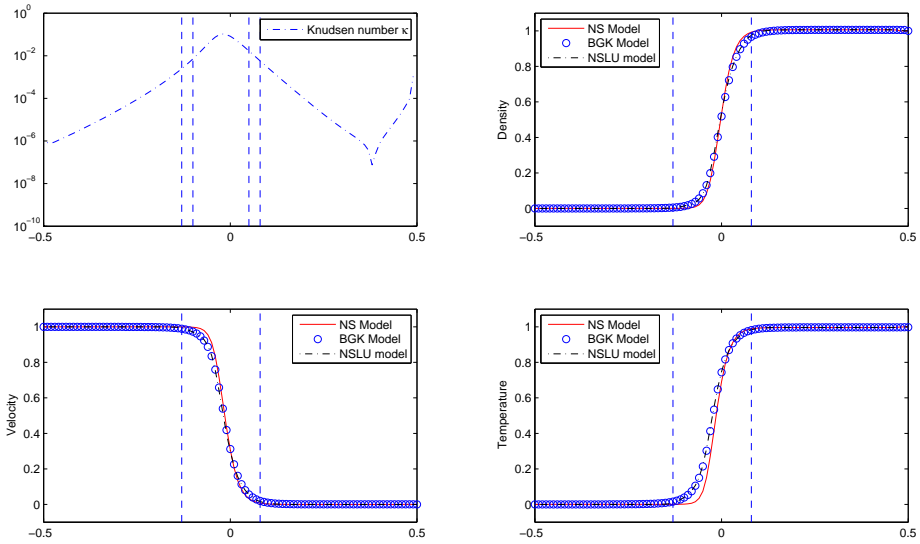
where

$$\tilde{S}_{k,j}^n = \left(-\frac{2((u_j^n - \xi_k)^2 - \theta_j^n)}{3\theta_j^n} Du_j^n + \frac{(u_j^n - \xi_k)((u_j^n - \xi_k)^2 - 3\theta_j^n)}{2(\theta_j^n)^2} D\theta_j^n \right) \mathcal{M}_{k,j}^n,$$

$$\hat{S}_{k,j}^n = \left(-\frac{2}{3}((u_j^n - \xi_k)^2 - 4\theta_j^n) Du_j^n + \frac{u_j^n - \xi_k}{2\theta_j^n}((u_j^n - \xi_k)^2 - 2\theta_j^n) D\theta_j^n \right) \mathcal{M}_{k,j}^n,$$

$$(5.66)$$

Now we choose a smaller kinetic region, i.e. the buffer-zone function $h(x) = 1$ in $[-0.1, 0.05]$ and $h(x) = 0$ in $[-0.5, -0.13]$ and $[0.08, 0.5]$, and linear between these intervals. Therefore the two buffer zones will be $[-0.13, -0.1]$ and $[0.05, 0.08]$.

Using the same data as the ELU1 model, figure 5.30 shows the results without the zero-moment projection.

We may also try a more stable scheme : SWS flux splitting for the Euler fluxes
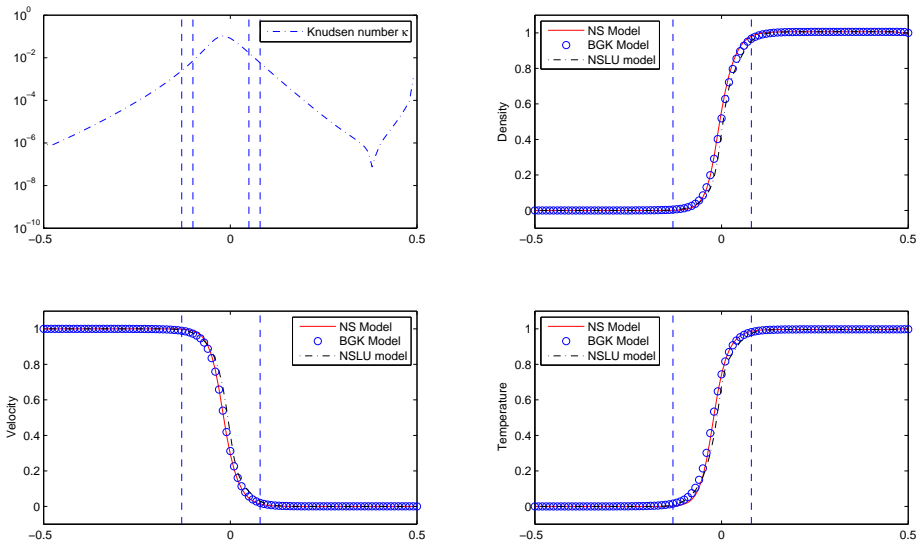
(a) 1st order
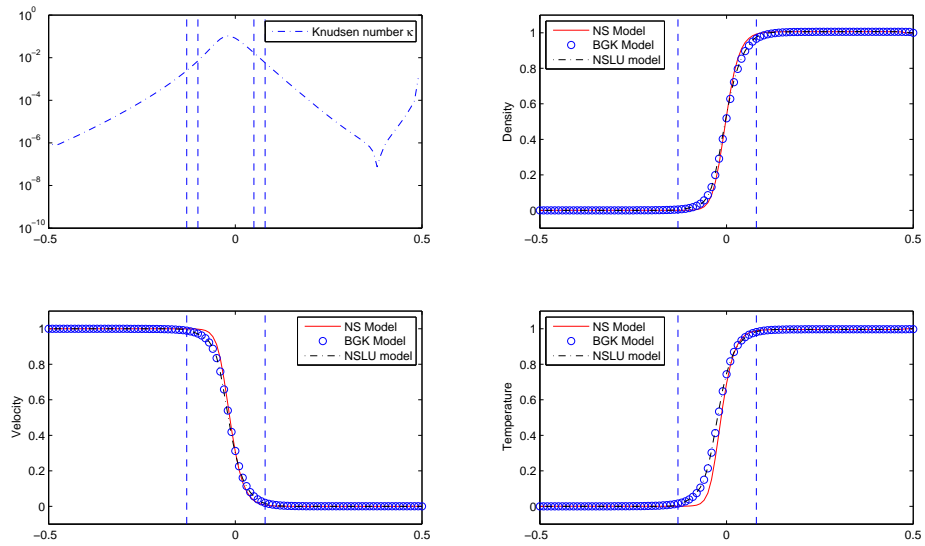
(b) 2nd order

Figure 5.30: NSLU for 1D3D BGK with KFVS, No Proj

and center-differencing scheme for the viscosity terms, i.e. the following:

$$D_t^- \rho_j^n + D^- F_{1,j}^{+,n} + D^+ F_{1,j}^{-,n} = 0,$$

$$D_t^- (\rho_j^n u_j^n) + D^- F_{2,j}^{+,n} + D^+ F_{2,j}^{-,n} + \tilde{D}(\tau_j^n T_{2,j}^n) + D^- \sum_k \xi_k^+ \xi_k \hat{g}_{k,j}^n$$

$$+ D^+ \sum_k \xi_k^- \xi_k \hat{g}_{k,j}^n = 0, \quad \text{where } \tilde{D}(\tau_j^n T_{2,j}^n) = D^- (-\frac{4}{3}[\kappa \rho \theta]_{j+1/2}^n D^+ u_j^n)$$

$$D_t^- (\rho_j^n ((u_j^n)^2 + \theta_j^n)) + D^- F_{3,j}^{+,n} + D^+ F_{3,j}^{-,n} + \tilde{D}(\tau_j^n T_{3,j}^n) + D^- \sum_k \xi_k^+ \xi_k^2 \tilde{g}_{k,j}^n$$

$$+ D^- \sum_k \xi_k^+ \hat{g}_{k,j}^n + D^+ \sum_k \xi_k^- \xi^2 p_{k,j}^n + D^+ \sum_k \xi_k^- \hat{g}_{k,j}^n = 0,$$

$$\text{where } \tilde{D}(\tau_j^n T_{3,j}^n) = D^- (-\frac{8}{3}[\kappa \rho u \theta]_{j+1/2}^n D^+ u_j^n - 5[\kappa \rho \theta]_{j+1/2}^n D^+ \theta_j^n)$$

$$D_t^- \tilde{g}_{k,j}^n + h_j (D^- \xi_k^+ + D^+ \xi_k^-) \tilde{g}_{k,j}^n = -h_j \tilde{S}_{k,j}^{n+1} - \frac{1}{\tau_j^{n+1}} h_j \tilde{g}_{k,j}^{n+1}$$

$$- h_j (D_t^- + D^- \xi_k^+ + D^+ \xi_k^-)(\mathcal{M}_{k,j}^n + \tau_j^n \tilde{S}_{k,j}^n),$$

$$\text{where } \tilde{S}_{k,j}^n = \left(-\frac{2((u_j^n - \xi_k)^2 - \theta_j^n)}{3\theta_j^n} Du_j^n + \frac{(u_j^n - \xi_k)((u_j^n - \xi_k)^2 - 3\theta_j^n)}{2(\theta_j^n)^2} D\theta_j^n \right) \mathcal{M}_{k,j}^n,$$

$$D_t^- \hat{g}_{k,j}^n + h_j (D^- \xi_k^+ + D^+ \xi_k^-) \hat{g}_{k,j}^n = -h_j \hat{S}_{k,j}^{n+1} - \frac{1}{\tau_j^{n+1}} h_j \hat{g}_{k,j}^{n+1}$$

$$- h_j (D_t^- + D^- \xi_k^+ + D^+ \xi_k^-)(\theta \mathcal{M}_{k,j}^n + \tau_j^n \hat{S}_{k,j}^n),$$

$$\text{where } \hat{S}_{k,j}^n = \left(-\frac{2}{3}((u_j^n - \xi_k)^2 - 4\theta_j^n) Du_j^n + \frac{u_j^n - \xi_k}{2\theta_j^n}((u_j^n - \xi_k)^2 - 2\theta_j^n) D\theta_j^n \right) \mathcal{M}_{k,j}^n,$$

$$(5.67)$$

Figure 5.31 shows the results for the first and second scheme without projection.

If the zero-moment projection is applied, it is hardly to tell the change from the

141
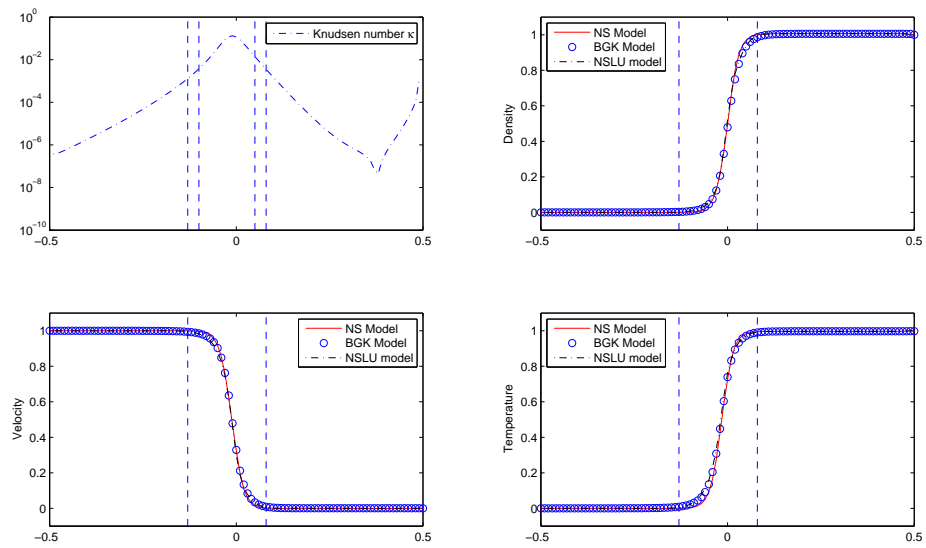
(a) 1st order

(b) 2nd order

Figure 5.31: NSLU for 1D3D BGK with SWS + CD, No Proj

142

macroscopic quantities' profile. To see the effects of the zero-moment projections, we may compare the profile of the heat fluxes.

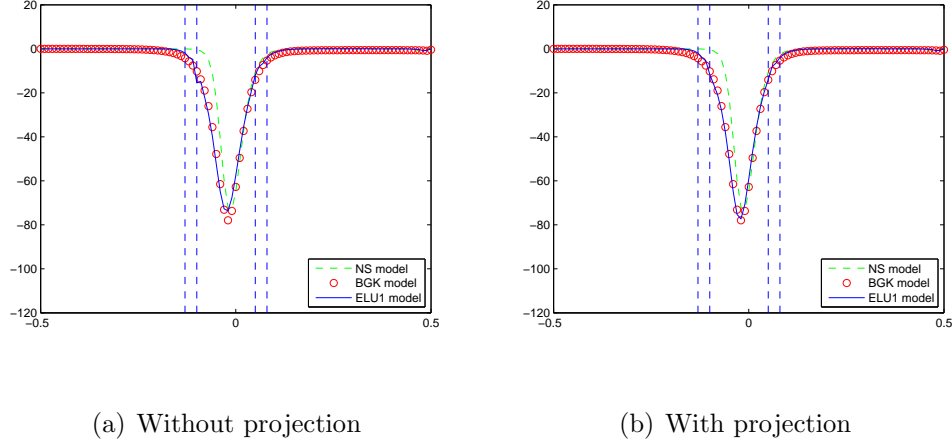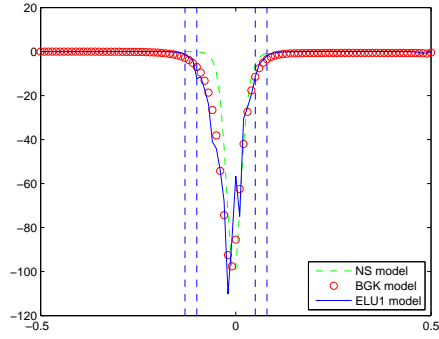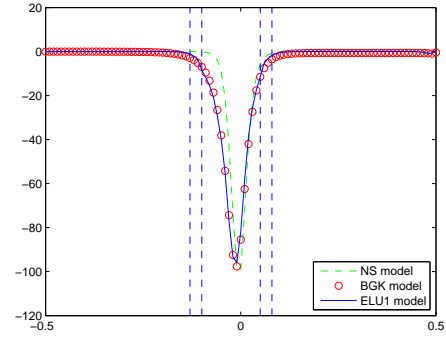(a) Without projection   (b) With projection

Figure 5.32: Heat flux of NSLU for 1D3D BGK with 1st order KFVS

From the comparison of heat fluxes in figure 5.32, 5.33, 5.34 and 5.35, we see the projection not only makes the heat flux smoother but also improves its accuracy, which can be observed from the better agreement of the valley of the heat flux between the NSLU model and the BGK model for the 2nd order SWS scheme.

Remark: From [46], we know the Navier-Stokes solutions is in agreement with the kinetic solution only when the shock is weak, i.e. the shock's Mach number < 2. Therefore in our numerical experiment, we choose the Mach number to be 2. Also for the choice of kinetic region, because the local Knudsen number is only a necessary condition to demarcate the regions [4], we need to choose a much bigger kinetic region to get a good approximation of a strong shock.
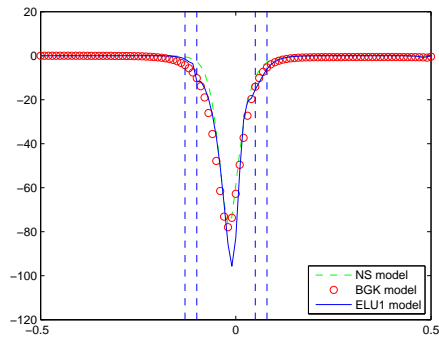
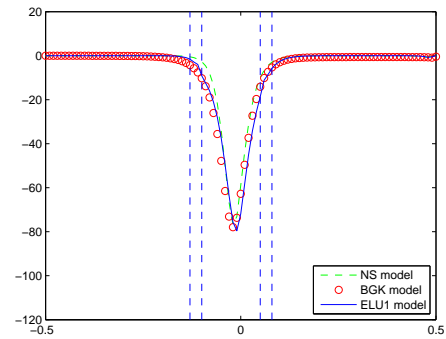(a) Without projection   (b) With projection

Figure 5.33: Heat flux of NSLU for 1D3D BGK with 2nd order KFVS

(a) Without projection   (b) With projection

Figure 5.34: Heat flux of NSLU for 1D3D BGK with 1st order SWS + CD
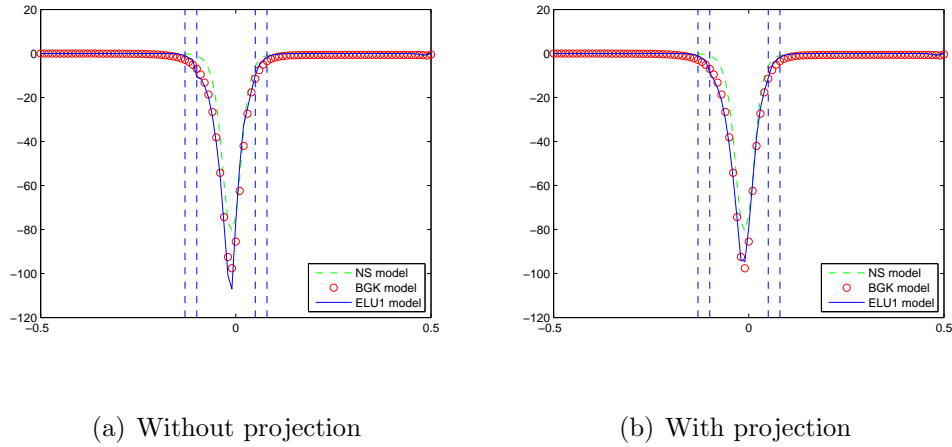
144

(a) Without projection   (b) With projection

Figure 5.35: Heat flux of NSLU for 1D3D BGK with 2nd order SWS + CD

5.4 Simulation of the 1D Semiconductor Device

The semiconductor device we consider here is the 1D GaAs n^+-n-n^+ diode of length $0.8\mu m$. It is often used to simulate the channel in MOSFET and MESFET devices. In [13], the authors give a benchmark comparisons of this device via four different kinds of semiconductor models.

We will use the following units:

$$\mu m = 10^{-6} meter, \quad 10^{-12} second, \quad 10^{-30} kg, \quad 10^{-18} Coulomb, \quad Kelvin,$$

The position of the device is $x \in I = [0, 0.8]$. The doping is defined by $\rho_d(x) = 10^6$ in $0 \le x \le 0.175$ and in $0.625 \le x \le 0.8$, and by $\rho_d(x) = 2 \times 10^3$ in $[0.225 \le x \le 0.575]$, with a smooth intermediate transition. This is also the device used in [3], except for a smooth transition of width 0.05 at the junctions.

145
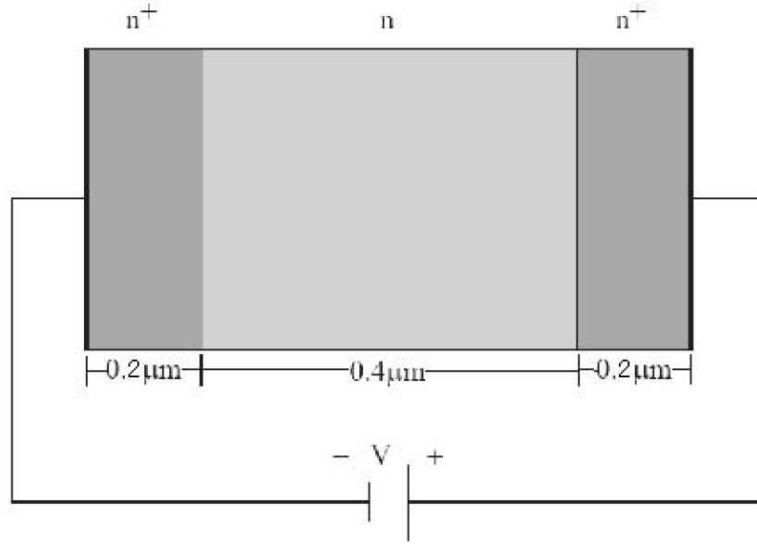
Figure 5.36: 1D GaAs n^+-n-n^+ diode

Here are other parameters: the lattice temperature $T_0 = 300$, the effective electron's mass $0.065 * 0.91$, the electric unit charge $e = 0.1602$, the Boltzmann constant $k_b = 0.138046 \times 10^{-4}$, the electric permittivity $\epsilon = 13.2 \times 8.85418$, [13].

Usually the relaxation time τ is given in terms of the mobility $\tau = \frac{m}{e}\mu$. Here we consider two different characterizations for μ:

1. Constant μ. We may have: $\mu = 0.14$.

2. Variable μ depending on the electric field E, used in drift-diffusion simulations to model saturation:

$$\mu(E) = \frac{2\mu_0}{1 + \sqrt{1 + 4(\mu_0|E|/v_d)^2}},$$

where $\mu_0 = 0.14$, $v_d = 0.11$. v_d here is taken to be the maximum of the velocity in the kinetic run with $V_{bias} = 1.0$ and $\mu = 0.14$ [9].

If we take $\mu = 0.14$, then the scaled mean free path $\varepsilon = \frac{\tau\sqrt{\theta}}{L} = 0.0171$ small. And $\alpha = \frac{eV_{bias}}{m\theta} = 38.7V_{bias}$ for LFS or $\gamma = \frac{\tau_0 eV_{bias}}{mL\sqrt{\theta}} = 0.662V_{bias}$ for $DCBS$. The scaled Debye length $\beta^2 = \frac{\epsilon V_{bias}}{e\rho_d L^2} = 0.57V_{bias}$ in the middle part of the device.

5.4.1 Drift-Diffusion Local Up-scaling(DrDiLU) Model

In the numerical test, we will use 160 points on the x-direction. On the ξ-direction, we choose $-1.3224 \leq \xi \leq 1.3224$ which is equal to 5 standard deviations and 25 points.

First we take $\mu_0 = 0.14$ and $V_{bias} = 0.05$, the results from the RT model and the DrDi model are shown in figure 5.37). From the profile of the electric field(bottom-left plot), we see the DrDi model fails to approximate the RT model around the doping steps, i.e. $x = 0.2$ and $x = 0.6$, where the electric field is high. This explains the big difference of the velocity's profiles between the DrDi model and the RT model (top-right plot in 5.37). If we look at the difference of the distribution functions obtained from these two models, i.e. the graph of $(f_r - f_d)/\rho_r$. Here subscript r denotes the RT model's result and d denotes the DrDi model's result, where f_d is defined as

$$f_d = \rho\mathcal{M}_\theta - \tau(\partial_x\rho + \frac{e}{m\theta}\rho E))\xi\mathcal{M}_\theta,$$

147

It is shown in figure 5.37. Also we can see the big difference between these two models around the doping steps. It implies we need to set these region to be the kinetic region if we want to get a more accurate result.

Then for the DrDiLU model, the kinetic regions are chosen to be $[0.18, 0.22]$ and $[0.52, 0.6]$. In other words, the transition function $h = 1$ in the kinetic regions, $h = 0$ in the regions $[0, 0.14] \bigcup [0.26, 0.48] \bigcup [0.64, 0.8]$. h is is linear and between 0 and 1 in all other regions.

The result of the three models when $V_{bias} = 0.1$ for the second order scheme is shown as the figure 5.38. From the velocity's plot(top right), we see the DrDiLU model has much better agreement with the RT model than the DrDi model, esp. around the doping steps.

Next we choose V_{bias} to be $0.05, 0.1, 0.15, 0.2, 0.25$ to get the I-V curve of the models. See figure 5.39. From the I-V curve we see the agreement of these three models is very good when the applied voltage is low(≤ 0.15).

We may also try the variable $\mu(E) = \frac{2\mu_0}{1+\sqrt{1+4(\mu_0|E|/v_d)^2}}$ and get the similar result. See figure 5.40.

When V_{bias} is increased, the electronic field becomes high and DrDi model can't be used to approximate the RT model. This can be shown from the big difference of the distribution functions of the RT model and the DrDi model in the n^- region. In this case both DrDi model and DrDiLU model fail. Instead we need to use HF

148
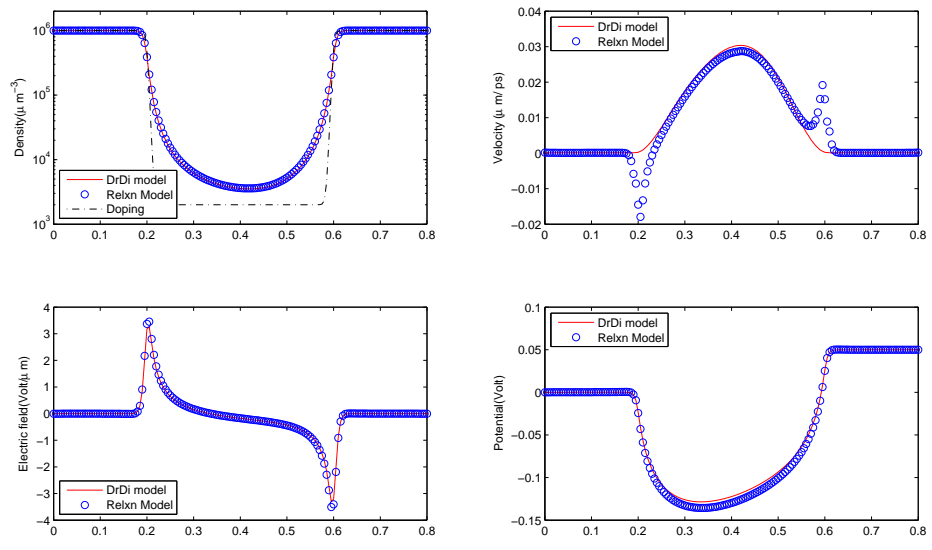
(a) Macro Quantities
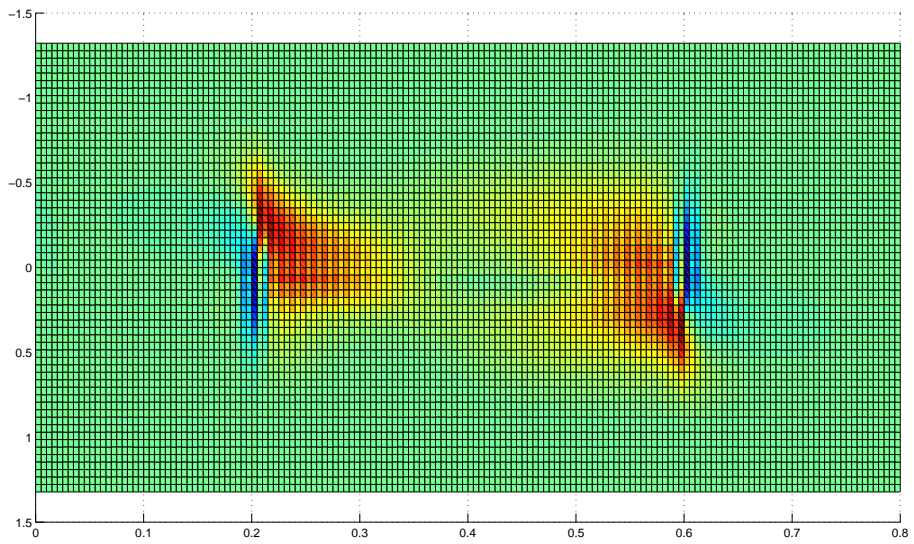
(b) Difference function

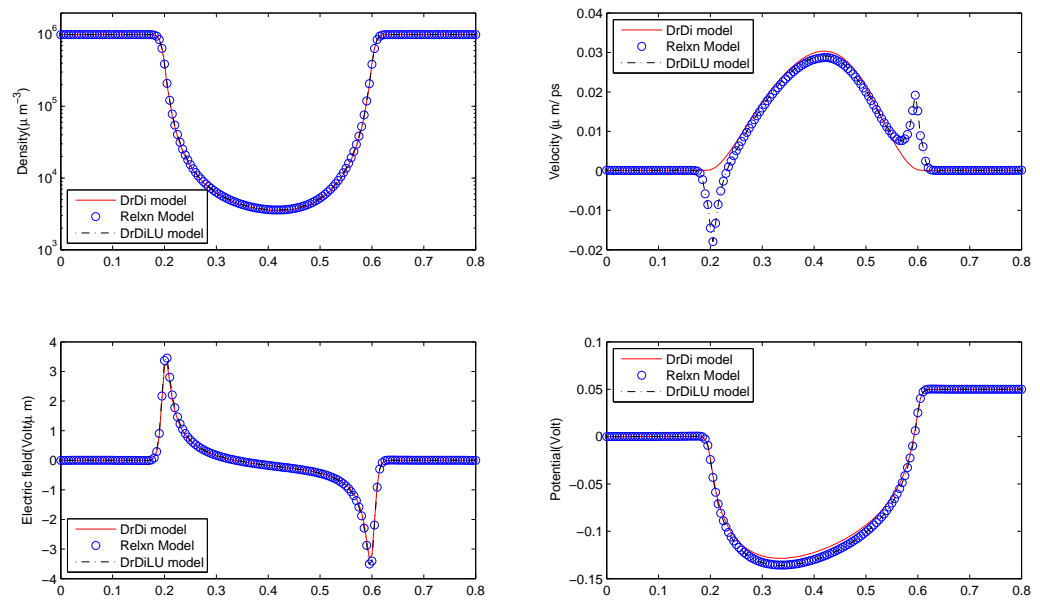Figure 5.37: Comparison of RT and DrDi, $V_{bias} = 0.05$

Figure 5.38: Comparison of Three models, $V_{bias} = 0.1$
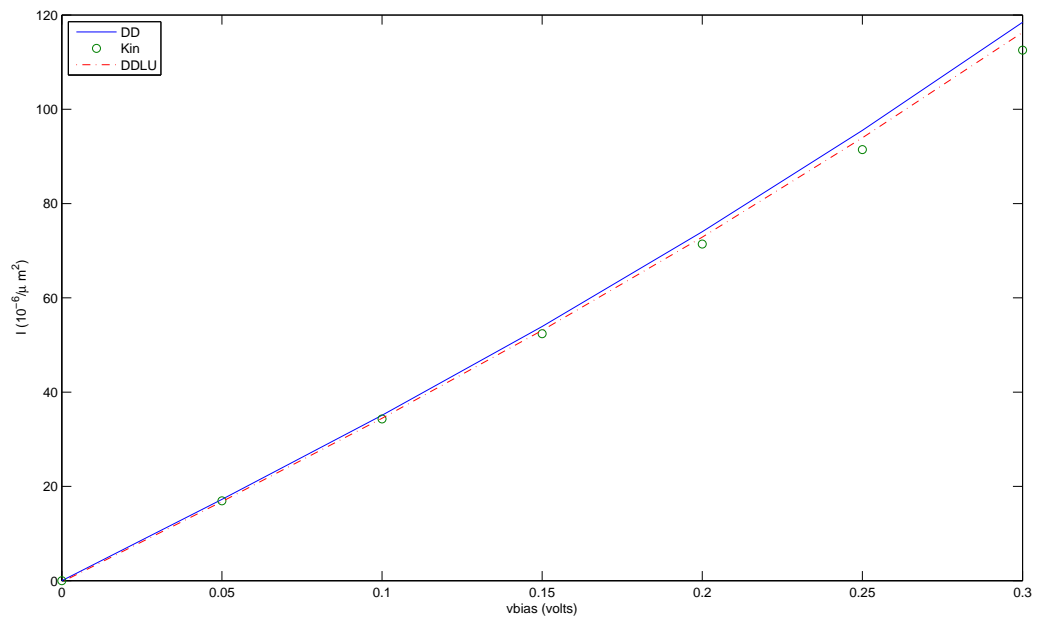
Figure 5.39: Comparison of Three models: I-V curves
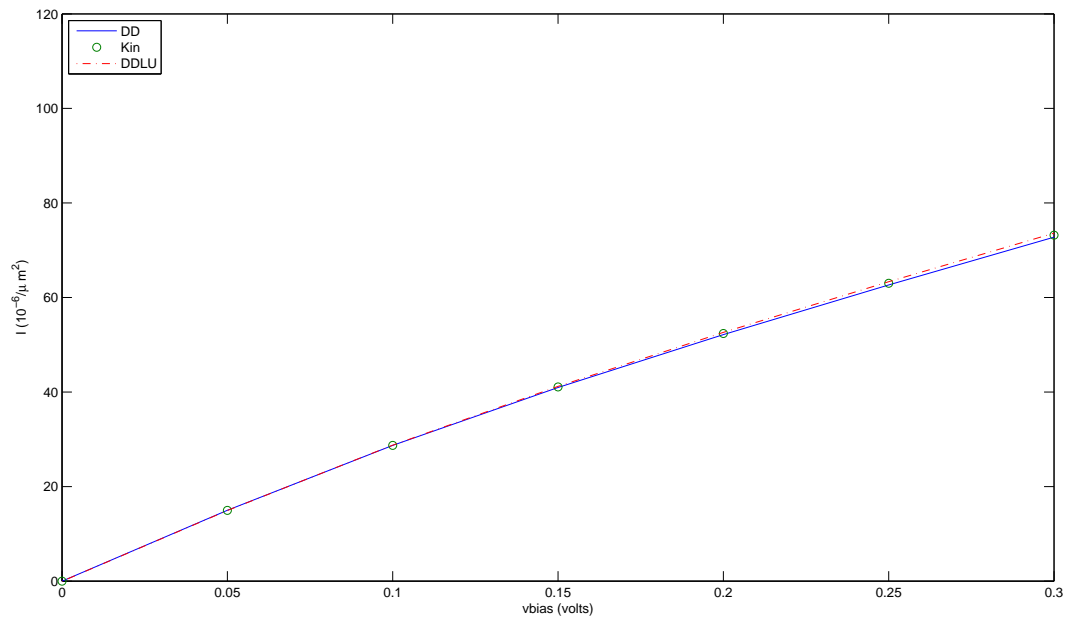
Figure 5.40: Comparison of Three models for variable $\mu(E)$: I-V curves

model to be the macroscopic model of the device. We may take $[0.25, 0.55]$ as the fluid region to apply the HF model and all other regions are kinetic regions where the RT model should be applied. In the computation, we choose 4 points overlap at the interface to get a smoother profile.

The result when $V_{bias} = 1$ is shown in figure 5.41.
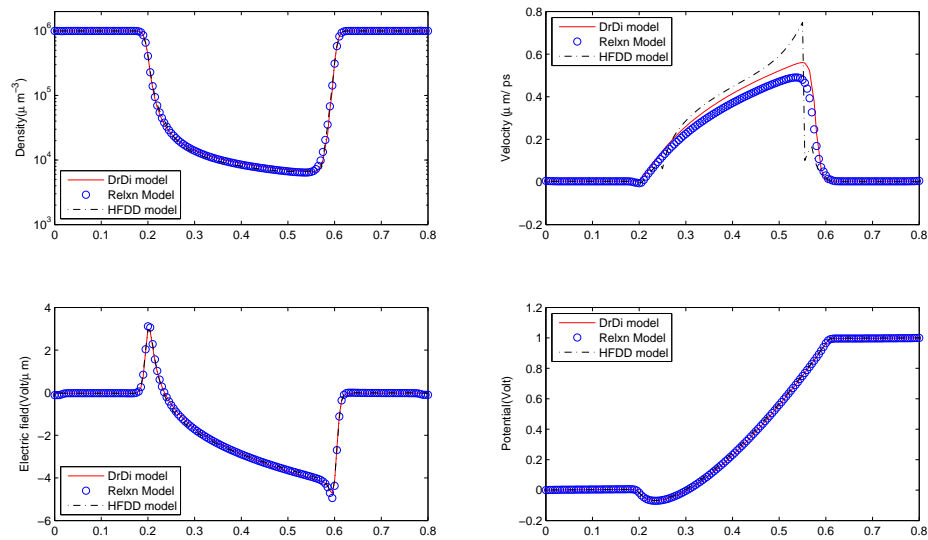
Figure 5.41: Comparison of Three models for variable $\mu(E) : V_{bias} = 1$

5.5 Simulation of 2D Planar Couette Flow

2D plannar Couette flow refers to the laminar flow of a viscous fluid in the space between two parallel plates, one of which is stationary and the other is moving with

a velocity in the plane of the surface. The flow is driven by virtue of viscous drag force acting on the fluid and the applied pressure gradient parallel to the plates.

The distance between the plates is $1m$ and the velocity of the walls are $\pm 0.5 Mach$, here 1 Mach corresponds $307.8m/s$. The temperature of the wall is $T = 273K$. The gas is argon whose parameters are mass $m = 6.63 \times 10^{-26} kg$, the coefficient of viscosity $\mu = 2.117^{-5} Nsm^{-2}$ and the density $n = 1.4 \times 10^{20} m^{-3}$.

Therefore the mean free path $\lambda = 0.0122m$. Therefore we need 100 cells so that the cell's size $\Delta x < \lambda$. We also choose 1/5 of mean free time to ensure that most of molecules can't pass a cell in one time step.

The diameter of the molecule is obtained from (4.62), [7], i.e.

$$\mu = \frac{5(mk_BT/\pi)^{1/2}}{16d^2}$$

Here μ is given so we get the diameter we need for DSMC is $d = 3.6284^{-10} m$.

The numerical result of viscosity comes from the Newton's formula, i.e: Shear Stress = Viscosity $\times$ Velocity Gradient. Therefore the tangential force $F = -\mu \frac{\partial u}{\partial y}$. Here $\frac{\partial u}{\partial y} = \frac{2w}{L}$. To get the viscosity, we only need to estimate the tangential force in the DSMC, which can be obtained by calculation of the momentum change of the molecules along the x-direction.

It is well-known that the DSMC's result converges very slowly. We may try to use ELU2 model with the stress tensor and heat flux obtained from the DSMC's result to get a smoother profile by means of the numerical viscosity of the Euler

fluxes without changing accuracy. Here is the ELU2 model we discussed before:

$$\partial_t \rho + \nabla_x \cdot (\rho \mathbf{u}) = 0,$$

$$\partial_t(\rho \mathbf{u}) + \nabla_x \cdot (\rho \mathbf{u} \otimes \mathbf{u} + \rho \theta I) + \nabla_x \cdot \tilde{\Sigma} = 0, \qquad (5.68)$$

$$\partial_t(\rho e) + \nabla_x \cdot ((\rho e + p)\mathbf{u}) + \nabla_x \cdot (\tilde{\Sigma} \cdot \mathbf{u} + \tilde{\mathbf{q}}) = 0,$$

where the viscosity and heat flux are the up-scaling terms

$$\tilde{\Sigma} = \langle \mathbf{c} \otimes \mathbf{c} f \rangle^2 - \frac{1}{3}\langle |\mathbf{c}|^2 f \rangle, \quad \tilde{\mathbf{q}} = \frac{1}{2}\langle \mathbf{c}|\mathbf{c}|^2 f \rangle, \qquad (5.69)$$

Here $\tilde{\Sigma}$ and $\tilde{\mathbf{q}}$ are obtained by sampling from the DSMC's result. To reduce the fluctuation of the up-scaling fluxes from DSMC, we use the fluxes obtained from the long time averaged result of DSMC as the up-scaling term for the moment equation.

We take 10000 simulate molecules totally, which means each represents 1.4×10^{17} real molecules and sample the DSMC's result after 20000 steps to supply the moment equation's initial condition. We choose the middle points of the cell as the grid point for the fluid equation and the same time step as DSMC.

To avoid boundary layer we use the DSMC's result close to the plates as the boundary condition of the fluid equation. Since DSMC is a first-order scheme so we apply the first-order scheme for the moment equations too.

In the computation we notice the conservation laws are lost due to the fluctuation of the boundary condition and the up-scaling terms which cause the density of ELU2's is much smaller and the temperature is much bigger compared with the

155

DSMC's result. To partially correct it, we enforce the conservation of mass and momentum in the following way:

$$\tilde{\rho} = \rho - \int \rho dx + \int \rho_0 dx, \quad \tilde{\mathbf{u}} = (\rho \mathbf{u} - \int (\rho \mathbf{u}) dx + \int \rho_0 \mathbf{u}_0 dx)/\tilde{\rho} \qquad (5.70)$$

where ρ_0 and $\mathbf{u}_0$ are the initial values. The figure 5.42 shows the result we get.
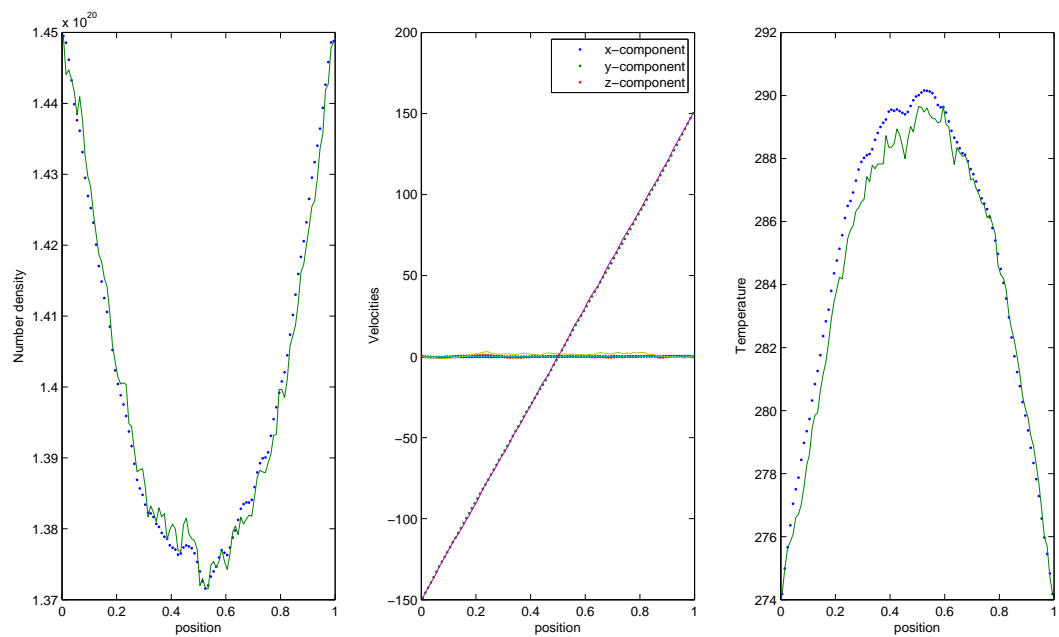

Figure 5.42: Comparison of Boltzmann equation (-) and ELU2 (.)

The solid line is the DSMC result and the dotted line is the ELU2 model's result. The density and velocities' profiles are good but the temperature's profile is a little big high.

Appendix A

Derivation of the Boltzmann Equation for Hard-Sphere Molecules

Assuming the molecules of a gas are hard, elastic and perfectly smooth spheres, the number of the molecules usually considered is extremely large $(2.7 \times 10^{19}/cm^3)$ at atmospheric pressure and $273K$, it is a hopeless task to attempt to describe the state the gas by specifying the positions and the velocities of every individual sphere. Therefore Maxwell and Boltzmann started to work with the one-particle probability density: $P^{(1)}(t, \mathbf{x}, \boldsymbol{\xi})$ which is a function of seven variables. Here $\mathbf{x} = (x_1, x_2, x_3)^T \in R^3, \boldsymbol{\xi} = (\xi_1, \xi_2, \xi_3)^T \in R^3$. Boltzmann wrote an evolution equation for $P^{(1)}$ by means of a heuristic argument with extra assumptions in the following way. [10]

For the exact dynamics of N molecules, we define $P^{(1)}(t, \mathbf{x}, \boldsymbol{\xi})$ as the probability density of finding one fixed particle (say the one labeled by 1) at a certain point $(\mathbf{x}, \boldsymbol{\xi})$ of the 6-dimension reduced phase space associated with the position and velocity of that particle at time t.

In the absence of collisions, $P^{(1)}$ would remain unchanged along the trajectory of the particle if there is no external force. Accordingly, we must evaluate the effects of collisions and have the following equation of $P^{(1)}$:

$$\frac{\partial P^{(1)}}{\partial_t} + \boldsymbol{\xi} \cdot \frac{\partial P^{(1)}}{\partial \mathbf{x}} = G - L, \tag{A.1}$$

157

where the gain term $Gd\mathbf{x}d\boldsymbol{\xi}dt$ gives the expected number of particles with position between $\mathbf{x}$ and $\mathbf{x} + d\mathbf{x}$ and velocity between $\boldsymbol{\xi}$ and $\boldsymbol{\xi} + d\boldsymbol{\xi}$ that enter these ranges of values because of a collision in the time interval between t and $t + dt$, the lost term $Ld\mathbf{x}_1 d\boldsymbol{\xi}dt$ gives the analogous number of particles disappearing from the same range in the same time interval.

For dilute gas, we assume the intermolecular collisions are overwhelmingly likely to be the binary collisions.
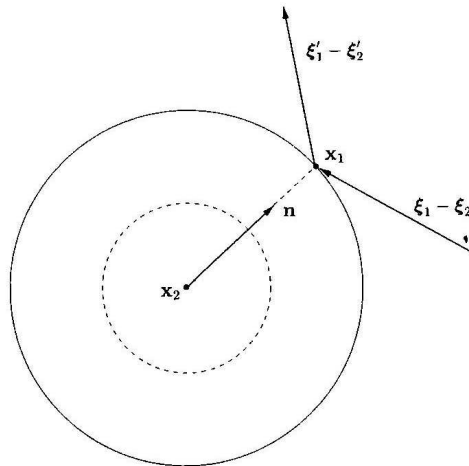
Figure 1.1. The directions of the relative velocities before and after the impact are bisected by the unit vector $\mathbf{n}$.

Consider these binary collisions are elastic, i.e. there is no interchange of translational and internal energy. When two particles with velocities $(\boldsymbol{\xi}, \boldsymbol{\xi}_1)$ collide, moment and kinetic energy must be conserved. The post-collision velocities $(\boldsymbol{\xi}', \boldsymbol{\xi}_1')$

158

are related to the pre-collision velocities $(\boldsymbol{\xi}, \boldsymbol{\xi}_1)$ by

$$\boldsymbol{\xi}' = \boldsymbol{\xi} - \mathbf{n}[\mathbf{n} \cdot (\boldsymbol{\xi} - \boldsymbol{\xi}_1)], \qquad \boldsymbol{\xi}_1' = \boldsymbol{\xi}_1 + \mathbf{n}[\mathbf{n} \cdot (\boldsymbol{\xi} - \boldsymbol{\xi}_1)], \qquad \text{(A.2)}$$

where $\mathbf{n}$ is the unit vector along $\boldsymbol{\xi} - \boldsymbol{\xi}'$.

In order to write L and G, we need another function $P^{(2)}$ that gives the probability density of finding, at time t, the first particle at $\mathbf{x}$ with velocity $\boldsymbol{\xi}$ and the second at $\mathbf{x}_1$ with velocity $\boldsymbol{\xi}_1$. We write $P^{(2)} = P^{(2)}(\mathbf{x}, \boldsymbol{\xi}, \mathbf{x}_1, \boldsymbol{\xi}_1, t)$.
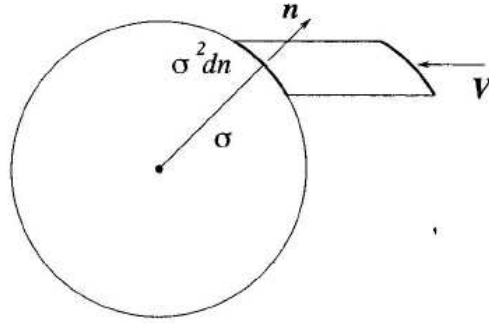
Figure 1.2. Calculation of the number of collisions between two molecules.

Let d be the diameter of the particle. From figure 1.2, the base area of the cylinder is $\mathrm{d}^2 d\Omega$ and the height is $|(\boldsymbol{\xi}_1 - \boldsymbol{\xi}) \cdot \mathbf{n}|$, where $d\Omega$ is the unit solid angle about the vector $\mathbf{n}$. In the spherical coordinates system, $d\Omega = \sin\theta d\theta d\epsilon$ where θ is the zenith angle and ϵ is the azimuth angle. Here θ is the angle between $\mathbf{n}$ and the relative velocity $\mathbf{V} = \boldsymbol{\xi}_1 - \boldsymbol{\xi}$. The relative speed $|\boldsymbol{\xi}_1 - \boldsymbol{\xi}|$ will be denoted by V. Then $\mathbf{V} \cdot \mathbf{n} = V \cos\theta$. We may also use $\chi = \pi - 2\theta$. Here χ is the deflection angle.

Fixing the first particle, we integrate over the sphere for all $\mathbf{n}$ and all the

159

possible velocities of the second particle to obtain

$$L = (N-1)\mathrm{d}^2 \int_{R^3} \int_{B^-} P^{(2)}(t,\mathbf{x},\boldsymbol{\xi},\mathbf{x}+\mathrm{d}\mathbf{n},\boldsymbol{\xi}_1)V\cos\theta d\Omega d\boldsymbol{\xi}_1, \qquad (\mathrm{A.3})$$

where B^- is the hemisphere corresponding to $0 \le \theta \le \frac{\pi}{2}$(the particles are moving toward each other before the collision) and $\mathbf{n} = (\sin\theta\cos\epsilon, \sin\theta\sin\epsilon, \cos\theta)$. Here we use $N-1$ because there are $N-1$ particles remaining if we fix the first particle. Similarly, we have

$$G = (N-1)\mathrm{d}^2 \int_{R^3} \int_{B^+} P^{(2)}(t,\mathbf{x},\boldsymbol{\xi},\mathbf{x}+\mathrm{d}\mathbf{n},\boldsymbol{\xi}_1)V(-\cos\theta)d\Omega d\boldsymbol{\xi}_1, \qquad (\mathrm{A.4})$$

where B^+ is the hemisphere corresponding to $\frac{\pi}{2} \le \theta \le \pi$(the particles are moving toward each other after the collision). We may change $\mathbf{n}$ into $-\mathbf{n}$ to have the same integration range as in L and then we have

$$G = (N-1)\mathrm{d}^2 \int_{R^3} \int_{B^-} P^{(2)}(t,\mathbf{x},\boldsymbol{\xi},\mathbf{x}-\mathrm{d}\mathbf{n},\boldsymbol{\xi}_1)V\cos\theta d\Omega d\boldsymbol{\xi}_1, \qquad (\mathrm{A.5})$$

Assuming the probability $P^{(2)}$ is continuous at a collision, we have

$$P^{(2)}(t,\mathbf{x},\boldsymbol{\xi},\mathbf{x}_1,\boldsymbol{\xi}_1) = P^{(2)}(t,\mathbf{x},\boldsymbol{\xi}',\mathbf{x}_1,\boldsymbol{\xi}_1') \qquad (\mathrm{A.6})$$

i.e.

$$G = (N-1)\mathrm{d}^2 \int_{R^3} \int_{B^-} P^{(2)}(t,\mathbf{x},\boldsymbol{\xi}',\mathbf{x}-\mathrm{d}\mathbf{n},\boldsymbol{\xi}_1')V\cos\theta d\Omega d\boldsymbol{\xi}_1, \qquad (\mathrm{A.7})$$

Consider the Boltzmann-Grad limit, i.e. let $N \to \infty, \mathrm{d} \to 0$ with $N\mathrm{d}^2$ finite, we may neglect the difference between $\mathbf{x}$ and $\mathbf{x} \pm \mathrm{d}\mathbf{n}$ in the expressions of L and G

160

and change $N - 1$ to be N. Also we may assume the probability of finding a pair of particles in a particular configuration before collision is simply the product of the probabilities of finding the individual particles in the two corresponding one-particle configuration (molecular chaos), i.e.

$$P^{(2)}(\mathbf{x}, \boldsymbol{\xi}, \mathbf{x}_1, \boldsymbol{\xi}_1, t) = P^{(1)}(t, \mathbf{x}, \boldsymbol{\xi}) P^{(1)}(t, \mathbf{x}_1, \boldsymbol{\xi}_1) \tag{A.8}$$

Therefore

$$G - L = N\mathrm{d}^2 \int_{R^3} \int_{B^-} \left(P^{(1)}(t, \mathbf{x}, \boldsymbol{\xi}') P^{(1)}(t, \mathbf{x}, \boldsymbol{\xi}_1') \right.$$
$$\left. - P^{(1)}(t, \mathbf{x}, \boldsymbol{\xi}) P^{(1)}(t, \mathbf{x}, \boldsymbol{\xi}_1) \right) V \cos\theta d\Omega d\boldsymbol{\xi}_1, \tag{A.9}$$

Let $f(t, \mathbf{x}, \boldsymbol{\xi})$ be the expected number density distribution of the particles at time t at the point $(\mathbf{x}, \boldsymbol{\xi})$ in the phase space. Therefore $f = NP^{(1)}$. Then the evolution of f for the hard-sphere monatomic particles is governed by the Boltzmann equation:

$$\frac{\partial f}{\partial t} + \boldsymbol{\xi} \cdot \nabla_{\mathbf{x}} f = Q(f, f), \tag{A.10}$$

The quadratic integral collision operator $Q(f, f)$ is

$$Q(f, f) = \int_{R^3} \int_{B^-} (f' f_1' - f f_1) \mathrm{d}^2 V \cos\theta d\Omega d\boldsymbol{\xi}_1, \tag{A.11}$$

Here $f = f(t, \mathbf{x}, \boldsymbol{\xi})$, $f_1 = f(t, \mathbf{x}, \boldsymbol{\xi}_1)$, $f' = f(t, \mathbf{x}, \boldsymbol{\xi}')$, $f_1' = (t, \mathbf{x}, \boldsymbol{\xi}_1')$.

Appendix B

List of Molecular Models

From A.11, we see the only difference of Boltzmann equations for different models is the collision term.

Plug the expression $d\Omega = \sin\theta d\theta d\epsilon$ into the collision term $Q(f, f)$ of the hard sphere model, we get

$$Q(f, f) = \int_{R^3} \int_0^{2\pi} \int_0^{\pi/2} (f'f_1' - ff_1) \mathrm{d}^2 V \cos\theta \sin\theta d\theta d\epsilon d\boldsymbol{\xi}_1, \qquad (B.1)$$

In terms of the deflection angle $\chi = \pi - 2\theta$, we may write $Q(f, f)$ as

$$Q(f, f) = \frac{1}{4} \int_{R^3} \int_B (f'f_1' - ff_1) V \mathrm{d}^2 d\Omega d\boldsymbol{\xi}_1 = \int_{R^3} \int_B (f'f_1' - ff_1) V \left(\frac{1}{4}\mathrm{d}^2\right) d\Omega d\boldsymbol{\xi}_1,$$
$$(B.2)$$

The disadvantage of hard sphere model is that its collision cross-section is independent of the relative speed V of two interacting molecules, which is not realistic. For a realistic molecular model, the molecular diameter should depend not only on the relative speed V of the two molecules, but also on the relative moving direction, or the deflection angle χ. In this case, we change $\frac{1}{4}\mathrm{d}^2$ to be $\sigma(V, \chi)d\Omega$ and call σ the differential cross-section. The Boltzmann equation for the general monatomic

162

molecules takes on the following form:

$$\frac{\partial f}{\partial t} + \boldsymbol{\xi} \cdot \nabla_{\mathbf{x}} f = Q(f, f), \tag{B.3}$$

where the quadratic integral collision operator $Q(f, f)$ is

$$Q(f, f) = \int_{R^3} \int_B (f' f_1' - f f_1) V \sigma d\Omega d\boldsymbol{\xi}_1, \tag{B.4}$$

The function $\sigma(V, \chi)$ summarizes the complicated details of the two-body interactions, and $V\sigma$ gives essentially the (unnormalized) probability density of a relative deflection χ for a pair of molecules having the relative speed V. Notice the total collision cross-section $\sigma_T = \int_B \sigma d\Omega$.

Here is a list of some generally used molecular models:

1. **Inverse Power Law Model (IPL).** The potential force $F = \kappa/r^\eta$. The differential cross-sections is written as:

$$\sigma d\Omega = W_0 \left\{ \kappa/(m_r V^2) \right\}^{2/(\eta-1)} dW_0 d\epsilon, \tag{B.5}$$

here $m_r = m/2$ is the reduced mass. Let b be the the miss-distance, then $W_0 = b(m_r V^2)^{1/(\eta-1)}$ is a dimensionless impact parameter which is shown to be a single variable function of the deflection angle χ.

Remark. For this model, we need to integrate W_0 from 0 to ∞ to get σ_T. In this case, the collision term cannot be expressed in terms of the elementary functions because of the unbounded total collision cross-section. Therefore a

finite cut-off of miss-distance or the deflection angle is necessary. Because of the arbitrary choice of this cut-off, it is not suitable to use this model to get the collision frequency or the mean free path.

2. **Maxwell model (MAX)**: This is a special case of inverse power law model with $\eta = 5$. The differential cross-section is

$$\sigma d\Omega = \frac{W_0}{V} \left\{ \frac{\kappa}{m_r} \right\}^{1/2} dW_0 d\epsilon, \tag{B.6}$$

This means the collision probability $V\sigma d\Omega = W_0 \left\{ \frac{\kappa}{m_r} \right\}^{1/2} dW_0 d\epsilon$ is independent of the relative speed in the Maxwell gas, which is unrealistic for the real gases. Since all the molecules have the same collision probability, the Maxwell model is widely used in the analytical study.

3. **Hard Sphere model (HS)**: This is the model we already discussed. It can be considered as the extreme case: $F = 0, r \geq d; F = \infty, r < d$, where d is the diameter of the molecule. The differential cross-section

$$\sigma d\Omega = \frac{1}{4} d^2 \sin \chi d\chi d\epsilon, \tag{B.7}$$

4. **Variable Hard Sphere model (VHS)**:

Other than extremely low temperature, the effective cross-section of real molecules decreases as V increases. The rate of change is directly related to the change of the viscosity coefficient μ with the temperature T. The HS model shows

$\mu \propto T^{0.5}$ while $\mu \propto T^{0.75}$ is the characteristic of real gas. The variable cross-section is needed to match the power of real gas.

If we integrate the inverse power law model with finite cut-off of W_0, which is equivalent to the finite cut-off of χ, we get

$$\sigma_T = \pi W_{0,m}^2 \left\{ \kappa/(m_r V^2) \right\}^{2/(\eta-1)} , \tag{B.8}$$

which shows the total cross-section is inversely proportional to $V^{4/(\eta-1)}$.

These observations led Bird [6] to introduce the variable hard sphere molecular model. In this model, the molecule is still considered as the hard sphere, but its diameter of a hard sphere molecule is a function of the relative speed V, i.e. $d = d_{ref}(V_{ref}/V)^\nu$ where the subscript $_{ref}$ denotes the reference values. It is shown in [7] if $\nu = 4/(\eta-1)$, then the variation of μ with T will be same as the inverse power law model, with $\mu \propto T^{\nu+1/2}$.

The VHS model is defined by the effective diameter at a particular reference temperature. Since VHS model combines a finite cross-section with a realistic temperature exponent w, it has permitted the definition of a mean free path and the Knudsen number. We also have $\chi = 2\cos^{-1}\frac{b}{d}$, which is the same as the HS model.

Appendix C

Break-downs of Macroscopic Model for Small κ

In order to use the ELU or NSLU model, the kinetic effects should be localized in the kinetic region which is defined by some criteria, like Knudsen number κ. Since the fluid model only describe the leading behavior of the motion of the gas using the expansion on κ, which is only a necessary condition, but not sufficient for the asymptotic behavior. We may see it more clearly in the following examples.

Example 1: the Jin-Xin relaxation model. If we take the relaxation rate $\kappa = 0.02$ in the fluid region and $\kappa = 1$ in the kinetic region. All other data is same as the moving shock in the numerical experiment. Using first order scheme, we may get the following graph (C.1):

The fluid regions are the left regions in the above graphs. Close to the boundary of the fluid region (the leftmost vertical dotted line), both Euler and Navier-Stokes solutions are quite different from the kinetic solutions. Therefore if we want to keep the accuracy, we need to choose a larger kinetic region such that the asymptotic property holds in all the fluid region. Here we should choose to kinetic region $[-0.05, 1]$ instead of $[0.05, 1]$.

Example 2: Another example is the high mach number stationary shock.
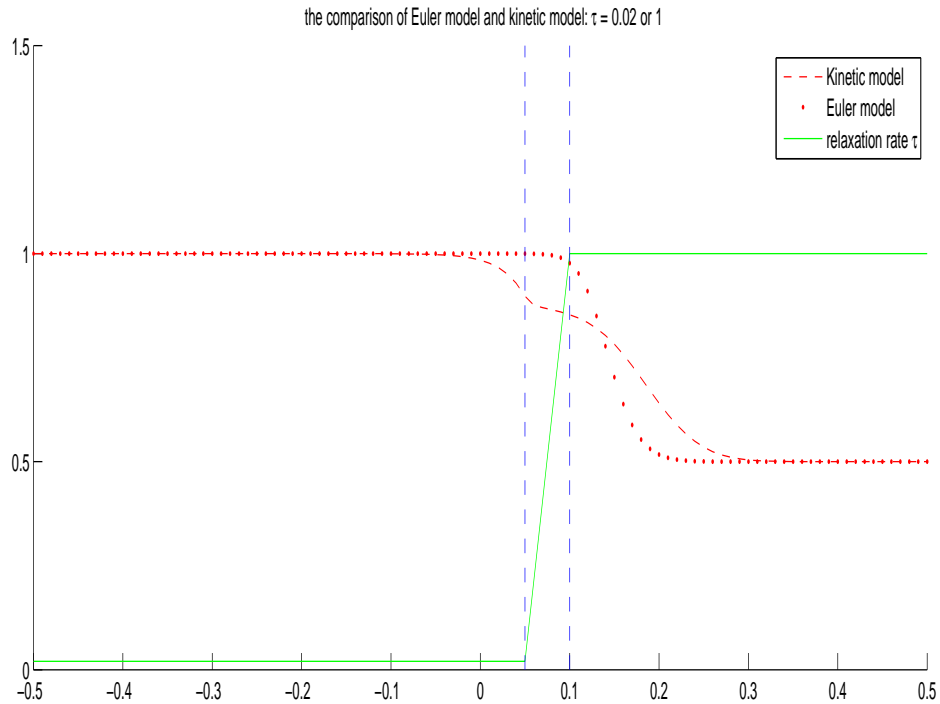
166

Figure C.1: Euler & Kinetic for Jin-Xin model, with fluid $\kappa = 0.02, 1$

The Navier-Stokes equations approximate the kinetic model only when the shock is weak, or the Mach number is < 2. Here is a picture copied from [46] which shows that the Navier-Stokes equation doesn't agree with the BGK model in the upstream part when Mach number is 5 although the local Knudsen number is small. See figure C.2. This is the shock-wave velocity profiles obtained in [32]. The BGK solutions follows closely the Navier-Stokes solution in the downstream, high-density portion
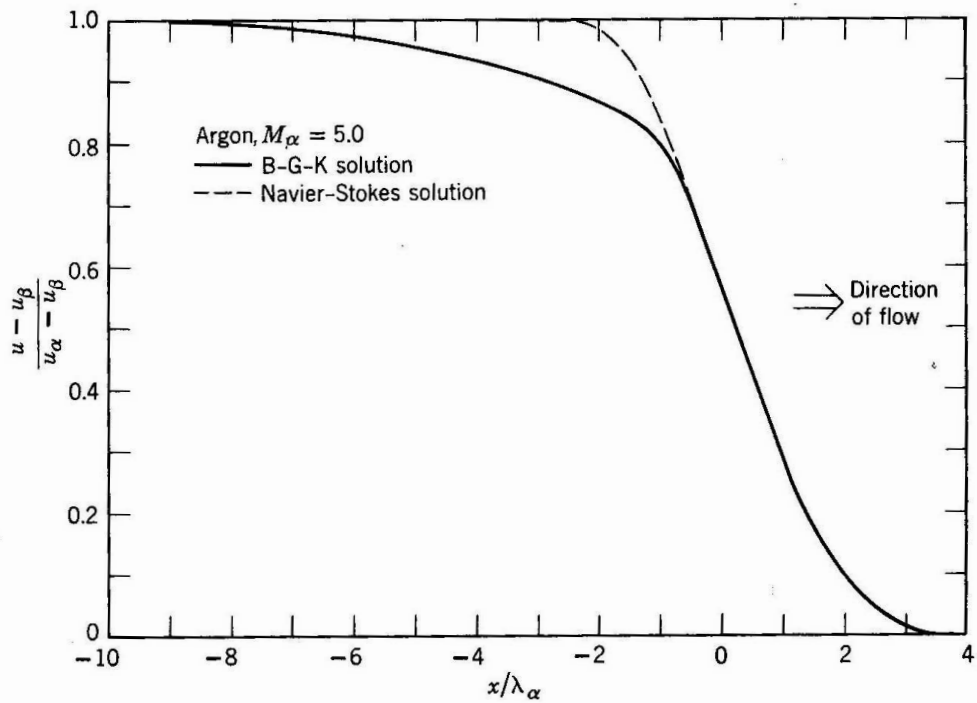
Fig. 4. Shock-wave velocity profiles according to the B-G-K and Navier-Stokes
solutions (after Liepmann, Narasimha, and Chahine, 1962).

Figure C.2: High Mach number stationary shock: BGK & NS

of the shock wave but gives a much thicker profile in the upstream region.

Appendix D

Zero-Moment Projections for the BGK Model

In this section, we will derive the zero-moment projection formula for the 1D1D

BGK model and the reduced dimension BGK model which are used in the numerical

experiments.

168

D.1 Zero-Moment Projection for 1D1D BGK Model

Since the normalized orthogonal basis of the space $(a + b\xi + c\xi^2)\mathcal{M}^{n+1}$ are

$$\chi_0 = \frac{1}{\sqrt{\rho}}\mathcal{M}^{n+1}, \quad \chi_1 = \frac{u - \xi}{\sqrt{\rho\theta}}\mathcal{M}^{n+1}, \quad \chi_2 = \frac{1}{\sqrt{2\rho}}\left(\frac{(u - \xi)^2}{\theta} - 1\right)\mathcal{M}^{n+1}, \quad \text{(D.1)}$$

Therefore the projection of g^{n+1} onto the space spanned by these three basis is

$$\mathcal{P}g^{n+1} = \sum_{i=0}^{2}[g^{n+1}, \chi_i]\chi_i, \quad \text{(D.2)}$$

after some simple computation, we get

$$\mathcal{P}g^{n+1} = \frac{1}{\rho}\left(\langle g^{n+1}\rangle + \frac{u - \xi}{\theta}\langle(u - \xi)g^{n+1}\rangle \right. \\ \left. + \frac{(u - \xi)^2 - \theta}{2\theta}(\frac{1}{\theta}\langle(u - \xi)^2 g^{n+1}\rangle - \langle g^{n+1}\rangle)\right)\mathcal{M}^{n+1}, \quad \text{(D.3)}$$

therefore the corrected g^{n+1} will be $\tilde{g}^{n+1} = g^{n+1} - \mathcal{P}g^{n+1}$.

D.2 Zero-Moment Projection for 1D3D BGK Model

To get the reduced dimension, we assume f is an even function w.r.t ξ_2 and ξ_3. Therefore the non-equilibrium part is also an even function w.r.t ξ_2 and ξ_3. For such a non-equilibrium $h(\boldsymbol{\xi})$, the projection of h to $\mathcal{M}_3$ is defined as $\mathcal{P}h = \sum_{i=0}^{4}[h, \chi_i]\chi_i$.

Let $f = \int_{R^2} h d\xi_2 d\xi_3, \quad g = \frac{1}{2}\int_{R^2}(\xi_2^2 + \xi_3^2)h d\xi_2 d\xi_3$, we have

$$[h, \chi_0] = \frac{1}{\sqrt{\rho}}\int_R f d\xi_1 = \frac{1}{\sqrt{\rho}}\langle f \rangle,$$

$$[h, \chi_1] = \frac{1}{\sqrt{\rho\theta}}\int_R (u - \xi_1) f d\xi = \frac{1}{\sqrt{\rho\theta}}\langle (u - \xi_1)f \rangle,$$

$$[h, \chi_2] = \frac{1}{\sqrt{\rho\theta}}\int_{R^3} \xi_2 h d\boldsymbol{\xi} = 0, [h, \chi_3] = \frac{1}{\sqrt{\rho\theta}}\int_{R^3} \xi_3 h d\boldsymbol{\xi} = 0,$$

$$[h, \chi_4] = \frac{1}{\sqrt{6\rho}}\int_R \left(\frac{(u - \xi_1)^2}{\theta} - 3\right)f + g d\xi_1 = \frac{1}{\sqrt{6\rho}}(\frac{1}{\theta}\langle(u - \xi_1)^2 f\rangle - 3\langle f\rangle + \frac{2}{\theta}\langle g\rangle),$$

$$\text{(D.4)}$$

After some computation, we get

$$\mathcal{P}h = \frac{1}{\rho}\left\{\langle f \rangle + \frac{u - \xi_1}{\theta}\langle(u - \xi_1)f\rangle \right.$$
$$\left. + \frac{(u - \xi_1)^2 + \xi_2^2 + \xi_3^2 - 3\theta}{6\theta}\left(\frac{1}{\theta}\langle(u - \xi_1)^2 f + 2g\rangle - 3\langle f\rangle\right)\right\}\mathcal{M}_3,$$

$$\text{(D.5)}$$

Therefore if we get $\mathcal{P}f = \int_{R^2} \mathcal{P}h d\xi_2 d\xi_3$, then

$$\mathcal{P}f = \frac{1}{\rho}\left\{\langle f \rangle + \frac{u - \xi_1}{\theta}\langle(u - \xi_1)f\rangle + \frac{(u - \xi_1)^2 - \theta}{6\theta}\left(\frac{1}{\theta}\langle(u - \xi_1)^2 f + 2g\rangle - 3\langle f\rangle\right)\right\}\mathcal{M},$$

$$\text{(D.6)}$$

Define $\mathcal{P}g = \frac{1}{2}\int_{R^2}(\xi_2^2 + \xi_2^2)\mathcal{P}h d\xi_2 d\xi_3$, we get

$$\mathcal{P}g = \frac{1}{\rho}\{\theta\langle f\rangle + (u - \xi_1)\langle(u - \xi_1)f\rangle$$
$$+ \frac{(u - \xi_1)^2 + \theta}{6}\left(\frac{1}{\theta}\langle(u - \xi_1)^2 f + 2g\rangle - 3\langle f\rangle\right)\}\mathcal{M},$$

$$\text{(D.7)}$$

Therefore the corrected f^{n+1}, g^{n+1} will be

$$\tilde{f}^{n+1} = f^{n+1} - \mathcal{P}f^{n+1}, \quad \tilde{g}^{n+1} = g^{n+1} - \mathcal{P}g^{n+1}, \tag{D.8}$$

170

Bibliography

[1] Andries, P., and Perthame, B., the ES-BGK Model Equation with Correct Prandtl Number, Proceedings of the 22nd International Symposium on Rarefied Gas Dynamics , American Institute of Physics, pp.426-433, (2001)

[2] Harold U. Baranger and John W. Wilkins, Ballistic electrons in an inhomogeneous submicron structure: Thermal and contact effects, Phys. Rev. B, Vol.30, Num.12 (1984)

[3] H.U. Barenger, J.W. Wilkins, Ballistic structure in the electron distribution function of small semiconducting structures: General features and specific trends, Phys. Rev. B36 (1987) 1487-1502.

[4] I.D. Boyd, G. Chen, and G.V. Candler, Predicting failure of the continuum fluid equations in transitional hypersonic flows, Phys. Fluids 7, 210 (1995).

171

[5] P.L.Bhatnagar, E.P.Gross, and M.Krook, A model for collision processes in gases. Small amplitude processes in charged and neutral one-component systems, Phys. Rev. 94, 511-525 (1954)

[6] G.A.Bird, Monte-Carlo simulation in an engineering context, Rarefied Gas Dynamics, S.S.Fischer, Ed., Vol. I,239-255, AIAA, New York (1981)

[7] G.A.Bird, Molecular gas dynamics and the direct simulation of gas flows, Oxford Science Publications (1994)

[8] J.-F. Bourgat, P. Le Tallec, M.D. Tidriri, Coupling Boltzmann and Navier-Stokes equations by friction, J. Comput. Phys 127 (1996) 227-245

[9] S. Chen, W. E, Y. Liu, C-W Shu, A discountinuous galerkin implementation of a domain decomposition method for kinetic-hydrodynamic coupling multi-scale problems in gas dynamics and device simulations, 1314-1330, 225, J. Compu. Physics, (2007)

[10] Carlo Cercignani, Rarefied Gas Dynamics, Cambridge University Press (2000)

[11] Carlo Cercignani, Mathematical Methods in Kinetic Theory, 2nd ed., Plenum Press (1990)

[12] S Stefanov, C Cercignani, Monte Carlo simulation of the Taylor-Couette flow of a rarefied gas, Journal of Fluid Mechanics 256, 199-213, Cambridge University Press (1993)

[13] C. Cercignani, I.M. Gamba, J.W. Jerome, C.-W. Shu, Device benchmark comparisons via kinetic, hydrodynamic, and high-field models, Comput. Meth. Appl. Mech. Eng. 181, 381C392 (2000)

[14] C.Cercignani, I.M.Gamba and C.D.Levermore. High field approximations to Boltzmann-Poisson system boundary conditions in a semiconductor. Appl. Math. Lett., 10:111-117, (1997)

[15] J.A. Carrillo, I.M.Gamba, A.Majorana and C.-W. Shu, A WENO-solver for the 1D non-stationary Boltzmann-Poisson system for semiconductor devices, J. Compu. Electron., 1, 365-370, (2002)

[16] H. Choi and J.-G. Liu, The reconstruction of upwind fluxes for conservation laws - Its behavior in dynamic and steady state calculations, Journal of Computational Physics. Vol. 144, no. 2, pp.237-256. 10 Aug. (1998)

[17] S. Y. Chou and D. Baganoff, Kinetic flux-vector splitting for the Navier-Stokes equations, J. Compu. Phys. 130, 217 (1997)

[18] P. Degond, S. Jin, and L. Mieussens, A smooth transition model between kinetic and hydrodynamic equations, J. Comput. Phys., 209 (2005)

[19] P. Degond, J.-G. Liu and L. Mieussens, Macroscopic fluid modes with localized kinetic upscaling effects, Multi-scale Model. Simul. 5 695–1043 (2006)

[20] W. E and B. Engquist, The heterogeneous multi-scale methods, Comm. Math. Sci., vol. 1, no. 1, pp. 87-132 (2003)

[21] W. E, B. Engquist, X. Li, W. Ren and E. Vanden-Eijnden, Heterogeneous multi-scale methods: A review, Comm. Comput. Phys., vol. 2, no. 3, pp.367-450 (2007)

[22] W. E and Z. Huang, A dynamic atomistic-continuum method for the simulation of crystalline materials, J. Comput. Phys., 182 (2002),

[23] Alejanoro L. Garcia, Numerical methods for physics, 2nd Ed. Prentice Hall (2000)

[24] E. Godlewski and P.-A. Raviart, Numerical approximation of hyperbolic systems of conservation laws, Springer (1996)

[25] D. Hash and H. Hassan, A Decoupled DSMC/NavierCStokes Analysis of a Transitional Flow Experiment, AIAA Paper 96-0353 (1996).

[26] A.B. Huang, P.F. Hwang, Test of statistical models for gases with and without internal energy states, Phys. Fluids 16 (4) 466C475 (1973).

[27] Holway, L. H., Kinetic Theory of Shock Structure Using an Ellipsoidal Distribution Function, Proceedings of the Fourth International Symposium on Rarefied Gas Dynamics, Academic Press, New York, pp. 193-215.11 (1966)

[28] S. Jin, C.-D. Levermore, Numerical schemes for hyperbolic conservation laws with stiff relaxation terms, J. Comput. Phys. 126 (2) 449C467 (1996)

[29] S. Jin, Z.P. Xin , The relaxation schemes for systems of conservation laws in arbitrary space dimensions, Comm. Pure Appl. Math. 48 235C277 (1995).

[30] K.Koura and H. Matsumoto, Variable soft sphere molecular model for inverse power-law or Lennard-Jones potential, Phys. Fluids A 3, 2459-2465 (1991)

[31] C.D. Levermore, Fluid dynamic limits of kinetic equations. I. formal derivations, J. Stat. Phys. 63, no. 1-2, 323-344 (1991)

[32] Liepmann, H.W., R. Narasimha, and M. T. Chahine, Structure of a Plane Shock Layer. Phys. Fluids, vol. 5, no. 11, pp.1313, (1962)

[33] T.-P. Liu, Hyperbolic Conservation Laws with Relaxation, Commun. Math. Phys. 108, pp.153-175 (1987)

[34] T.-P. Liu, T. Yang and S.-H. Yu, Energy method for the Boltzmann equation, Phys. D 188, pp.178-192 (2004)

[35] J.C. Maxwell, Phil. Trans. R. Soc. I, Appendix (1879)

[36] J. Mandel and S. Deshpande, Kinetic flux vector splitting for Euler equations, Compu. Fluids 23, 447(1994)

[37] L. Mieussens, Discrete velocity model and implicit scheme for the BGK equation of rarefied gas dynamics, Math. Models and Meth. in Appl. Sci., Vol. 10, No.8 (2000)

[38] P.A.Markowich, C.A. Ringhofer and C.Shmeiser, Semiconductor Equations, springer, New York, 1990

[39] Taku Ohwada, Boltzmann schemes for the compressible Navier-Stokes equations, Vol. 585, pp. 321-328, AIP Conf. Proc. (2001)

[40] T. Ohwada, Structure of normal shock waves: Direct numerical analysis of the Boltzmann equation for hard-sphere molecules, Phys. Fluids A, 5 (1993)

[41] Natalini, R., Convergence to equilibrium for the relaxation for the relaxation approximations of conservation laws. Comm. Pure Appl. Math. v49. pp.795-823 (1996)

[42] P.S. Prasanth and Jose K. Kakkassery, Direct simulation Monte Carlo (DSMC): A numerical method for transition-regime flows: Review, J. Indian Inst. Sci., 86, May-June (2006)

[43] J. L. Steger and R. F.Warming, Flux vector splitting of the inviscid gasdynamic equations with application to finite difference methods, J. Comput. Phys. 40, 263 (1981).

[44] P. Le Tallec and F. Mallinger, Coupling Boltzmann and Navier-Stokes Equations by Half Fluxes, J. Comput. Phys. 136, 51-67 (1997)

[45] B. van Leer, Flux vector splitting for the Euler equations, in Lecture Notes in Physics (Springer-Verlag, New York, Vol. 170, p. 354, (1981)

[46] W. G. Vincenti and C. H. Kruger, Jr. , Introduction to physical gas dynamics, John Wiley & Sons, Inc. (1965)

[47] W. Wagner, A convergence proof for Bird's direct simulation Monte Carlo method for the Botlzamnn equation, J. Stat. Phys. 66, 1011-1044 (1992)

[48] G.J. Wagner, E. G. Karpov, and W. K. Liu, Molecular dynamics boundary conditions for regular crystal lattices, Comput. Methods Appl. Mech. Engrg., 193 (2004)